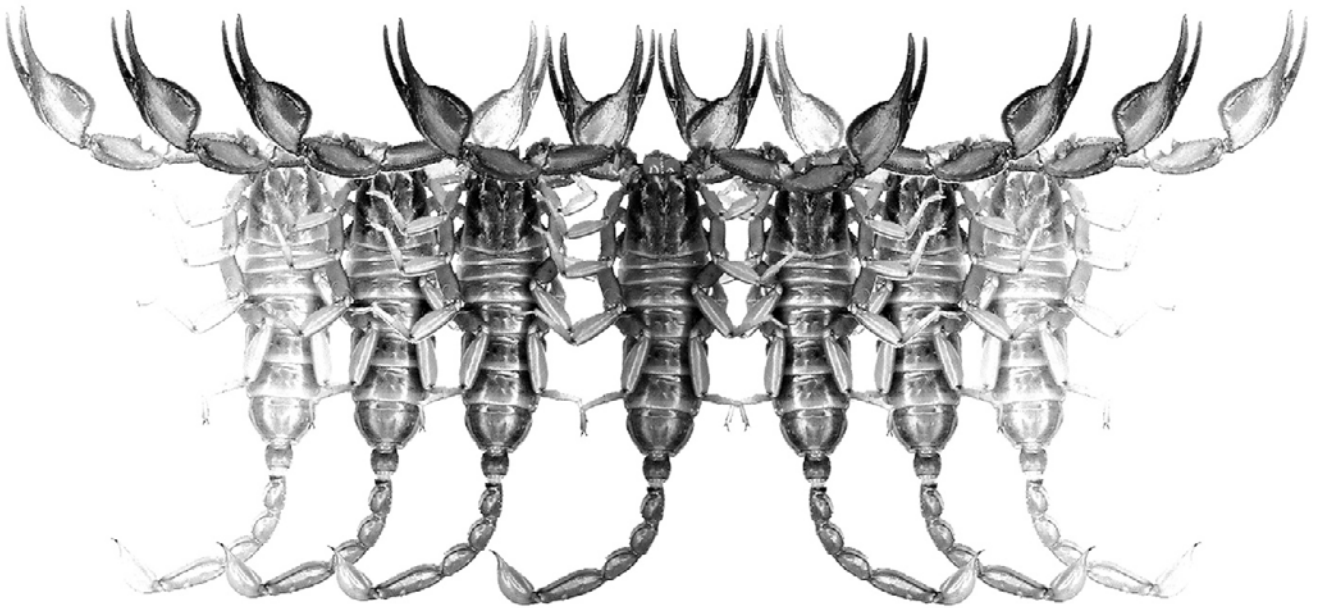


Euscorpium

Occasional Publications in Scorpiology



**Clustered setation on the pedipalps of buthid
scorpions (Scorpiones: Buthidae)**

Graeme Lowe & Victoria Tang

October 2024 — No. 398

Euscorpius

Occasional Publications in Scorpiology

EDITOR: **Victor Fet**, Marshall University, 'fet@marshall.edu'

ASSOCIATE EDITOR: **Michael E. Soleglad**, 'msoleglad@gmail.com'

TECHNICAL EDITOR: **František Kovařík**, 'kovarik.scorpio@gmail.com'

Euscorpius is the first research publication completely devoted to scorpions (Arachnida: Scorpiones). *Euscorpius* takes advantage of the rapidly evolving medium of quick online publication, at the same time maintaining high research standards for the burgeoning field of scorpion science (scorpiology). *Euscorpius* is an expedient and viable medium for the publication of serious papers in scorpiology, including (but not limited to): systematics, evolution, ecology, biogeography, and general biology of scorpions. Review papers, descriptions of new taxa, faunistic surveys, lists of museum collections, and book reviews are welcome.

Derivatio Nominis

The name *Euscorpius* Thorell, 1876 refers to the most common genus of scorpions in the Mediterranean region and southern Europe (family Euscorpiidae).

Euscorpius is located at: <https://mds.marshall.edu/euscorpius/>
Archive of issues 1-270 see also at: <http://www.science.marshall.edu/fet/Euscorpius>

(Marshall University, Huntington, West Virginia 25755-2510, USA)

ICZN COMPLIANCE OF ELECTRONIC PUBLICATIONS:

Electronic (“e-only”) publications are fully compliant with ICZN (*International Code of Zoological Nomenclature*) (i.e. for the purposes of new names and new nomenclatural acts) when properly archived and registered. All *Euscorpius* issues starting from No. 156 (2013) are archived in two electronic archives:

- **Biotaxa**, <http://biotaxa.org/Euscorpius> (ICZN-approved and ZooBank-enabled)
- **Marshall Digital Scholar**, <http://mds.marshall.edu/euscorpius/>. (This website also archives all *Euscorpius* issues previously published on CD-ROMs.)

Between 2000 and 2013, ICZN *did not accept online texts* as “published work” (Article 9.8). At this time, *Euscorpius* was produced in two *identical* versions: online (*ISSN 1536-9307*) and CD-ROM (*ISSN 1536-9293*) (laser disk) in archive-quality, read-only format. Both versions had the identical date of publication, as well as identical page and figure numbers. **Only copies distributed on a CD-ROM** from *Euscorpius* in 2001-2012 represent published work in compliance with the ICZN, i.e. for the purposes of new names and new nomenclatural acts.

In September 2012, ICZN Article 8. What constitutes published work, has been amended and allowed for electronic publications, disallowing publication on optical discs. From January 2013, *Euscorpius* discontinued CD-ROM production; only online electronic version (*ISSN 1536-9307*) is published. For further details on the new ICZN amendment, see <http://www.pensoft.net/journals/zookeys/article/3944/>.

Publication date: 5 October 2024

<http://zoobank.org/urn:lsid:zoobank.org:pub:34AFE347-FAFA-43C5-8627-7EEA8188DF8A>

Clustered setation on the pedipalps of buthid scorpions (Scorpiones: Buthidae)

Graeme Lowe¹ & Victoria Tang²

¹Monell Chemical Senses Center, Philadelphia, Pennsylvania 19104-3308, USA; email: loweg@monell.org

²Zhangyang Rd. 200120, Pudong New District, Shanghai, China; email: jibril.flueqel@gmail.com

<http://zoobank.org/urn:lsid:zoobank.org:pub:34AFE347-FAFA-43C5-8627-7EEA8188DF8A>

Summary

Chaetotaxy of the external pedipalp femur and distal ventral pedipalp movable finger was studied in 120 species, 69 genera and 17 families of scorpions. Setation was generally denser in the ‘Buthus’ group, a major arid-adapted buthid lineage distributed across Palearctic deserts. On the external femur, macrosetae formed a prominent cluster, the ‘distal external macrosetal cluster’ (DEMC); on the distal ventral movable finger they formed a dense patch, the ‘distal ventral macrosetal cluster’ (DVMC). In other buthids and non-buthids, the DEMC and DVMC were mostly absent, except in a few arid-adapted genera. Relative setation densities of DEMC and DVMC in different species depended strongly on size, being denser in larger species and sparser in smaller species, while absolute density varied only weakly with size (mean spacing of setae ~200 µm in DEMC, ~40 µm in DVMC). Ontogenetic variation followed similar trends. Multivariate morphometric analyses revealed taxonomic differences in setation patterns. The ‘Buthus’ group, other buthids, and non-buthids, were partially separable according to their spatial profiles of setation. In the ‘Buthus’ group, major genera were separable by spatial and density profiles of setation. In buthids, there were taxonomic differences in external femoral trichobothriotaxy. The ‘Buthus’ and Tityus’ groups were largely separable by proximodistal positioning of trichobothrium e_1 . Relative setation densities of DEMC and DVMC were positively correlated, in that species with dense DEMCs also tended to have dense DVMCs. In the buthid *Olivierus martensii*, DEMC and DVMC were observed to brush the median ocelli during sponge-bathing. In all examined buthids, the DEMC was located where it would contact the ipsilateral median ocellus during femoral articulation. Both DEMC and DVMC may assist in the ocular grooming of desert buthids, by removing sand and dust from surfaces of the median ocelli.

Introduction

The exoskeleton of scorpions bears numerous setae with diverse morphologies and distribution patterns. Comparative studies of scorpion setation place heavy emphasis on the description and analysis of trichobothrial patterns on the pedipalps (e.g., Fet & Rechkin, 1989; Fet et al., 2005; Soleglad & Fet, 2001; Vachon, 1972, 1974, 1975; and a great many subsequent works). Trichobothriotaxy is applied widely in the diagnosis and description of taxa at all levels from families down to species, and in phylogenetic analysis. However, the systematic study of configurations of other types of setae (chaetotaxy) is also a potential source of taxonomic characters. Tarsal chaetotaxy has proven informative in the lower-level taxonomy of genera and species in various scorpion lineages. Diagnostic value has been attached to numbers and positions of setiform macrosetae on the basitarsus and telotarsus of vaejovids (e.g., González-Santillán & Prendini, 2013; Haradon, 1983, 1984a, 1984b, 1985; McWest, 2009) and buthids (e.g., Lowe & Kovařík, 2019, 2022); and to numbers of spiniform macrosetae on the telotarsus of bothriurids (e.g., Kovařík & Ojanguren Affilastro, 2013) and Scorpionoidea

(e.g., Francke, 1977, 1978; Kovařík et al., 2017; Kraepelin, 1894; Purcell, 1899; Prendini, 2000; Prendini & Loria, 2020; Santibáñez-López et al., 2013; Soleglad et al., 2005; Stahnke, 1967, 1968). The arrangement of macrosetae on carinae or intercarinal surfaces of the metasoma can exhibit consistent interspecies differences in vaejovids (e.g., González-Santillán & Prendini, 2013; Haradon, 1983, 1984a, 1984b, 1985; Jain et al., 2022, 2023), bothriurids (e.g., Kovařík & Ojanguren Affilastro, 2013), hadrurids (e.g., Soleglad et al., 2011; Williams, 1970), hormurids (Monod et al., 2023), and buthids (e.g., Cain et al., 2021; Lowe, 2001; Teruel & Turiel, 2020; Vachon, 1952).

Chaetotaxy of pedipalp segments has received less attention. In vaejovids, Haradon (1984a, 1984b, 1985) described numbers and positions of macrosetae on the external femur, internal patella, and chela manus in different species of *Paruroctonus*. Macrosetal counts on these segments were also provided in some other descriptions of vaejovids (e.g., Hughes, 2011; Jain et al., 2022, 2023; Sissom et al., 2016). On the pedipalp fingers, two specialized pairs of small, subdistal macrosetae were reported in a number of buthids (Armas, 1977; Cruz & Armas, 1980; Fet et al., 2006). Recently, Lowe & Fet (2024) investigated the occurrence of these ‘Cruz-

Armas sensilla' (CAS) in a larger sample of buthids. In all examined buthids, at least one pair of CAS was observed. In addition, small landmark macrosetae (termed SPS, or subrow proximal sensilla) were located immediately proximal to each proximal enlarged denticle of median denticle subrows of the fingers. Conversely, in non-buthids, the CAS and SPS macrosetae were invariably replaced by subdistal and subrow proximal fluorescent microsetae. These findings showed that non-trichobothrial pedipalp setation can be informative in higher level phylogeny.

The aim of this paper is to continue the systematic study of pedipalp setation. We focus on the external surface of the femur, and the distal ventral surface of the chela movable finger. These areas have been largely neglected in taxonomic descriptions. Illustrations or photographs of the external aspect of the femur were only occasionally published (e.g., Contreras Félix & Navarrete Heredia, 2024; González-Santillán et al., 2019; Kovařík & Lowe, 2019; Kovařík & Njoroge, 2021; Lourenço, 1984, 1998, 2007; Lourenço & Pham, 2010; Lowe, 2018; Lowe et al., 2019; Lowe & Kovařík, 2022; Monod et al., 2013, 2023; Prendini, 2004; Prendini & al., 2006; Prendini et al., 2021; Tang, 2022a, 2022b, 2023; Tang et al., 2023, 2024; Vachon, 1974, 1977), and are absent in the vast majority of descriptive works. The main structures on the external femur are the external median carina (aka retromedian carina, retrolateral dorsosubmedian carina, dorsal-outer crest, exterior-median keel), one to four external trichobothria, and macrosetae whose numbers and positions vary between taxa. In buthids, external macrosetae appear to be more numerous and are often gathered in the distal half of the femur on the infracarinal surface. Vachon (1952) roughly indicated these in dorsal illustrations of the femur, and termed them “*soies accessoires*”. Subsequently, they were termed “*external accessory bristles*” by Levy et al. (1973), and “*distal-outside accessory bristles*” by Levy & Amitai (1980). These authors did not present detailed descriptions and counts of macrosetae, only reporting either their absence, or the presence of a few or many. Lowe (2001, 2010b, 2010c, 2010d, 2018), Lowe & Kovařík (2016), and Lowe et al. (2014, 2019) termed them “*distal external accessory macrosetae*” and reported their arrangements and counts. Here, we introduce the term ‘distal external macrosetal cluster’ (abbreviated DEMC) to refer to this group of infracarinal macrosetae in the distal half of the segment (Figs. 1–6). We analyze the numbers and spatial distributions of DEMC setae, and investigate their occurrence in buthids and other scorpion families.

Illustrations or photographs of the ventral surface of the chela movable finger were often published as part of figures showing ventral views of the entire chela. However, at these low magnifications, finer details of the ventral chaetotaxy cannot be resolved. In some buthids, there appears to be a distal tuft or cluster of macrosetae. Here, we introduce the term ‘distal ventral macrosetal cluster’ (abbreviated DVMC) to refer to this distal cluster (Figs. 238–241). We analyze the numbers and spatial distributions of DVMC setae, and investigate their occurrence in buthids and other scorpion families.

Methods, Material & Abbreviations

Imaging. Studied material was preserved in 70% ethyl or isopropyl alcohol. Adult specimens were selected for examination, unless otherwise stated. Pedipalp segments were viewed by UV fluorescence after removing specimens from liquid storage (Volschenk, 2005). The UV source was an array of light-emitting diodes with peak emission 395 nm (half peak width ~10 nm) (Lowe et al., 2003). Images were recorded with Canon EOS 7D Mark II and Canon EOS 5DsR cameras. For imaging at lower magnification, we used Canon EF 100 mm f/2.8, Canon MP-E 65 mm f/2.8 1–5X, or Laowa 25 mm f/2.8 2.5–5X macro lenses, with or without Kenko extension tubes. For imaging at higher magnification, we used Mitutoyo M Plan Apo 5X/ 0.14, 10X/ 0.28 or 20X/ 0.42 objectives, attached to Canon EF 70–200 f/4 IS USM, Canon EF 100–400 mm f/4.5–5.6 IS USM, or Raynox DCR-150 tube lenses. A 475 nm long pass emission filter blocked UV excitation light from reaching the camera sensor. For microscopic imaging of cuticular sections, we used an Olympus BX51 microscope with UPlanSApo 20X/ 0.75 objective. Cuticular sectioning methods, fluorescence light sources and filters were as described in Lowe & Fet (2024). Focus stacking was performed by SR90 or THK2001A rails, controllers and software (<https://www.mjkzz.com>), and Zerene Stacker software (Zerene Systems LLC, Washington, USA). Image scales were determined by photographing microscope stage micrometer calibration slides. When necessary, scale bars were corrected for rescaling factors introduced by stacking software (typically 1–3%). Carapace measurements were recorded under a stereo microscope equipped with an ocular micrometer.

Analysis. Non-linear RAW conversion of images was performed in-camera, and post-processing was performed in Paintshop Pro X (Corel Corporation, Ontario, Canada). Brightness and contrast were adjusted to clearly display setation patterns. Figures of the external femur (Figs. 1–6, 7–161, 218–225) show either segments of the right pedipalp, or segments of the left pedipalp displayed in mirror image for comparison (Figs. 9, 10, 15, 16, 20, 23, 24, 26–28, 57, 59, 72, 79, 94, 95, 109, 110, 116, 120, 125, 126, 136, 138, 141, 143, 145–146, 157). Figures of the ventral movable finger (Figs. 238–398) show either fingers of the left pedipalp, or fingers of the right pedipalp displayed in mirror image for comparison (Figs. 241–251, 256–259, 264–267, 272–273, 280–281, 294–295, 300–301, 304–307, 310–311, 314–321, 328–331, 334–337, 340–341, 350–352, 354–356, 359, 363, 365, 367, 376–378, 388, 390, 393, 397, 402). Figs. 411–418 of the ventral movable finger show either fingers of the right pedipalp, or fingers of the left pedipalp displayed in mirror image for comparison (Figs. 411, 414). Macrosetae were identified by their dark non-fluorescent shafts (i.e., ‘Type N’ sensillae), which distinguished them from microsetae whose shafts were normally fluorescent (i.e., ‘Type F’ sensillae) (Lowe & Fet, 2024). Setation patterns were extracted directly from focus-stacked images, and as such represent 2D projections of patterns on 3D surfaces. Patterns were digitized

by manual placement of position markers over socket insertions of individual macrosetae and trichobothria (Figs. 161, 399, 402). If setae were truncated at their bases, markers were placed over empty sockets identified as macrosetal sockets. Identification was based on similarity to sockets of nearest intact macrosetae, and difference from sockets of nearest intact microsetae. Marker coordinates were analyzed with ImageJ 1.52a (Schneider et al., 2012). Cumulative distribution functions (CDFs) of setation patterns and nearest neighbor distances (NNDs) between setae were computed using scripts coded in Origin 7.0 (OriginLab, Massachusetts, USA). Multivariate analysis was performed in NCSS 2023 version 23.0.1 (NCSS LLC, Utah, USA).

Observation of sponge bathing behavior. Adult male *Olivierus martensii* were procured online from Linyi City, Shandong Province, China. Scorpions were housed individually in plastic jars with dry sand substrate (jar diameter ca. 8.3 cm, substrate depth ca. 0.5 cm). If necessary, carapaces were cleaned to remove original dust or excrement. After a one-week acclimation period, 2–3 ml of water was added to the substrate in each container. To elicit sponge bathing behavior, loess dust was deposited evenly over the carapace by a flour sifter (mesh size ca. 0.3 mm). The anterior tergites were covered by a piece of clay to locally restrict the applied dust to the carapace. Adhesion of dust was facilitated by misting with a water sprayer bottle. Videos of sponge bathing activity were recorded with a Samsung Galaxy Note10+ (SM-N9760) mobile phone.

Nomenclature and terminology. Morphological terminology mostly follows Stahnke (1971). Trichobothrial nomenclature follows Vachon (1974). Nomenclature of major buthid lineages follows Štundlová et al. (2020), Lowe & Kovařík (2022) and Lowe & Fet (2024).

Abbreviations. 1D, one-dimensional; 2D, two-dimensional; 3D, three-dimensional; CAS, Cruz–Armas sensillum/ sensilla; CDF, cumulative distribution function; DEMC, distal external macrosetal cluster; DVMC, distal ventral macrosetal cluster; ECMS, external carinal macrosetal series; FKCP, private collection of Frantisek Kovařík, Prague, Czech Republic; FMNH, Field Museum of Natural History, Chicago, USA; NHMB, Naturhistorisches Museum Basel, Switzerland; NND, nearest neighbor distance; PCA, principal components analysis; R, Pearson's correlation coefficient; SD, standard deviation; UPGMA, unweighted pair-group method with arithmetic mean; USNM, Smithsonian National Museum of Natural History (aka United States National Museum), Washington D.C., USA; UV, ultraviolet; VT, private collection of Victoria Tang, Shanghai, China. Standard abbreviations of International System of units are used.

Material examined. Specimens are deposited in the collection of the first author, unless otherwise indicated. Corresponding figure numbers are listed in parentheses at the end of each species entry. Most, but not all examined species and specimens are shown in the figures. Elevation data are cited as recorded on collection labels, in either feet (') or meters (m).

BUTHIDAE

BUTHUS GROUP

Aegaeobuthus gibbosus (Brullé, 1832): 1♂1♀, Turkey, Iskenderun env., Topbogazi Pass, 800 m a. s. l., 7.V.1988, leg. A. Plutenko (7–8, 164, 244–245).

Androctonus australis (Linnaeus, 1758): 1♂1♀, Egypt, 2008 (9–10, 165, 241–243, 402–404).

Androctonus cf. crassicauda (Olivier, 1807): 1♂, Iran, Markazi Province, Delijan–Mahalat, 33°52'08.6"N 50°28'04.3"E, 1610 m a. s. l., V.2014, leg. Masihpour, Hayader & Behmam, FKCP (11, 248–249); 1♀, Iran, Tehran Province, Firooz kooh, Semnan road, Pirdeh, 35°42'43"N 52°49'19"E, 2559 m a. s. l., V.2012, leg. Rabiei, Barzegar and Fallahpour, FKCP (12, 250–251); 1♀2♂juv.1♀juv, Oman, Batinah coast, 10–15 km W of Barka, Abyad pipeline road, dunes, *Acacia* woodland, 23°41.16'N 57°43.61'E, < 50 m a. s. l., 13.X.1993, leg. G. Lowe, A. S. Gardner & S. M. Farook (219, 221–223); 1♂1♂juv., Oman, Batinah coast, ca. 11 km W. of Barka, 23°40.62'N 57°45.77'E < 50 m a. s. l., sand dunes, sand flats, *Acacia* woodland, 13.X.1993; leg. G. Lowe, A. S. Gardner, S. M. Farook (218, 224); 1♂juv, Oman, near Yitti, 23°30.54'N 58°38.46'E, 0 m a. s. l., UV detection, wadi near village, trees, soft sand, 1.X.1995; leg. G. Lowe, M. D. Gallagher & A. Al-Baluchi (220); 1♂juv, Oman, Wahiba Sands, 24°09'N 58°23'E, 2.II.1986; leg. M.D. Gallagher, Oman Eastern Sands Project, NHMB (223).

Anomalobuthus lowei Teruel, Kovařík & Fet, 2018: 1♀, holotype, Kazakhstan, 75 mi. N of Alma-Ata, Ili River, 17.V.1993, leg. A. Feodorov (19, 246–247).

Apistobuthus pterygocercus Finnegan, 1932: 1♂1♀, Oman, NW of Montesar, S of Wadi Muqshin, UV detection on sand, humpy dunes, sparse vegetation, 19°29.17'N 54°36.89'E, 200 m a. s. l., 6.X.1994, leg. G. Lowe & M. D. Gallagher (13, 166, 238–240, 252–253, 399–401); 1♀, Oman, between Qarn Alam & Ghaba North, 21°22'02"N 57°05'28"E, 150 m a. s. l., on coarse grit, on top of dusty alluvium, in shallow depression with *Acacia ehrenbergiana*, with sand mounds at base, 21.II.1996, leg. M. D. Gallagher MDG8755, NHMB (14); 2♀2♂juv., Oman, Wadi Atiyah, 18°17.09'N 53°14.45'E, 260 m a. s. l., 28.IX.1995, leg. G. Lowe, M. D. Gallagher & A. Dunsire (411–415).

Apistobuthus susanae Lourenço, 1998: 1♂1♀, Iran, Khoozestan Province, Omidiyeh, 30°57'49"N 49°31'47"E; leg. S. Navidpour (15–16, 161–163, 256–259).

Buthacus nigroaculeatus Levy et al., 1973: 1♂1♀, Oman, Wadi Muqshin, near Montesar, 19°27'58"N 54°57'20"E, 140 m a. s. l., open ground, level sand and some scrub, 12.XII.1996, leg. I. D. Harrison & M. D. Gallagher, MDG 8822, NHMB (17–18, 167, 264–267); 1♂, Oman, Wadi Muqshin, NW of Montesar, 19°27.68'N 54°37.2'E, 195 m a. s. l., UV detection on sand, sandy flat in wadi, patchy dunes, *Prosopis* and *Zygophyllum*, 6.X.1994, leg. G. Lowe & M. D. Gallagher (1–2).

Butheolus gallagheri Vachon, 1980: 1♂, Oman, Salalah, leg. A. Ullrich (254–255).

- Butheolus harrisoni* Lowe, 2018: 1♀, paratype, Oman, Jabal Qamr, deep wadi between steep winding roads, UV detection on gravel in wadi, 16°52.3'N 53°43.28'E, 140 m a. s. l., 27.IX.1995, leg. M. D. Gallagher (21–22, 260–263).
- Buthus mardochei* Simon, 1878: 1♂, Morocco, Ait Saoun, 12.III.1999 (20, 268–269).
- Compsobuthus acutecarinatus* (Simon, 1882): 1♀, Oman, Jabal Qara, Nejd Desert, wadi below Ayun, 17°13.4'N 53°54.36'E, 600 m a. s. l., 20.X.1993, leg. G. Lowe (27).
- Compsobuthus levyi* Kovařík, 2012: 1♂, Jordan, Balqa Governorate, 32°11.058'N 35°47.956'E, 292 m a. s. l., XI.2016, leg. A. Ullrich.
- Compsobuthus maindroni* (Kraepelin, 1900): 1♀, Oman, Al Hamra area, N of Bahla, 23°04'50.53"N 57°21'58.09"E, 700 m a. s. l., 19:00–20:30 h, rocky wadi, 4.III.1996, leg. J. Dundon 115 (31, 270–271).
- Compsobuthus matthiesseni* (Birula, 1905): 1♂1♀, Iran, Hamadan Province, 35 km SE of Hamadan, Gonbad vill. env., ca. 2000 m a. s. l., 7–8.V.1996, leg. V. Šejna (23–24, 272–275).
- Compsobuthus nematodactylus* Lowe, 2009: 1♂, paratype, Oman, Musandam peninsula, mountain road S. of Khasab, 20°0.32'N 56°12.69'E, 980 m a. s. l., 28.IX.1994, leg. G. Lowe (32, 276–277).
- Compsobuthus polisi* Lowe, 2001: 1♂1♀, paratypes, Oman, Wadi Dirif, 18°57.51'N 57°21.73'E. 20 m a. s. l., 19:00–20:00 h, 24.IX.1995, leg. G. Lowe & M. D. Gallagher (25–26, 278–279).
- Gint banfasae* Kovařík & Lowe, 2019: 1♂, paratype Somaliland, Shanshade vill., 08°39'35"N 45°55'49"E, 790 m a. s. l., 29–31.VIII.2018, leg. F. Kovařík et al. (28).
- Gint gaitako* Kovařík et al., 2013: 1♂1♀, paratypes, Ethiopia, Oromia State, Borana Prov., 04°25'31.5"N 38°58'14"E, 1171 m a. s. l., 27–28.VI.2013, leg. F. Kovařík (29–30).
- Hottentotta hottentotta* (Fabricius, 1787): 1♀, Cameroon, North Province, 20 km N. of Garoua, Sudanian scrub savanna 20.XI.1980, 250 m a. s. l., leg. R. L. Aalbu (33, 280–281).
- Hottentotta jayakari* (Pocock, 1895): 1♂1♀, Oman, Route 13, ca. 5.9 km E. of junction Wadi Mistal road, wadi near palm plantation, with water, UV detection, rock & earthen wall, 23°21.33'N 57°38.21'E, 460 m a. s. l., 26.IX.1994, leg. G. Lowe & M. D. Gallagher (35–36, 284–287).
- Hottentotta minax occidentalis* (Vachon & Stockmann, 1968): 1♀, Cameroon, Northern Province. 10 km N. of Waza, 25.VI.1980, 300 m a. s. l. Sahelian flood plain, leg. R. L. Aalbu (34).
- Hottentotta pellucidus* Lowe, 2010: 1♂1♀, paratypes, Oman, Jabal Bani Jabir, UV detection, rocky terrain, 22°49.6'N 59°1.59'E, 1640 m a. s. l., 14.IX.1995, leg. G. Lowe, M. D. Gallagher & J. Dundon (37–38, 168, 282–283).
- Hottentotta rugiscutis* (Pocock, 1897): 1♀, India, Madras, II.1993 leg. M. Veselý.
- Hottentotta saxinatans* Lowe, 2010: 1♀, paratype, Oman, Jabal Shams, UV detection, wide gravel wadi, on boulders, 23°14.31'N 57°11.64'E, 1900 m a. s. l., 14.X.1993, leg. G. Lowe & M. D. Gallagher (288–289).
- Hottentotta trilineatus* (Peters, 1861): 2♂2♀, Kenya, S. Magadi, Lake Magadi env., 6.XII.1997, leg. M. Snížek (39–42, 290–291).
- Kraepelinia palpator* (Birula, 1903): 1♂juv., Turkmenistan, Badghyz, Eroilanduz, 35°42'04"N 61°48'53", 348 m a. s. l., 7.IV.2002, leg. A. Gromov (51, 348).
- Leiurus abdullahbayrami* Yağmur, Koc & Kunt, 2009: 1♂, paratype, Turkey, 1 km S. of Eski Şarkaya Village, Şehitkamal District, Gaziantep Province, 37°12'44"N 37°07'45"E, 1000 m a. s. l., 23.VI.2007, leg. E. A. Yağmur & M. Yalçın (43, 292–293); 1♀, Turkey, 2 km E of Çaybaşı Village, Oğuzelli District, Gaziantep Province, 36°47'47"N 37°35'15"E 546 m a. s. l., 18.VII.2010, leg. E. A. Yağmur & M. Özkörük (44).
- Leiurus haenggii* Lowe, Yağmur & Kovařík, 2014: 1♂, Yemen, 8.VI.2010, leg. M. Heule (3–4); 1♀, Yemen, captive bred, 8.VI.2010, ex. M. Heule (47, 294–295);
- Leiurus hebraeus* (Birula, 1908): 1♀, Jordan, 32°11.058'N 35°47.956'E, 292 m a. s. l., leg. A. Ullrich (49, 296–297).
- Leiurus macroctenus* Lowe, Yağmur & Kovařík, 2014: 1♂1♀, paratypes, Oman, Dhuai, 21°06.26'N 58°22.292'E, 70 m a. s. l., low aeolinite hilltop & slope to sand, edge of trees, 21.X.1997, leg. M. D. Gallagher & I. D. Harrison, MDG 8889 (45–46, 169, 298–299).
- Leiurus quinquestriatus* (Ehrenberg, 1828): 1♀, Egypt, 2007, ex. F. Kovařík (48).
- Liobuthus kessleri* Birula, 1898: 1♂1♀, Uzbekistan, between Bukhara and Gazli, 11.V.2002, leg. V. Fet (50, 52, 170, 300–301).
- Mesobuthus afghanus* (Pocock, 1889): 1♀, Turkmenistan, Lebap Province, Karakum Desert, Repetek Nature Reserve, 18.IV.2002, leg. V. Fet (54, 306–307); 1♂, Turkmenistan, Badghyz Reserve, leg. K. Atmuradov (53); 1♂, Turkmenistan, Badghyz, Eroilanduz, IV.2002, leg. V. Fet & A. Gromov (304–305).
- Mesobuthus thersites* (C. L. Koch, 1839): 1♂1♀, China, Xinjiang Uygur Autonomous Region, Bayingolin Mongol Autonomous Prefecture, Qiemo County, near Bage'airike Township, 38°12'15.9"N 85°31'57.7"E, 1171 m a. s. l., 22.VII.2023, leg. Q. Du, VT (171); 1♂1♀, Kazakhstan, Baigakum, 44°20'37"N 66°27'09"E (55–56, 308–309).
- Microbuthus gardneri* Lowe, 2010: 1♀, paratype, Oman, Jabal Ukhayr, UV detection bottom of rocky slope on edge of wadi on sand between small rocks, 18:45–21:15 h, 22°42.34'N 58°47.58'E, 486 m a. s. l., 13.XII.2001, leg. A. Winkler (79, 349).
- Neobuthus amoudensis* Kovařík et al., 2018: 1♀, paratype, Somaliland, Borama campus, around university, 09°56'49"N 43°13'23"E, 1394 m a. s. l., 11–12.IX.2017, leg. F. Kovařík.
- Neobuthus ferrugineus* (Kraepelin, 1898): 1♀, Djibouti, Barra Yer (Petite Barre), 11°18'33.56"N 42°42'39.17"E, 585 m a. s. l., 6.II.2017, leg. F. Kovařík (61, 300–301).
- Odontobuthus bidentatus* (Lourenço & Pezier, 2002): 1♂, Iran, Bushehr Prov., Tangestan, Farshanbeh, 28°52'53"N 51°18'43"E, 95 m a. s. l., XI.2007, leg. Masihpour, Bahrani & al. (57); 1♀, Iran; Khuzestan Province, Omidiyeh, 30°57'49"N 49°31'47"E, 56 m a. s. l., V.2007, leg. Hayader & Bahrani (58, 172, 310–311).

Odontobuthus brevidigitus Lowe, 2010: 1♂, paratype, Oman, Ghubrah, resting on wall of ministry house by front door, at night, 23°35.64'N 58°23.79'E, 10 m a. s. l., 30.IX.1995, leg. G. Lowe (59); 1♀, topoparatype, Oman, Batinah plain, c. 4 km W of Seeb, sabkha, *Prosopis* & palms, colony of burrows, <0.5 m depth in fine soil, 23°41.39'E 58°06.93'E, 0 m a. s. l., 22.X.1993, leg. G. Lowe & A. S. Gardner (60, 312–313).

Olivierus fuscus (Birula, 1897): 1♀, Tajikistan, leg. A. Federov (62).

Olivierus gorelovi (Fet et al., 2018): 1♀, Kazakhstan, 75 km N of Alma-Ata, Ili River, VI.1993, leg. I. Skorkin (63, 314–315).

Olivierus kreuzbergi (Fet et al., 2018): 1♀, Uzbekistan, Babatag Mountains, 4.V.2002, leg. V. Fet (64, 322–323).

Olivierus longichelus (Sun & Zhu, 2010): 1♂, China, Xinjiang Uygur Autonomous Region, Bortala Mongol Autonomous Prefecture, Jinghe Co., 44°29'03.7"N 82°53'12.3"E, 485 m a. s. l., 6.VIII.2023, leg. Q. Du, VT (67, 173, 316–317); 1♀, China, Xinjiang Uygur Autonomous Region, Bortala Mongol Autonomous Prefecture, Bole City, nr Dalete Town, 44°48'06.3"N 82°04'14.1"E, 496 m a. s. l., 5.VIII.2023, leg. Qiu Du, VT; 1♀, China, Xinjiang Uygur Autonomous Region, Changji Prefecture, Wujiaqu City, 44°33'42.0"N 87°36'55.0"E, 351 m a. s. l., 3.IX.2023, leg. Q. Du, VT (68, 318–319).

Olivierus martensii (Karsch, 1879): 1♀, breeding farm, ex. C. P. Kristensen; 2♂1♀, China, Henan Province, Luoyang City, procured online, VT (65–66); 40♂1♀, China, Shandong Province, Linyi City, procured online, VT (5–6, 200, 424–435); 1♂1♀, albino, procured online in China, VT.

Olivierus przewalskii (Birula, 1897): 1♂, China, Xinjiang Uygur Autonomous Region, Ili Kazakh Autonomous Prefecture, Ghulja Co., nr Yingyeer Town, 43°59'47.9"N 81°09'02.7"E, 685 m a. s. l., 3.VIII.2023, leg. Q. Du, VT (69, 320–321); 1♀, China, Xinjiang Uygur Autonomous Region, Kashgar Prefecture, Yarkant Co., nr Kalasu Township, 38°18'15.2"N 77°31'51.5"E, 1186 m a. s. l., 29.VII.2023, leg. Q. Du, VT (70).

Orthochirus glabrifrons (Kraepelin, 1903): 1♂1♀, Oman, Jabal Bani Jabir, 22°49.93'N 59°01.06'E, 1610 m a. s. l., UV detection, shallow rocky depression, & surrounding rocky slopes, with grass, shrubs & trees, 14.IX.1995, leg. G. Lowe, M. D. Gallagher & J. Dundon (73–74, 324–325).

Orthochirus gromovi Kovařík, 2004: 1♂1♀, paratypes, Turkmenistan, Lebap Province, Karakum Desert, Repetek Nature Reserve, sands, 38°33'57–59"N 63°09'46"–10'13" E, ca. 200 m a. s. l., leg. A. V. Gromov (71–72, 174, 326–327).

Orthochirus zagrosensis Kovařík, 2004: 1♀, Iran, Bandar-e Gonave, 15.X.2002, leg. M. Kaftan (75).

Picobuthus wahibaensis Lowe, 2010: 1♀, paratype, Oman, 4 km N of Al Nuqdah, sand, grass & *Heliotropium* hummocks, 20°53'N 58°44.533'E, 10 m a. s. l., 29.I.1997, leg. I. D. Harrison & M. D. Gallagher, MDG 8844 (80, 350).

Razianus zarudnyi (Birula, 1903): 1♀, Iran, Khuzestan Province, 35 km E of Gach Saran, 6.II.1964, leg. J. Neal, USNM (76, 328–329).

Somalibuthus sabae Kovařík & Njoroge, 2021: 1♂1♀, paratypes, Kenya, Kiwayu Island, Lamu County, 1°59'36.32"S 41°17'08.59"E, 14.XII.2020, leg. S. Douglas–Hamilton (77–78, 330–331).

Trypanothacus barnesi Lowe et al., 2019: 1♂, paratype, Oman, wadi SE of Thumrait, slightly raised sedimentary plateau under sheet wood, 17°42'N 53°59'E, 9.X.1997, leg. J. N. Barnes (332–333, 428); 1♀, paratype, Oman, Yalooni, Jiddat Al Harasis, 19°57'N 57°06'E, XII.1988, Yalooni 185, NHMB (82).

Vachoniolus gallagheri Lowe, 2010: 1♂, paratype, Oman, sandy wadi W. of Ghabah, UV detection, low dunes & scrub, near sabkha, windy, 21°23.89'N 57°09.56'E, 185 m a. s. l., 5.X.1994, leg. G. Lowe & M. D. Gallagher (83).

Vachoniolus globimanus Levy, Amitai & Shulov, 1973: 1♀, United Arab Emirates, Nahel, nr Sweihan, 24°27'N 55°20'E ca. 225 m a. s. l., rolling sand with vegetation, 14.IX.2001, leg. G. Feulner (84, 175, 334–335).

Xenobuthus anthracinus (Pocock, 1895): 1♂, Oman, S of Thumrait; Nejd Desert, 17°30.77'N 54°02.82'E, 600 m a. s. l., UV detection, silty plain, edge of small vegetated wadi, fine silty soil, open plain, rock outcrops, 19.X.1993, 23:02 h, leg. G. Lowe, NHMB (85); 1♀, Oman, S of Thumrait, Nejd Desert, 17°30.76'N 54°02.76'E, 580 m a. s. l., UV detection, edge of small vegetated wadi, open plain, fine silty soil, rock outcrops, 16.X.1993, 19:28 h, leg. G. Lowe, NHMB (86).

Xenobuthus xanthus Lowe, 2018: 1♂, holotype, Oman, Jabal Zulul, escarpment above Ash Shuwaymiyah, 17°57.12'N 55°39.28'E, 215 m a. s. l., UV detection on ground, silt and gravel, rocky bowl surrounded by rocky cliffs and slopes, 26.IX.1995, 00:45 h, leg. G. Lowe, M.D. Gallagher, NHMB (87); 1♀, paratype, Wadi Shuwaymiyah, 17°55.94'N 55°31.47'E, 50 m a. s. l., under rock on mound of sandy soil, near permanent water seepage site on northern edge of wide vegetated wadi, 25.IX.1995, 19:15 h, leg. G. Lowe, M.D. Gallagher, NHMB (88).

OTHER BUTHIDS

ANANTERIS–ISOMETRUS GROUP

Babycurus centrurimorphus Karsch, 1886: 1♂, Kenya, Kabernet, town center, under stones, II.1989, leg. P. Brownell (89, 351).

Isometroides vescus (Karsch, 1880): 1♂, Australia, South Australia, pitfall, Tractor Dam. South Olary Plain, c. 33°18'S 139°34'E, 5.X.1992 (353); 1♀, Australia, South Australia, South Olary Plain, pitfall, National Parks and Wildlife Service Survey, ca. 32°30'S 140°10'E, X.1992.

Isometrus maculatus (DeGeer, 1778): 1♀, USA, Hawaii, Honolulu Co., Wai'anae Valley Road, ~2.5 mi. NE of Route 98, 12.I.1984, leg. G. Lowe (90, 352).

Langxie feti Tang, Jia & Liu, 2023: 1♀, China, Tibet Autonomous Region, Nyingchi Prefecture, Zayü County, Golag Township, 29°06'39.0"N 97°58'26.0"E, 2429 m a. s. l., 14–16.IX.2022, leg. Q.–Q. Jia, VT (91, 354)

Lychas mucronatus (Fabricius, 1798): 1♀, Indonesia, Maumere, Flores Island, 1984, 15.VII.2003, leg. M. Braunwalder (92, 355).

Lychas scutillus C. L. Koch, 1845: 1♂1♀, Thailand, Thaleban, 18.I.2013, leg. H. Bringsløe (93, 356).

Reddyanus bilyi (Kovařík, 2003): 1♂, Australia, New South Wales, Route 81, Rifle Creek, E. of Mt Molloy, 17.III.1987, leg. G. Lowe (94, 357).

CHARMUS–UROPLECTES GROUP

Grosphus madagascariensis (Gervais, 1843): 1♂1♀, Madagascar, Moramanga env., Anjirio, 10.II.1995 (95–96, 358).

Parabuthus abyssinicus Pocock, 1901: 1♀1♂, Ethiopia, Sodora, 1400 m a. s. l., IV.1994, leg. R. Lízler (97–98, 336–337).

Parabuthus granulatus (Ehrenberg, 1831): 1♂, RSA, Rehoboth, 10.III.1999, leg. R. Lízler (99).

Parabuthus transvaalicus Purcell, 1899: 1♀, Zimbabwe, 30 km N of Beltbridge, Tongwe env., 7.XII.1998, leg. S. Bečvář (100, 176, 338–339).

Teruelius ankarana (Lourenço & Goodman, 2003): 2♂3♀, Madagascar, Antsiranana Province, Ankarana National Park, 126 m a. s. l., 12°57'43.4"S 49°07'13.48"E, leg. M. Häckel (101–102, 340–341).

Teruelius flavopiceus (Kraepelin, 1900): 1♂1♀, Madagascar, Antsiranana Province, Diego Suarez env., E. of Ramena, village, ca. 50 m a. s. l., 12°15'9.95"S 49°21'31.05"E, ex. M. Trýzna, leg. M. Häckel (103, 177, 342–343).

Teruelius grandidieri (Kraepelin, 1900): 1♂, Madagascar, Toliara Province, Tsimanampetsotsa National Park, Mitoho Camp, 10 m a. s. l., 43°45.138'E 24°02.838'S, leg. M. Häckel (104).

Uroplectes flavoviridis Peters, 1861: 1♀, Zimbabwe, Maleme Rest camp, Matopos National Park, 7–12.II.1988, leg. J. Minshall.

Uroplectes planimanus (Karsch, 1879): 1♂1♀, Botswana, Maun, Island Safari Lodge, 15–29.I.1997, leg. M. Snížek (105–106).

Uroplectes vittatus (Thorell, 1876): 1♂1♀, Botswana, Nata, 9–14.I.1997, leg. M. Snížek (107–108, 178, 359).

TITYUS GROUP

Alayotityus sierramaestrae Armas, 1973: 1♂, Cuba (110, 360).

Centruroides bicolor (Pocock, 1898): 1♂, Costa Rica, Puntarenas Province, ca. 25 mi. NW of San Vito, 9.VIII.1989, leg. S. D. Miller (115, 361).

Centruroides edwardsii (Gervais, 1843): 1♂, Costa Rica, Guanacaste Province, Playas del Coco, 1989, leg. S. D. Miller (117, 179, 344–345).

Centruroides gracilis (Latreille, 1804): 1♂, USA, Florida, Dade Co., Miami, 15.VIII.1985, leg. G. Gwin (113); 1♀, Cuba; Santiago de Cuba City, 8.VIII.1988, leg. R. Teruel (114).

Centruroides koesteri Kraepelin, 1912: 1♀, Costa Rica, Prov. Puntarenas, Mata de Limon, UV detection, IV.1991, leg. S. D. Miller (116, 346–347).

Centruroides margaritatus (Gervais, 1841): 1♂1♀, Ecuador, coastal south–central region, 1992, leg. S. D. Miller (111–112, 180).

Centruroides nigrimanus (Pocock, 1898): 1♂, Mexico; Oaxaca, 1 mi. E of Yagul ruin, 5800' a.s.l., *Acacia* scrub, nr limestone caves, 2.VII.1982, leg. R. L. Aalbu (118).

Heteroctenus junceus (Herbst, 1800): 1♂, Cuba, Santiago de Cuba, Siboney, UV detection on ground, 24.III.2003, leg. R. Teruel (119); 1♀, Cuba, leg. R. Teruel (120, 362).

Microtityus jaumei Armas, 1974: 1♀, Cuba (121, 363).

Tityus championi Pocock, 1898: 1♂, Costa Rica, Prov. Puntarenas, ~25 mi. NW San Vito, 9.VIII.1989, leg. S. D. Miller (123, 364).

Tityus dedoslargos Francke & Stockwell, 1987: 1♂, Costa Rica, Quepos, III.1991, leg. S. D. Miller (365); 1♀, Costa Rica, Puntarenas, S.E. Quepos, 19:00 h, UV detection, forest floor, 20.IV.1994, leg. S. D. Miller (124).

Tityus ecuadorensis Kraepelin, 1896: 1♂, Ecuador, Zumba, on and under stones, X.1992, leg. S. D. Miller (122).

NON–BUTHIDS

PSEUDOCHACTIDAE

Qianxie solegladi Tang, 2022: 1♀, China, Yunnan Province, Kunming City, Luquan County, Wumeng Township, Zhongping Village, 25°53'45.24"N 102°43'28.92"E, 1192 m a. s. l., 29.IV.2022, leg. H. He, VT (126, 370).

Pseudochactas ovchinnikovi Gromov, 1998: 1♀, Uzbekistan, Babatag Mts, 38°01'39"N 68°14'45"E, 763 m a. s. l., 4.V.2002, leg. V. Fet (125, 369).

CHAERILIDAE

Chaerilus hofereki Kovařík, et al., 2014: 2♂, Vietnam, Binh Thuan Province, Phan Thiet, ca. 10°56'N 108°06'E, III.2014, bred from paratypes (138, 368).

BOTHRIURIDAE

Brachistosternus artigasi Cekalovic, 1974: 1♂, Chile, Iquique Prov., Alto Patache, III–IV.1998, leg. A. Ugarte (129, 182, 366).

Brachistosternus donosoi Cekalovic, 1974: 1♂, Chile, Iquique Prov., Alto Patache, III–IV.1998, leg. A. Ugarte (127).

Brachistosternus mattonii Ojanguren–Affilastro, 2005: 1♂, Chile, Iquique Province, Alto Patache, III–IV.1998, leg. A. Ugarte (128, 367).

ANUROCTONIDAE

Anuroctonus phaiodactylus (Wood, 1863): 1♂1♀, USA; Nevada; Lincoln Co., Bristol Well, ~12.9 mi. NW of Pioche, 7.3 mi. W of Route 93, charcoal kilns, 38°06'N 114°41.50' W, 5440' a. s. l., excavated from burrows, 15.VIII.1990, leg. G. Lowe, S. C. Williams, V. F. Lee, J. Chinn & R. Bechtel (133, 181, 371).

BELISARIIDAE

Belisarius xambeui Simon, 1879: 1♀, Spain, Catalonia, Tortellà, Girona, DGG773, 12.III.1996; leg. J. Nebot (134, 372).

CARABOCTONIDAE

Hadruides maculatus (Thorell, 1876): 1♂, Peru, Huancayo (131, 375).

CHACTIDAE

Brotheas gervaisii Pocock, 1893: 1♂, French Guyana, Kawa, ex. M. E. Braunwalder (136, 371).

Brotheas granimanus Pocock, 1898: 1♀, French Guiana, Kawa (373).

EUSCORPIIDAE

Euscorpius deltshevi Fet et al., 2014: 1♀, Bulgaria, Vratsa, 290 m a. s. l., 8.V.1999 (135, 374).

HADRURIDAE

Hadrurus obscurus Williams, 1970: 1♀juv., USA, California, Kern Co., Jawbone Canyon Rd, UV detection, wash with rocky cliffs & slopes, 35°18.87'N 118°05.29'W, 883 m a. s. l., 2.VIII.1997, leg. G. Lowe & B. Hébert (132, 183, 376).

IURIDAE

Iurus dufourei (Brullé, 1832): 1♀, Greece, Sparta, Gythio, Selinita, 3.VIII.1993, leg. P. Crucitti (130, 377).

SCORPIOPIIDAE

Scorpiops cf. *tibetanus* Hirst, 1911: 1♂, China, Tibet Autonomous Region, Nyenchen Tanglha Mts, Lhasa nord, 3800 m a. s. l., 30.V.1996, leg. V. Major (137, 378) (misidentified as *S. hardwickii* in Kovařík (2000) and Lowe & Fet (2024)).

VAEJOVIDAE

Catalinia andreas (Gertsch & Soleglad, 1972): 1♀, USA, California, San Diego Co., Otay Mountain, 10.VI.1976, leg. D. Faulkner (139, 379).

Chihuahuanus crassimanus (Pocock, 1898): 1♂, USA, Texas, Brewster Co., Route 2627, 0.9 mi. NW of La Linda, Heath Canyon, 29°27.5'N 102°50'W, 840' a. s. l., UV detection, roadcut, 3.IX.1991, leg. G. Lowe & B. Hébert (388).

Kochius hirsuticauda (Banks, 1910): 1♂, USA, California, Kern Co., Jawbone Canyon Rd, 35°18.87'N 118°05.29'W, 883 m a. s. l., UV detection, wash with rocky cliffs & slopes, 2.VIII.1997, leg. G. Lowe, B. Hébert (140, 380).

Kovarikia angelena (Gertsch & Soleglad, 1972): 1♀, USA, California, Los Angeles Co. Glendora Mountain Rd, above Little Dalton Canyon, Angeles National Forest, UV detection on rocky soil roadcut, 34°9.64'N 117°50.51'W, ca. 500 m a. s. l., 13.XI.1998, leg. G. Lowe & B. Hébert (141).

Paravaejovis spinigerus (Wood, 1863): 1♀, USA, Arizona, Mohave Co., Old Kingman Highway, UV detection, base of roadcut, 35°13.038'N 114°24.425', 3249' a. s. l., 29.IX.2011, leg. G. Lowe (142, 184, 381).

Paruroctonus gracilior (Hoffmann, 1931): 1♂1♀, USA, Texas, Brewster Co., Route 170, 3.9 mi. E of Lajitas, 29°16'45"N 103°43'20"W, 2540' a. s. l., UV detection, edge of road and roadcut, 2.IX.1991, leg. G. Lowe & B. Hébert (143–144, 383–384).

Paruroctonus hirsutipes Haradon, 1984: 1♀, USA, California, Imperial Co., 3.8 mi. W of Ogilby, Algodones Dunes, 32°48'45"N 114°54'W, 270' a. s. l., UV detection on sand dune, 11.IX.1991, leg. G. Lowe & W. R. Icenogle (145, 382).

Pseudouroctonus apacheanus (Gertsch & Soleglad, 1972): 1♂, USA, Arizona, Graham Co., Pinaleno Mountains, Swift Trail, below Arcadia Campground, 6500' a. s. l., UV

detection, roadcut, 20.IX.2003, leg. G. Lowe & B. Hébert (259–261, 799); 1♀, USA, Arizona, Cochise Co., Southwestern Research Station, 5 mi. W of Portal, 16.VII.1976, leg. S. C. Johnson (146, 385).

Serradigitus torridus Williams & Berke, 1986: 1♀, USA, California, Kern Co., Jawbone Canyon Rd, 35°18.87'N 118°05.29'W, 883 m a. s. l., UV detection, dry wash with rocky cliffs & slopes, 2.VIII.1997, leg. G. Lowe, B. Hébert (147, 387).

Smeringurus mesaensis (Stahnke, 1957): 1♂, USA, California, San Bernardino Co., 35°4.809'N 118°16.185'W, 1113' a. s. l., UV detection on sand, area of sand dunes and sand hummocks, 22.IX.2011, leg. G. Lowe (149); 1♀, USA, Arizona, Mohave Co., Polaris Road, 34°46.094'N 114°28.157'W, 634' a. s. l., open creosote scrub, 24.IX.2011, leg. G. Lowe (150, 389).

Smeringurus vachoni (Stahnke, 1961): 1♀, USA, California, Inyo Co., Route 178, 0.5 mi. W. of Shoshone, UV detection, low rocky hills, 20.VII.1985, leg. G. Lowe & B. Hébert, A²S/253 (151, 390).

Stahnkeus subtilimanus (Soleglad, 1972): 1♂, USA, California, Riverside Co., Berdoo Canyon Rd, 3–4 mi. NE Dillon Rd, UV detection, rocky canyon walls & slopes, 23.VII.1987, leg. G. Lowe, C. P. Kristensen, B. Hébert & B. Firstman, A²S/290 (148, 386).

Vejovoidus longiunguis (Williams, 1969): 1♂, Mexico, Baja California Norte, 11.3 km N. of Guerrero Negro, 5.VII.1979, leg. R. L. Aalbu (152, 185, 391–392).

DIPLOCENTRIDAE

Diplocentrus whitei (Gervais, 1844): 1♂, USA, Texas, Brewster Co., Route 170, 3.9 miles E. of Lajitas, 29°16'45"N 103°43'20"W, El. 2540' a. s. l., UV detection on sandy shoulder of road, 2.IX.1991, leg. G. Lowe & B. Hébert (155, 395).

HORMURIDAE

Hadogenes troglodytes (Peters, 1861): 1♂, Zimbabwe, N. of Chisumbanje, Rupisi, Niauxta riv., 28.XI.1998, leg. M. Snížek (153, 186, 394).

Hormurus waigiensis (Gervais, 1843): 1♀, Australia, Queensland, Crystal Cascades, IV.1987, leg. G. Lowe (154, 393).

SCORPIONIDAE

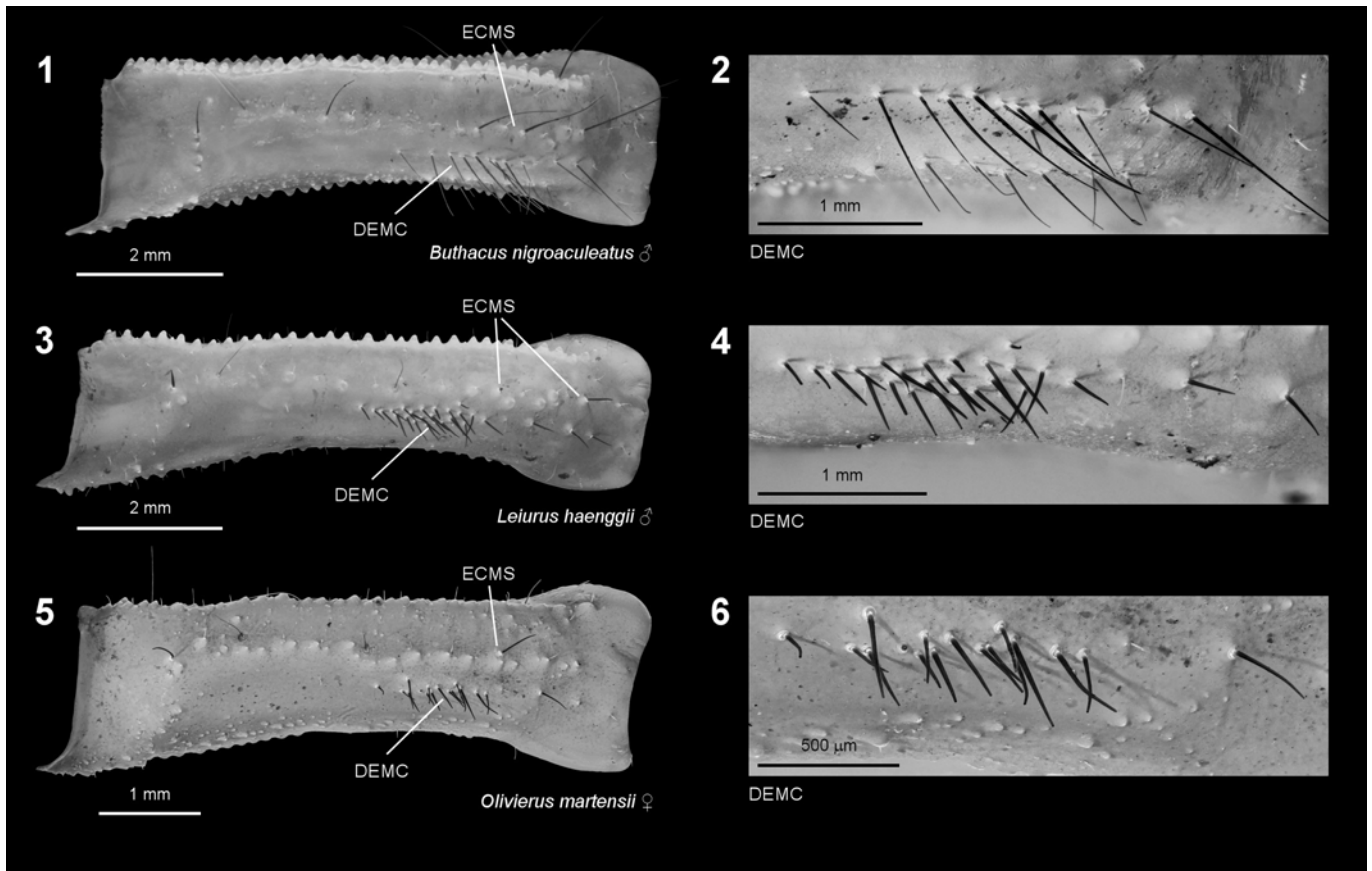
Opisthophthalmus glabrifrons Peters, 1861: 1♂1♀, Zimbabwe, N. of Chisumbanje, Rupisi, Niauxta Riv., 26.XI.1998, leg. M. Snížek (156, 396).

Pandinoides cavimanus (Pocock, 1888): 1♀, Kenya, Voi (Tsavo), 22.XI–2.XII.1996, leg. M. Snížek (157, 187, 397).

URODACIDAE

Urodacus hoplurus Pocock, 1898: 1♀, Australia, WA, Gill Pinnacle, Schwerin Mural Crescent (range of hills), 24°54'S 128°46'E, VII.1963, leg. P. Aitken & N. B. Trindle (159).

Urodacus novaehollandiae Peters, 1861: 1♀, Australia, South Australia, Aldinga Conservation Park, 35°17'S 138°28'E, 3–13.IV.1987; leg. E. G. Matthews (160, 398).



Figures 1–6. Clustered macrosetae on the external aspect of the pedipalp femur in the ‘Buthus’ group (Buthidae). **Figures 1–2.** *Buthacus nigroaculeatus*, male. **Figures 3–4.** *Leiurus haenggii*, male. **Figures 5–6.** *Olivierus martensii*, female. ECMS: external carinal macrosetal series. DEMC: distal external macrosetal cluster. Views of whole femur (1, 3, 5), and magnified views of DEMC (2, 4, 6). Scale bars: 2 mm (1, 3), 1 mm (2, 4–5), 500 μm (6). UV fluorescence.

Results

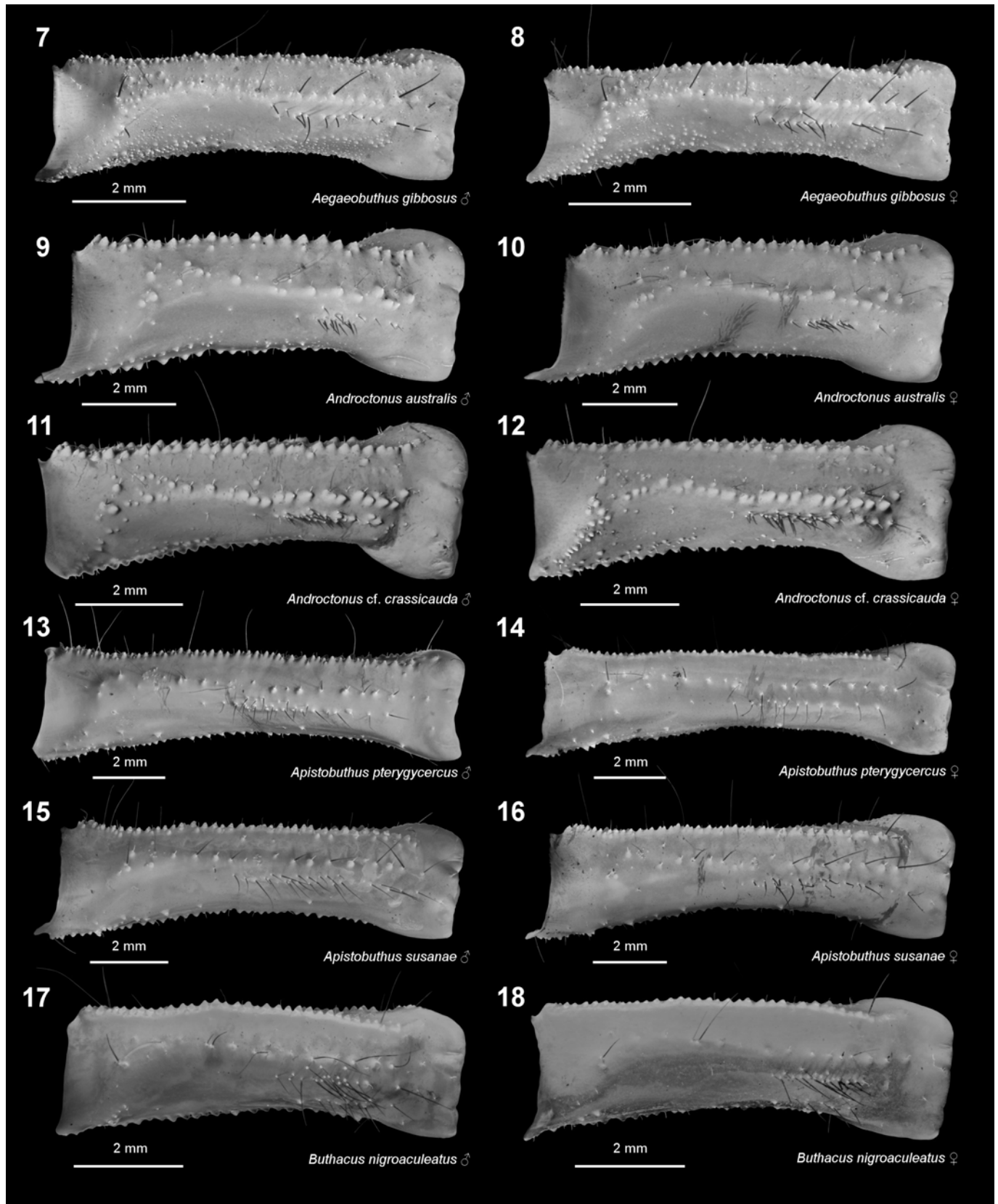
Patterns of macrosetae on the external surface of the pedipalp femur

We studied setation on the external femur by UV fluorescence imaging. Macrosetae were identified by their dark non-fluorescent shafts (Type N), which distinguished them from microsetae whose shafts were fluorescent (Type F) (Lowe & Fet, 2024). Figs. 1, 3 and 5 show external views of the femur of representative buthids belonging to the ‘Buthus’ group (Fet et al., 2005): *Buthacus nigroaculeatus*, *Leiurus haenggii*, and *Olivierus martensii*. Each femur bears two trichobothria, e_1 and e_2 , the orthobothriotaxic state in buthids. The external femoral surfaces are divided into upper and lower halves by an external median carina marked by granules. The carina begins near the base of the femur, at the edge of a large basal concavity that accommodates the trochanter. It runs longitudinally, slightly dorsal to median in the proximal half of the segment, before transitioning to a more median path in the distal half. At the transition point, the carina bends below trichobothrium e_2 , so that both trichobothria remain slightly dorsal to the carina. Setation is sparse along the carina, with only 2–5 non-clustered

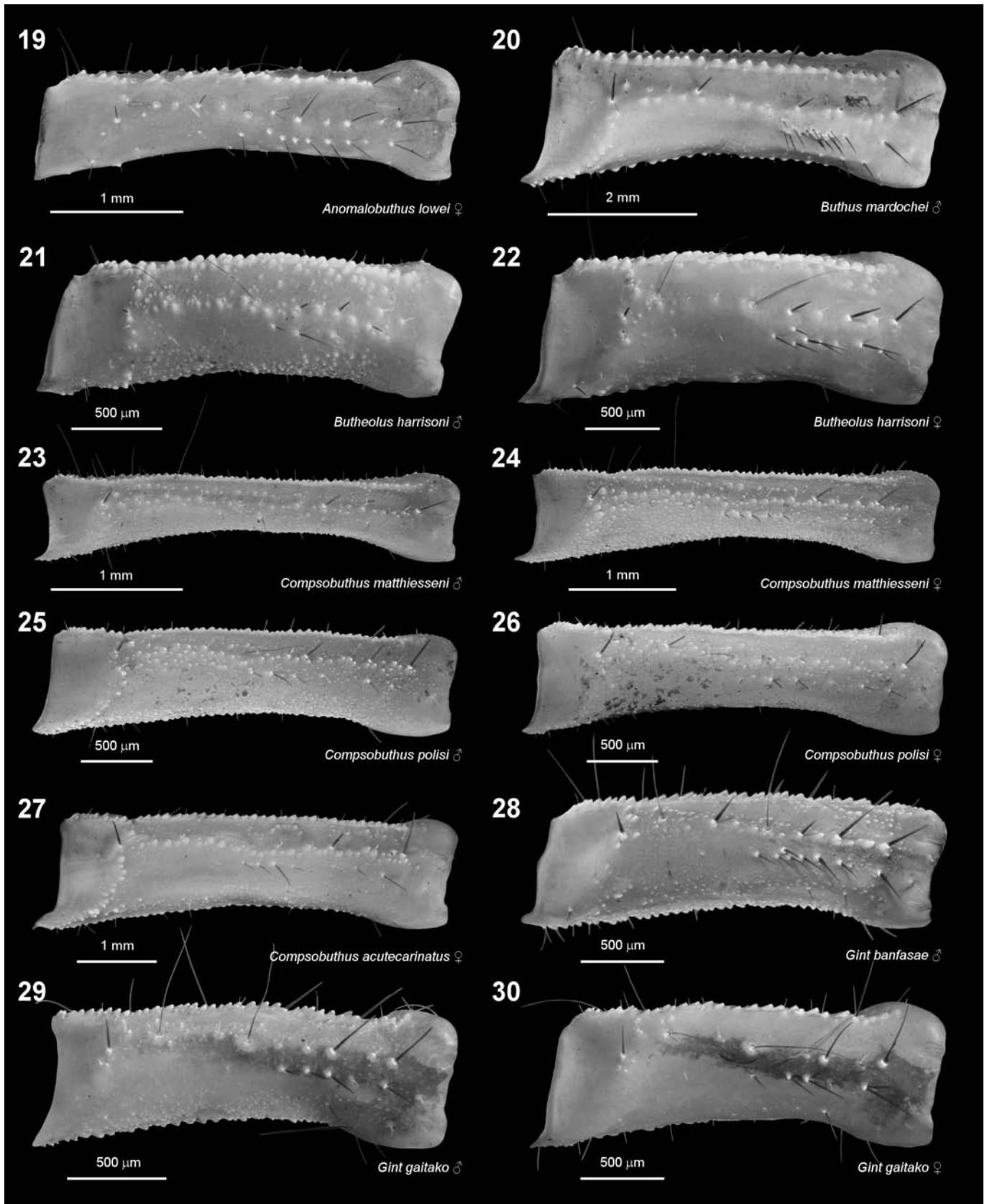
macrosetae, herein termed the ‘external carinal macrosetal series’ (ECMS). One macroseta is at the proximal limit of the carina where it is a convenient landmark. Most of the external femoral surface lacks macrosetae except for a narrow infracarinal strip in the distal half of the segment. The more proximal part of this strip is occupied by a dense, linear cluster of over a dozen macrosetae, herein termed the ‘distal external macrosetal cluster’ (DEMC). More distally, the setae become much sparser, and may be separated from the main cluster by a gap. However, such a gap was not always clear in other specimens, and for the purpose of enumeration, we defined the ‘DEMC’ to include all macrosetae in the distal ventral quadrant.

Does the distinctive setation pattern with a DEMC occur in other buthids, or other families? To address this, we examined the external femur of 85 species (40 genera) of buthids, and 35 species (29 genera) of non-buthids. We sampled all four major buthid lineages and 16 non-buthid families.

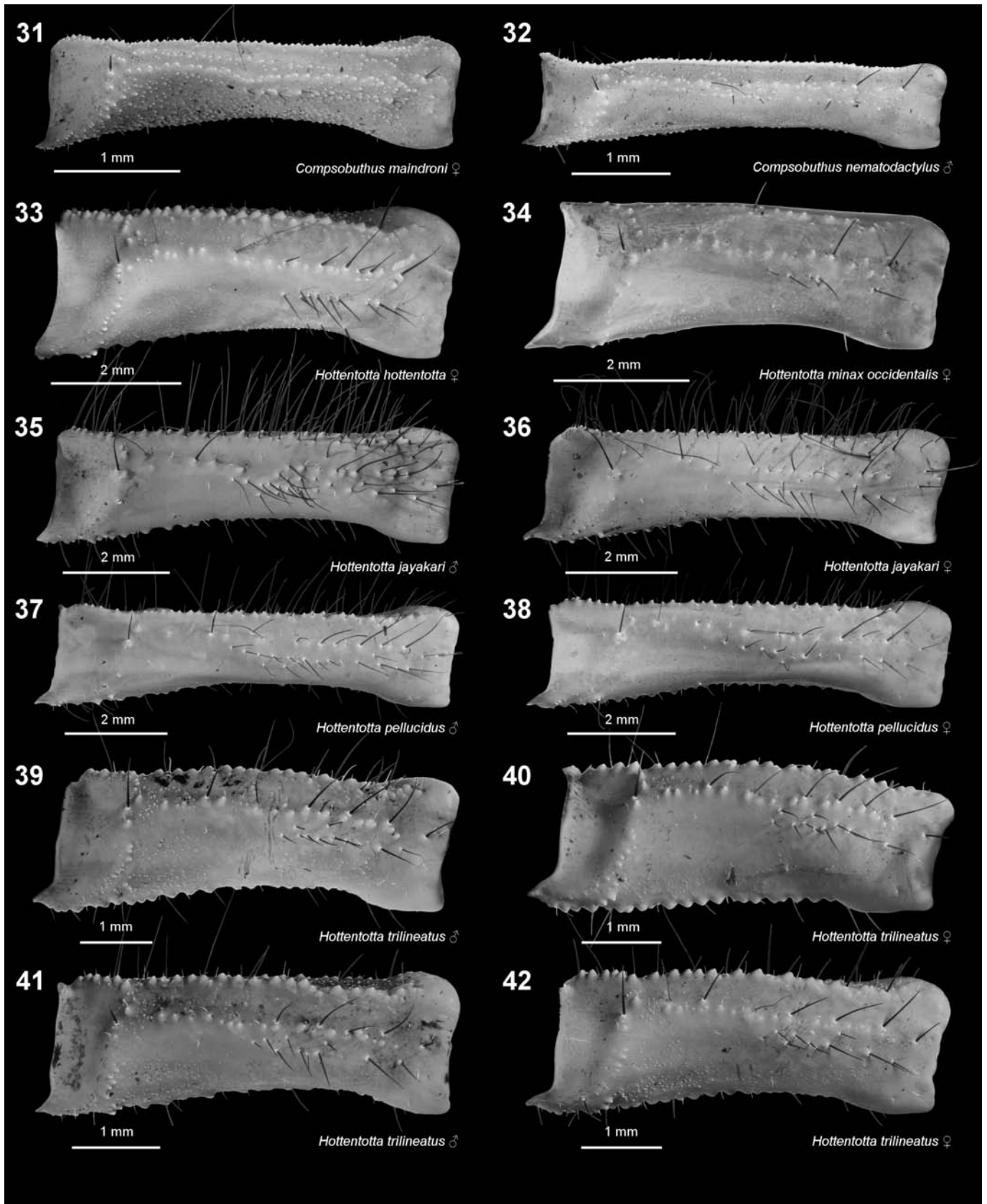
BUTHIDAE. BUTHUS GROUP (Figs. 1–88). *Aegaeobuthus gibbosus*, *Androctonus australis*, *Androctonus* cf. *crassicauda* (populations in Iran & Oman), *Anomalobuthus lowei*, *Apistobuthus pterygocercus*, *Apistobuthus susanae*, *Buthacus nigroaculeatus*, *Butheolus gallagheri*, *Butheolus harrisoni*, *Buthus mardochei*,



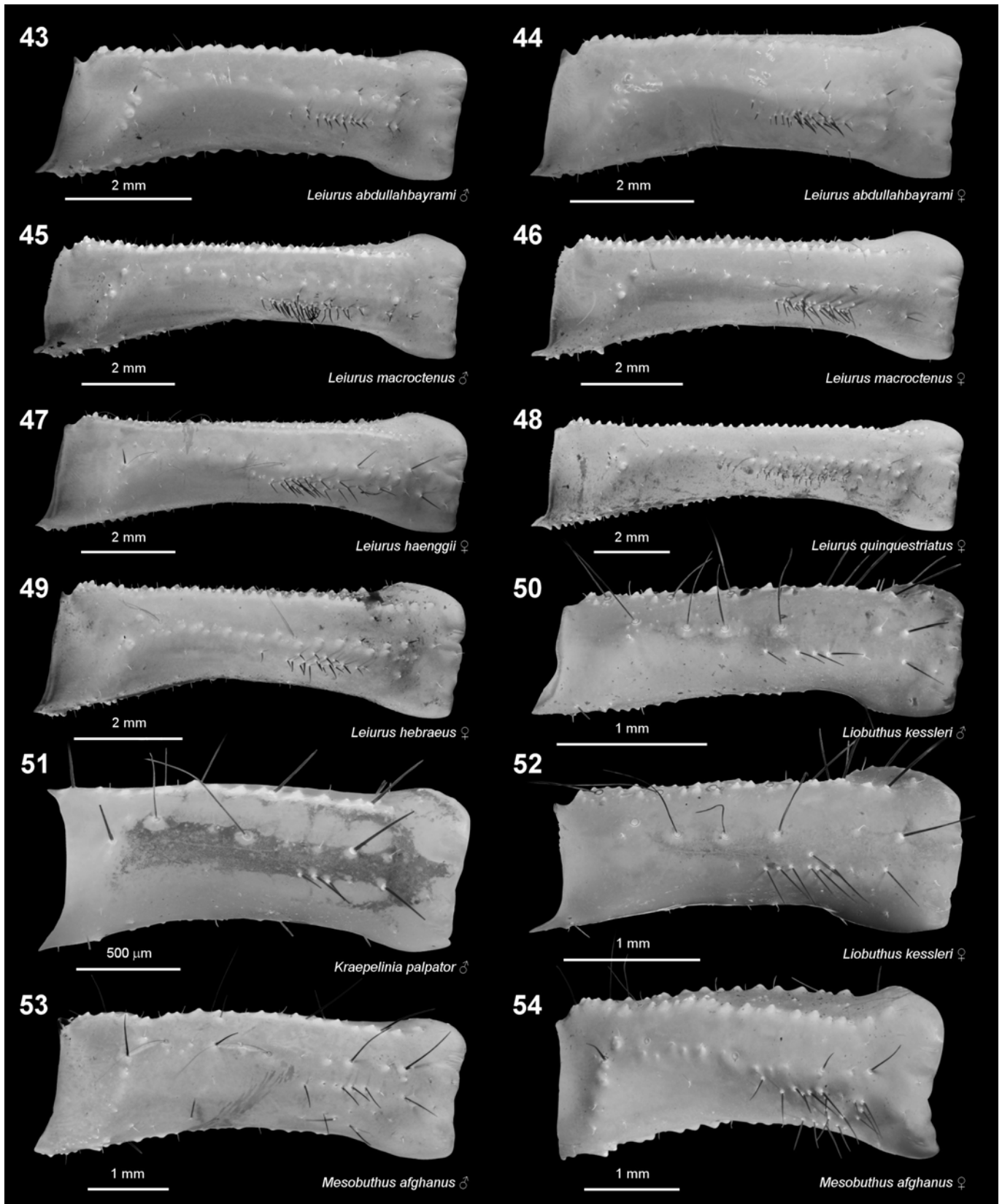
Figures 7–18. Pedipalp femur, external aspect. Buthidae, ‘Buthus’ group. **Figures 7–8.** *Aegaeobuthus gibbosus*, male (7) and female (8). **Figures 9–10.** *Androctonus australis*, male (9) and female (10). **Figures 11–12.** *Androctonus cf. crassicauda* (Iran), male (11) and female (12). **Figures 13–14.** *Apistobuthus pterygocercus*, male (13) and female (14). **Figures 15–16.** *Apistobuthus susanae*, male (15) and female (16). **Figures 17–18.** *Buthacus nigroaculeatus*, male (17) and female (18). Scale bars: 2 mm. UV fluorescence.



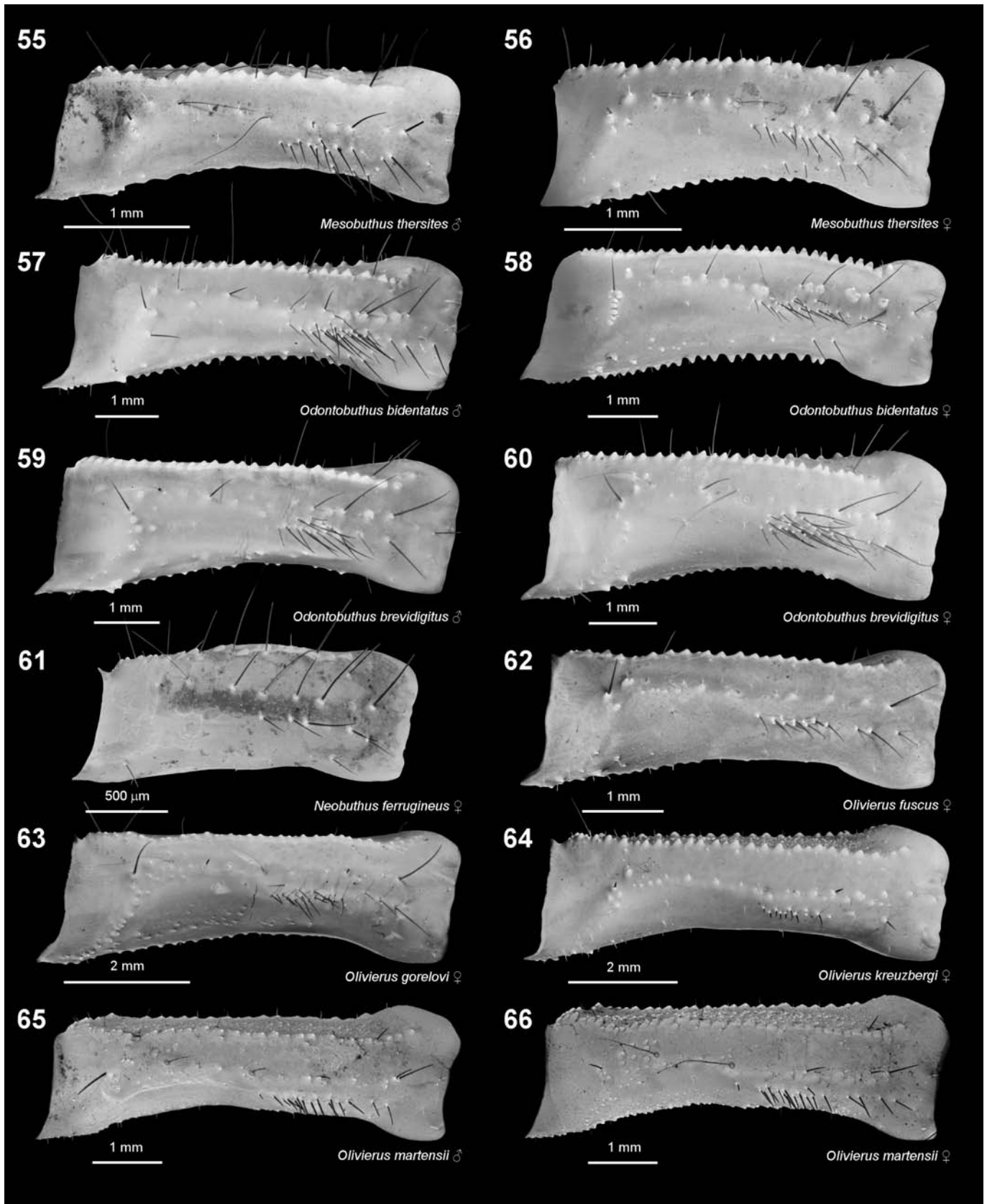
Figures 19–30. Pedipalp femur, external aspect. Buthidae, ‘Buthus’ group. **Figure 19.** *Anomalobuthus lowei*, female. **Figure 20.** *Buthus mardochei*, male. **Figures 21–22.** *Butheolus harrisoni*, male (21) and female (22). **Figures 23–24.** *Compsobuthus matthiesseni*, male (23) and female (24). **Figures 25–26.** *Compsobuthus polisi*, male (25) and female (26). **Figure 27.** *Compsobuthus acutecarinatus*, female. **Figure 28.** *Gint banfasae*, male. **Figures 29–30.** *Gint gaitako*, male (29) and female (30). Scale bars: 2 mm (20), 1 mm (19, 23–24, 27), 500 μm (21–22, 25–26, 28–30). UV fluorescence.



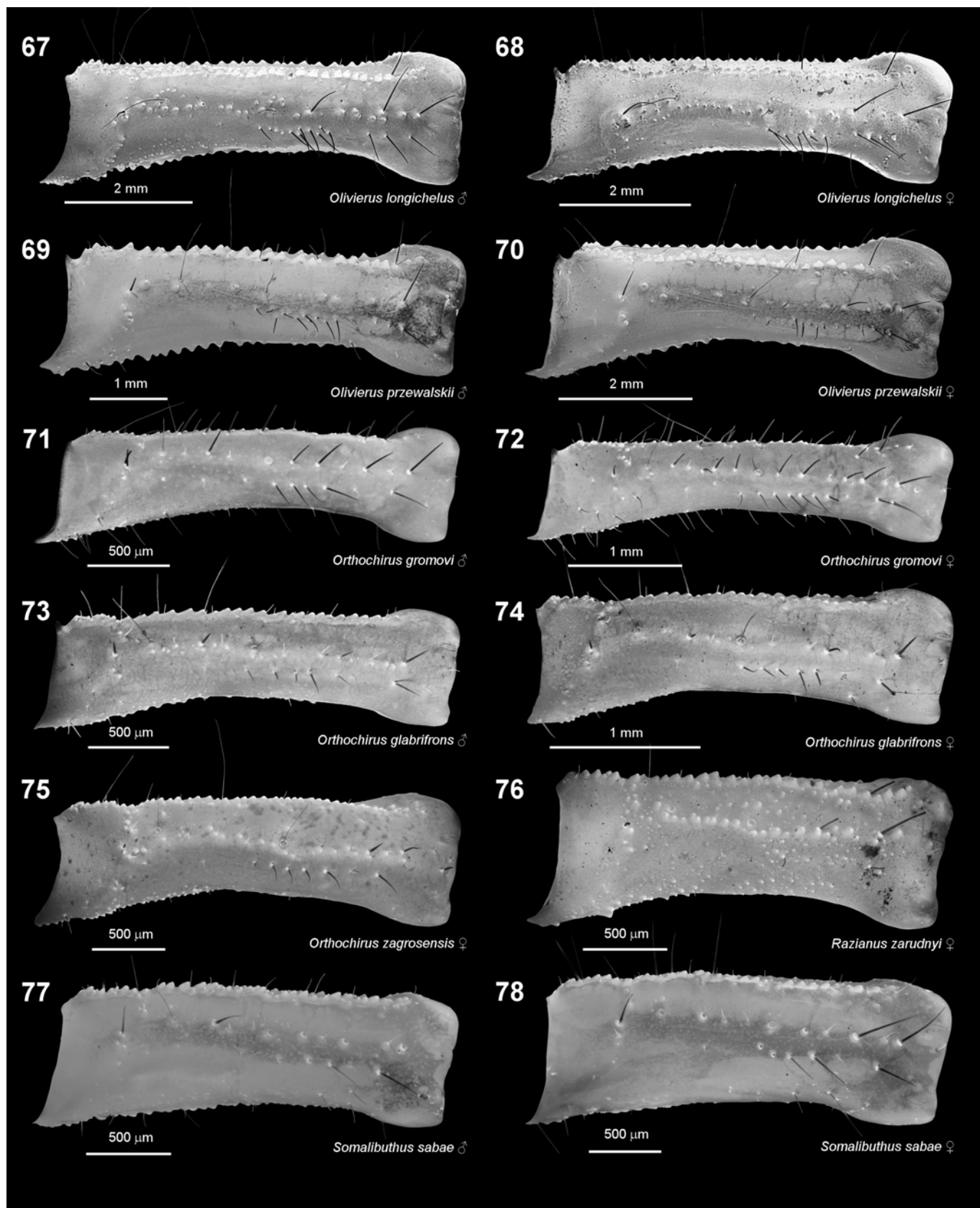
Figures 31–42. Pedipalp femur, external aspect. Buthidae, ‘Buthus’ group. **Figure 31.** *Compsobuthus maindroni*, female. **Figure 32.** *Compsobuthus nematodactylus*, male. **Figure 33.** *Hottentotta hottentotta*, female. **Figure 34.** *Hottentotta minax occidentalis*, female. **Figures 35–36.** *Hottentotta jayakari*, male (35) and female (36). **Figures 37–38.** *Hottentotta pellucidus*, male (37) and female (38). **Figures 39–42.** *Hottentotta trilineatus*, male (39, 41) and female (40, 42). Scale bars: 2 mm (33–38), 1 mm (31–32, 39–42). UV fluorescence.



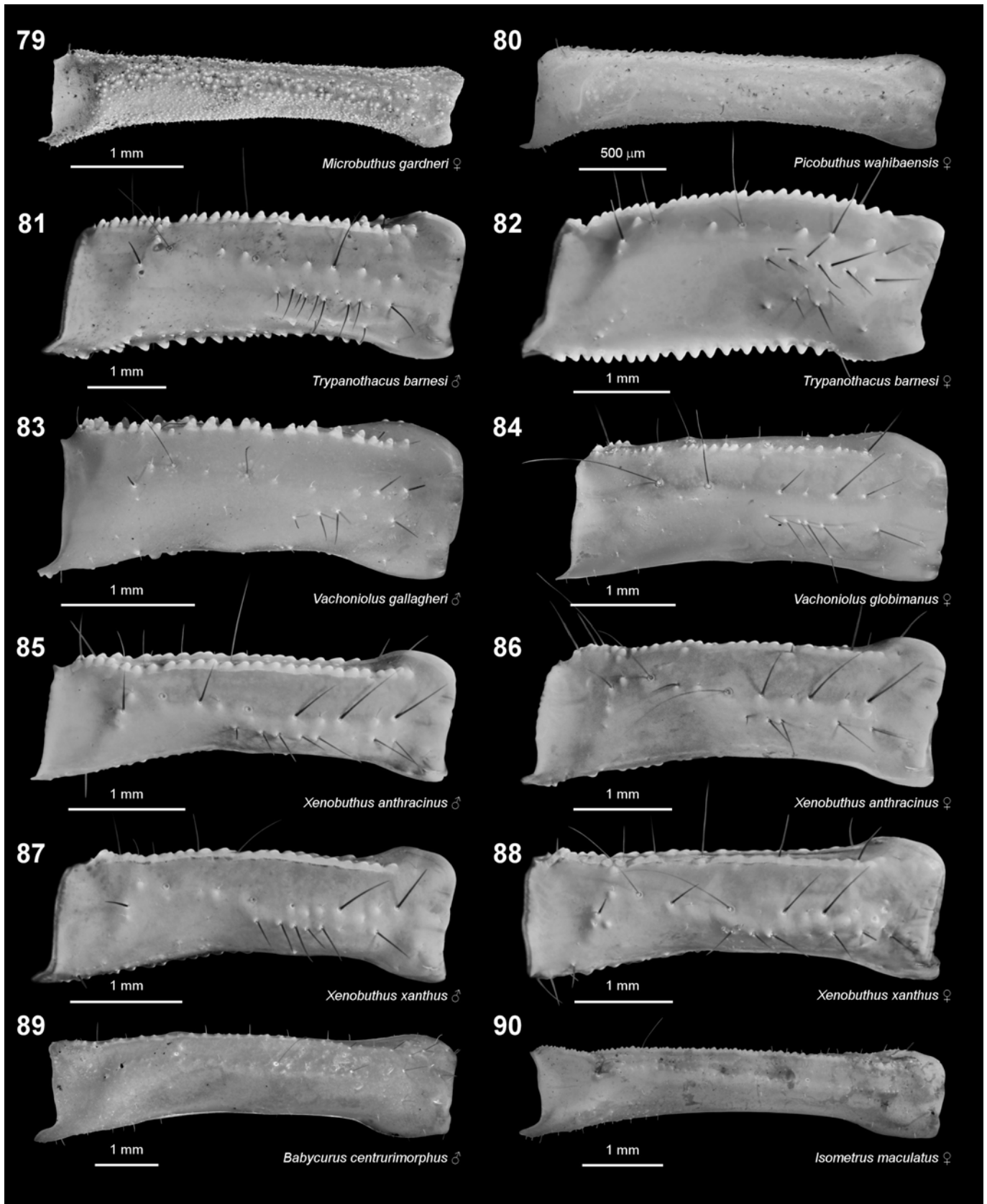
Figures 43–54. Pedipalp femur, external aspect. Buthidae, ‘Buthus’ group. **Figures 43–44.** *Leiurus abduallahbayrami*, male (43) and female (44). **Figures 45–46.** *Leiurus macroctenus*, male (45) and female (46). **Figure 47.** *Leiurus haenggii*, female. **Figure 48.** *Leiurus quinquestriatus*, female. **Figure 49.** *Leiurus hebraeus*, female. **Figures 50, 52.** *Liobuthus kessleri*, male (50) and female (52). **Figure 51.** *Kraepelinia palpator*, male. **Figures 53–54.** *Mesobuthus afghanus*, male (53) and female (54). Scale bars: 2 mm (43–49), 1 mm (50, 52–54), 500 µm (51). UV fluorescence.



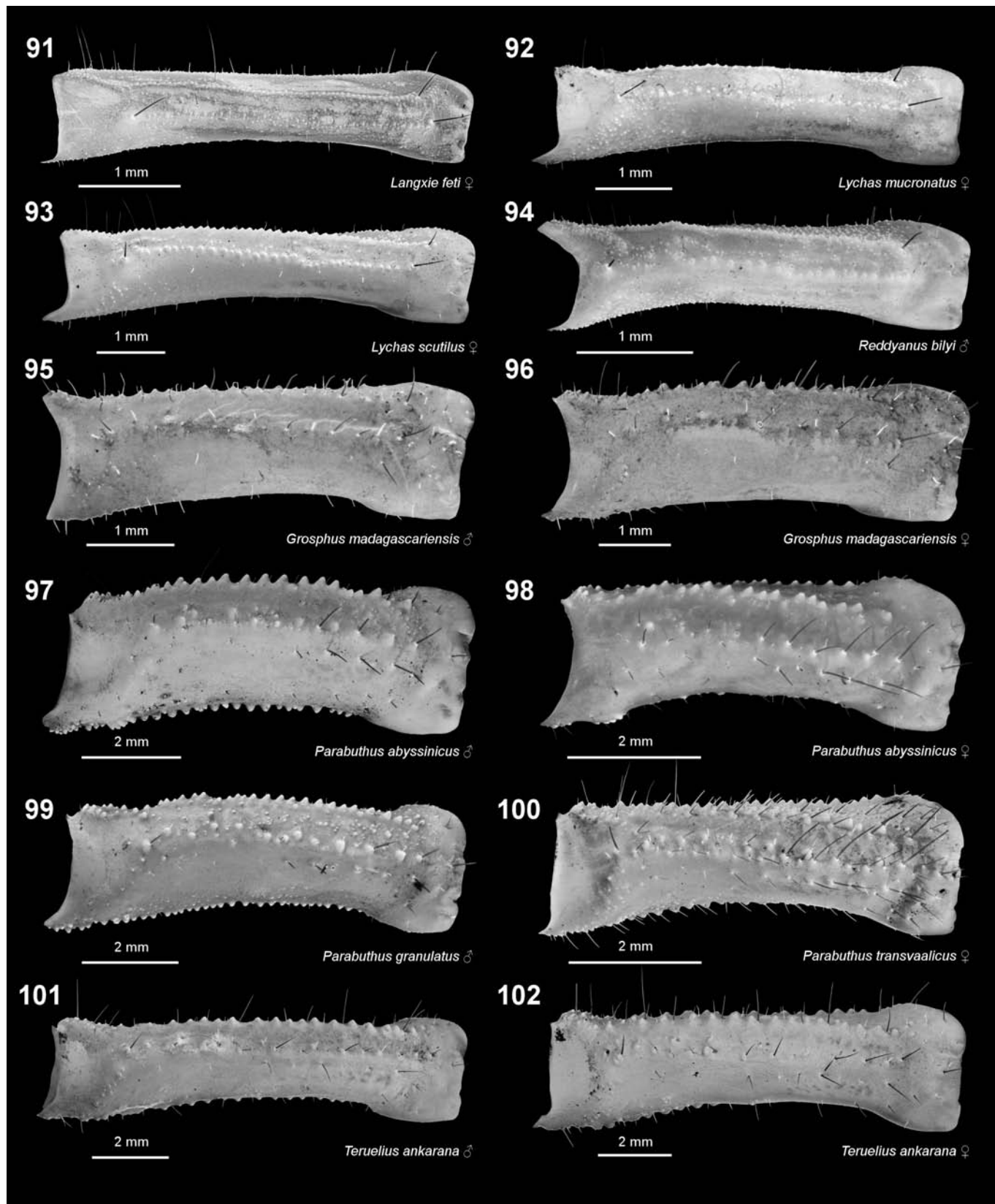
Figures 55–66. Pedipalp femur, external aspect. Buthidae, ‘Buthus’ group. **Figures 55–56.** *Mesobuthus thersites*, male (55) and female (56). **Figures 57–58.** *Odontobuthus bidentatus*, male (57) and female (58). **Figures 59–60.** *Odontobuthus brevidigitus*, male (59) and female (60). **Figure 61.** *Neobuthus ferrugineus*, female. **Figure 62.** *Olivierus fuscus*, female. **Figure 63.** *Olivierus gorelovi*, female. **Figure 64.** *Olivierus kreuzbergi*, female. **Figures 65–66.** *Olivierus martensii*, male (65) and female (66). Scale bars: 2 mm (63–64), 1 mm (55–60, 62, 65–66), 500 μm (61). UV fluorescence.



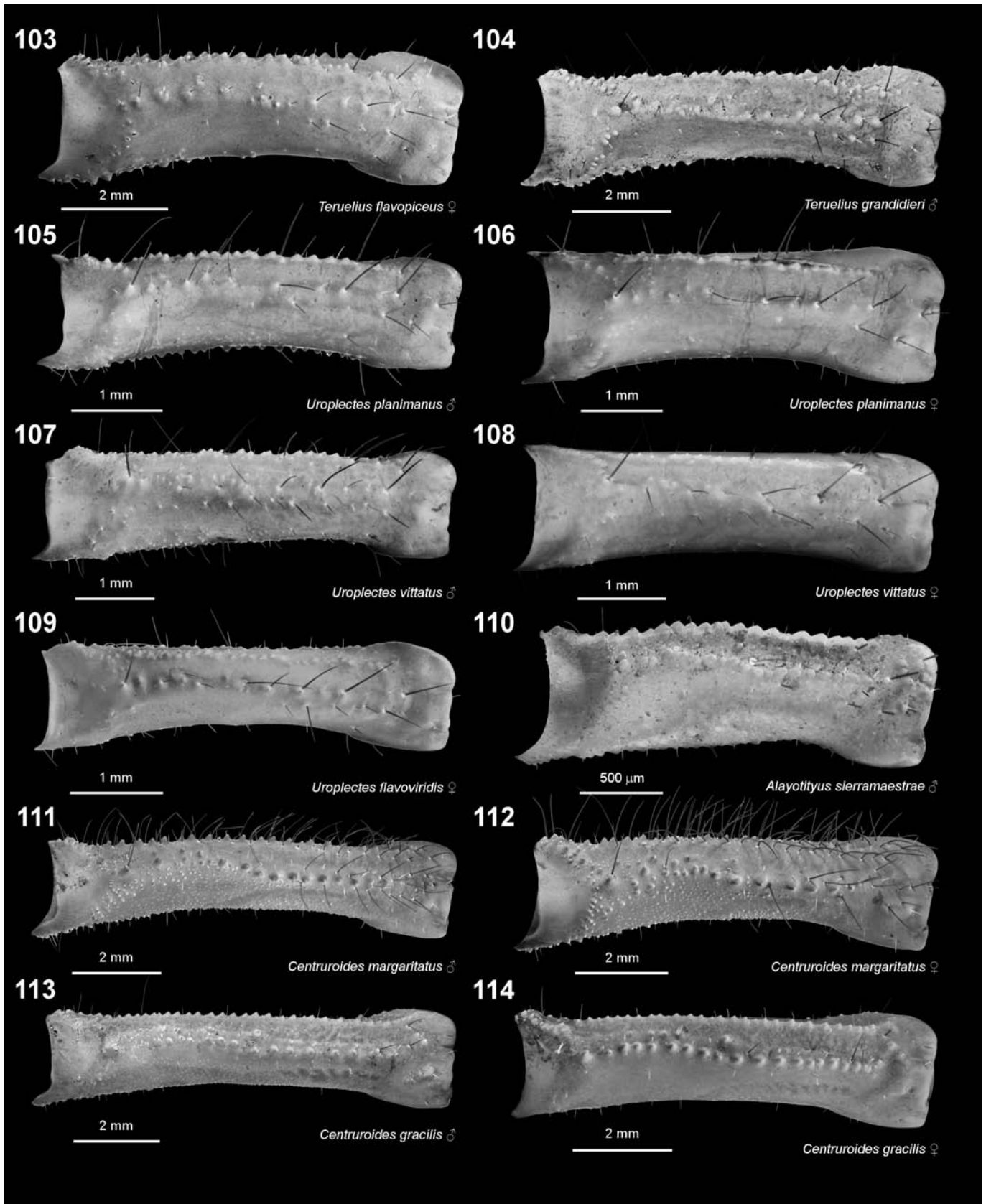
Figures 67–78. Pedipal femur, external aspect. Buthidae, ‘Buthus’ group. **Figures 67–68.** *Olivierus longichelus*, male (67) and female (68). **Figures 69–70.** *Olivierus przewalskii*, male (69) and female (70). **Figures 71–72.** *Orthochirus gromovi*, male (71) and female (72). **Figures 73–74.** *Orthochirus glabrifrons*, male (73) and female (74). **Figure 75.** *Orthochirus zagrosensis*, female. **Figure 76.** *Razianus zarudnyi*, female. **Figures 77–78.** *Somalibuthus sabae*, male (77) and female (78). Scale bars: 2 mm (67–68, 70), 1 mm (69, 72, 74), 500 μm (71, 73, 75–78). UV fluorescence.



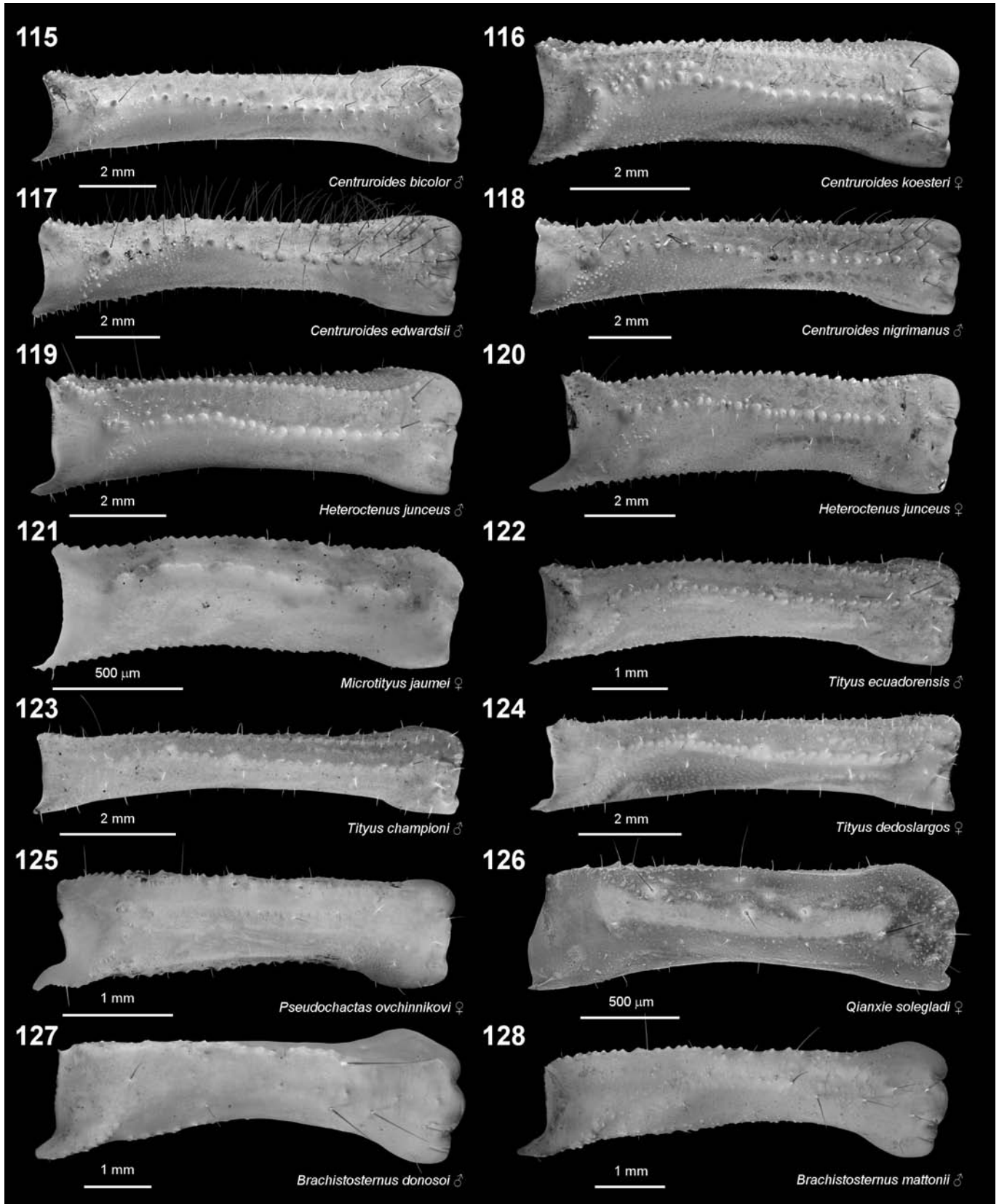
Figures 79–90. Pedipalp femur, external aspect. Buthidae, ‘Buthus’ group (79–88) and ‘Ananteris–Isometrus’ group (89–90). **Figure 79.** *Microbuthus gardneri*, female. **Figure 80.** *Picobuthus wahibaensis*, female. **Figures 81–82.** *Trypanothacus barnesi*, male (81) and female (82). **Figure 83.** *Vachoniolus gallagheri*, male. **Figure 84.** *Vachoniolus globimanus*, female. **Figures 85–86.** *Xenobuthus anthracinus*, male (85) and female (86). **Figures 87–88.** *Trypanothacus barnesi*, male (87) and female (88). **Figure 89.** *Babycurus centrurimorphus*, male. **Figure 90.** *Isometrus maculatus*, female. Scale bars: 1 mm (79, 81–90), 500 µm (80). UV fluorescence.



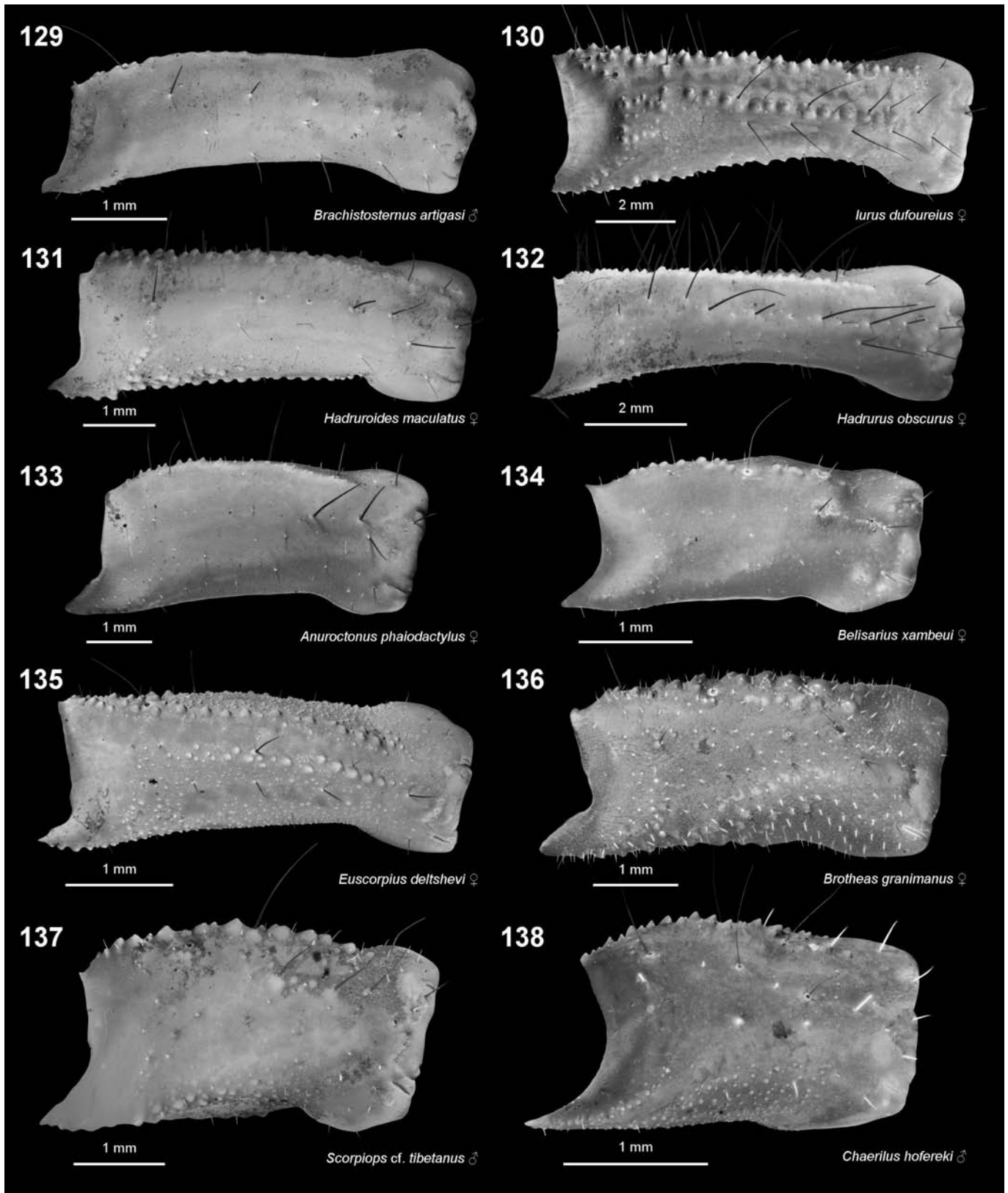
Figures 91–102. Pedipalp femur, external aspect. Buthidae, ‘Ananteris–Isometrus’ group (91–94) and ‘Charmus–Uroplectes’ group (95–102). **Figure 91.** *Langxie feti*, female. **Figure 92.** *Lychas mucronatus*, female. **Figure 93.** *Lychas scutillus*, female. **Figure 94.** *Reddyanus bilyi*, male. **Figures 95–96.** *Grosphus madagascariensis*, male (95) and female (96). **Figures 97–98.** *Parabuthus abyssinicus*, male (97) and female (98). **Figure 99.** *Parabuthus granulatus*, male. **Figure 100.** *Parabuthus transvaalicus*, female. **Figures 101–102.** *Teruelius ankarana*, male (101) and female (102). Scale bars: 2 mm (97–102), 1 mm (91–96). UV fluorescence.



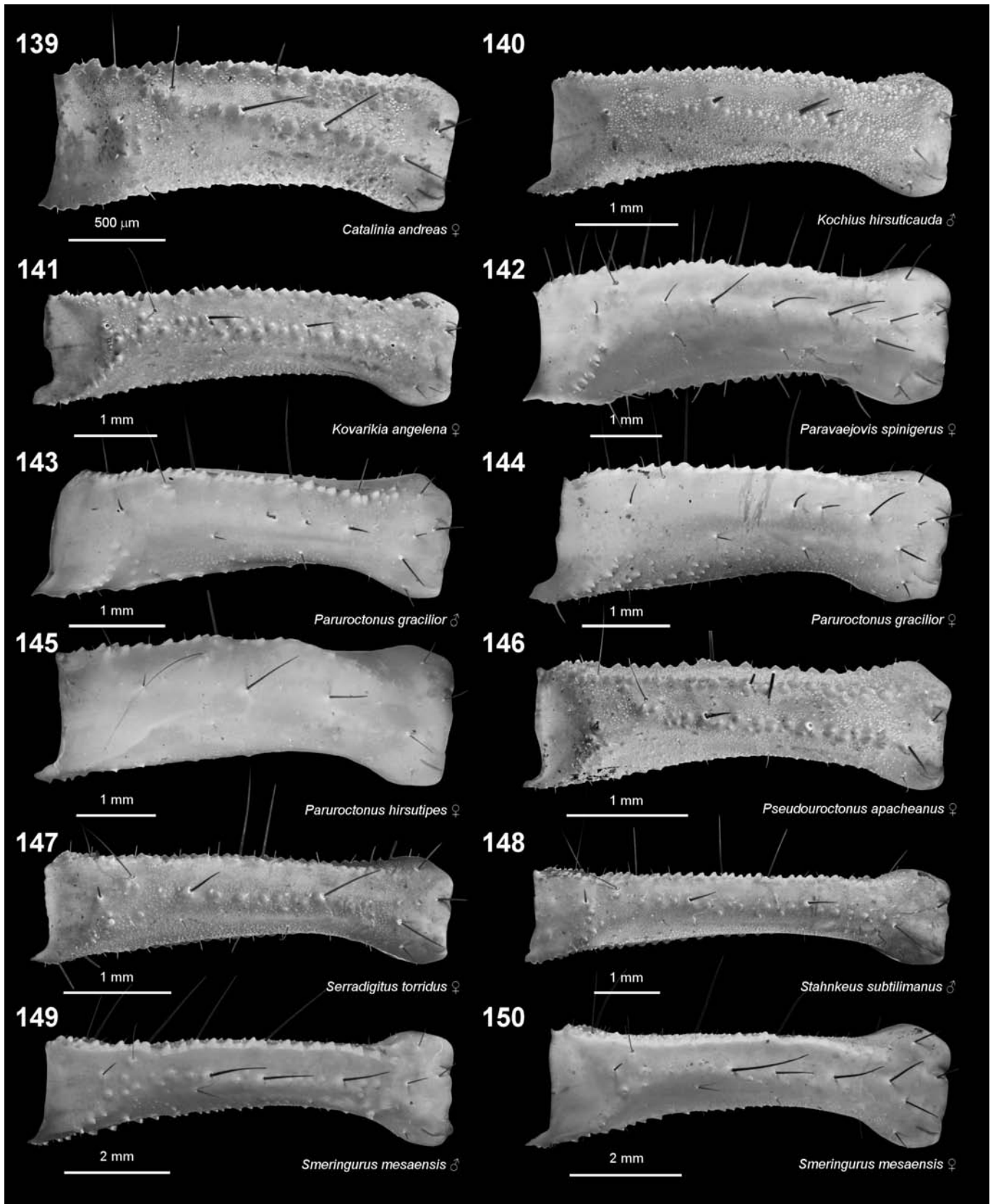
Figures 103–114. Pedipalp femur, external aspect. Buthidae, ‘Charmus–Uroplectes’ group (103–109) and ‘Tityus’ group (110–114). **Figure 103.** *Teruelius flavopiceus*, female. **Figure 104.** *Teruelius grandidieri*, female. **Figures 105–106.** *Uroplectes planimanus*, male (105) and female (106). **Figures 107–108.** *Uroplectes vittatus*, male (107) and female (108). **Figure 109.** *Uroplectes flavoviridis*, female. **Figure 110.** *Alayotityus sierramaestrae*, male. **Figures 111–112.** *Centruroides margaritatus*, male (111) and female (112). **Figures 113–114.** *Centruroides gracilis*, male (113) and female (114). Scale bars: 2 mm (103–104, 111–114), 1 mm (105–109), 500 μm (110). UV fluorescence.



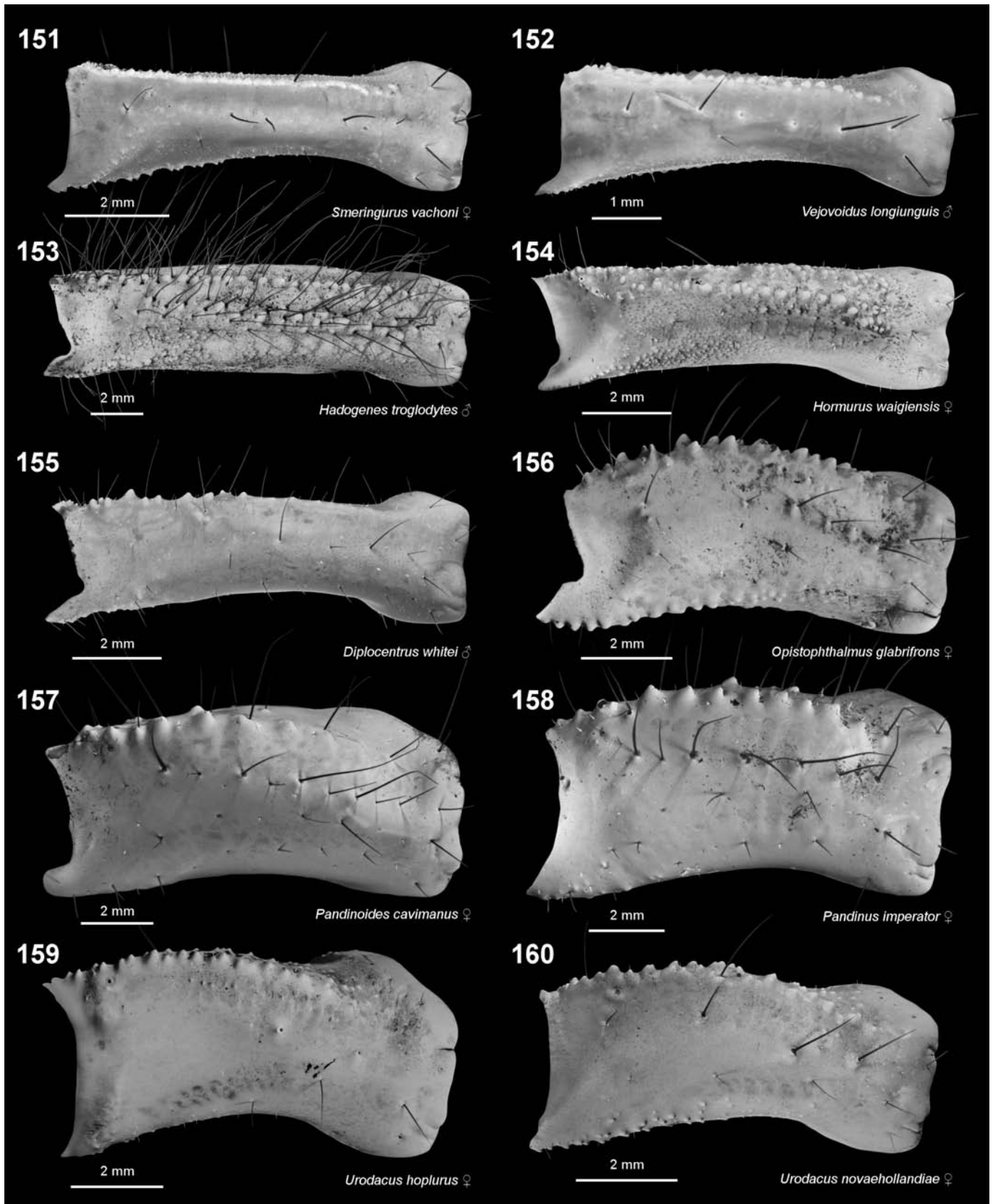
Figures 115–128. Pedipalp femur, external aspect. Buthidae, ‘Tityus’ group (115–124); Pseudochactidae (125–126); and Bothriuridae (127–128). **Figure 115.** *Centruroides bicolor*, male. **Figure 116.** *Centruroides koesteri*, female. **Figure 117.** *Centruroides edwardsii*, male. **Figure 118.** *Centruroides nigrimanus*, male. **Figures 119–120.** *Heteroctenus junceus*, male (119) and female (120). **Figure 121.** *Microtityus jaumei*, female. **Figure 122.** *Tityus ecuadorensis*, male. **Figure 123.** *Tityus championi*, male. **Figure 124.** *Tityus dedoslargos*, female. **Figure 125.** *Pseudochactas ovchinnikovi*, female. **Figure 126.** *Qianxie solegladi*, female. **Figure 127.** *Brachistosternus donosoi*, male. **Figure 128.** *Brachistosternus mattonii*, male. Scale bars: 2 mm (115–120, 123–124), 1 mm (122, 125, 127–128), 500 µm (121, 126). UV fluorescence.



Figures 129–138. Pedipalp femur, external aspect. Bothriuridae (129); Iuridae (130); Caraboctonidae (131); Hadruridae (132); Anuroctonidae (133); Belisariidae (134); Euscorpiidae (135); Chactidae (136); Scorpipidae (137); and Chaerilidae (138). **Figure 129.** *Brachistosternus artigasi*, male. **Figure 130.** *Iurus dufourei*, female. **Figure 131.** *Hadrurides maculatus*, female. **Figure 132.** *Hadrurus obscurus*, female. **Figure 133.** *Anuroctonus phaiodactylus*, female. **Figure 134.** *Belisarius xambeui*, female. **Figure 135.** *Euscorpius deltshevi*, female. **Figure 136.** *Brotheas granimanus*, female. **Figure 137.** *Scorpiops cf. tibetanus*, male. **Figure 138.** *Chaerilus hofereki*, male. Scale bars: 2 mm (130, 132), 1 mm (129, 131, 133–138). UV fluorescence.



Figures 139–150. Pedipalp femur, external aspect. Vaejovidae. **Figure 139.** *Catalinia andreas*, female. **Figure 140.** *Kochius hirsuticauda*, male. **Figure 141.** *Kovarikia angelena*, female. **Figure 142.** *Paravaejovis spinigerus*, female. **Figures 143–144.** *Paruroctonus gracilior*, male (143) and female (144). **Figure 145.** *Paruroctonus hirsutipes*, female. **Figure 146.** *Pseudouroctonus apacheanus*, female. **Figure 147.** *Serradigitus torridus*, female. **Figure 148.** *Stahnkeus subtilimanus*, male. **Figures 149–150.** *Smeringurus mesaensis*, male (149) and female (150). Scale bars: 2 mm (149–150), 1 mm (140–148), 500 μm (139). UV fluorescence.



Figures 151–160. Pedipalp femur, external aspect. Vaejovidae (151–152); Hormuridae (153–154); Diplocentridae (155); Scorpionidae (156–158); and Urodacidae (159–160). **Figure 151.** *Smeringurus vachoni*, female. **Figure 152.** *Vejovoidus longiunguis*, male. **Figure 153.** *Hadogenes troglodytes*, male. **Figure 154.** *Hormurus waigiensis*, female. **Figure 155.** *Diplocentrus whitei*, male. **Figure 156.** *Opisththalmus glabrifrons*, female. **Figure 157.** *Pandinoides cavimanus*, female. **Figure 158.** *Pandinus imperator*, female. **Figure 159.** *Urodacus hophilurus*, female. **Figure 160.** *Urodacus novaehollandiae*, female. Scale bars: 2 mm (151, 153–160), 1 mm (152). UV fluorescence.

Compsobuthus acutecarinatus, *Compsobuthus levyi*, *Compsobuthus maindroni*, *Compsobuthus matthiesseni*, *Compsobuthus nematodactylus*, *Compsobuthus polisi*, *Gint banfasae*, *Gint gaitako*, *Hottentotta hottentotta*, *Hottentotta jayakari*, *Hottentotta minax occidentalis*, *Hottentotta pellucidus*, *Hottentotta rugiscutis*, *Hottentotta saxinatans*, *Hottentotta trilineatus*, *Kraepelinia palpator*, *Leiurus abdullahbayrami*, *Leiurus haenggii*, *Leiurus hebraeus*, *Leiurus macroctenus*, *Leiurus quinquestriatus*, *Liobuthus kessleri*, *Mesobuthus afghanus*, *Mesobuthus thersites*, *Microbuthus gardneri*, *Neobuthus amoudensis*, *Neobuthus ferrugineus*, *Odontobuthus bidentatus*, *Odontobuthus brevidigitus*, *Olivierus fuscus*, *Olivierus gorelovi*, *Olivierus kreuzbergi*, *Olivierus longichelus*, *Olivierus martensii*, *Olivierus przewalskii*, *Orthochirus glabrifrons*, *Orthochirus gromovi*, *Orthochirus zagrosensis*, *Picobuthus wahibaensis*, *Razianus zarudnyi*, *Somalibuthus sabae*, *Trypanothacus barnesi*, *Vachoniolus gallagheri*, *Vachoniolus globimanus*, *Xenobuthus anthracinus*, and *Xenobuthus xanthus*: external median carina sparsely setose, bearing < 10 relatively long ECMS setae; proximal landmark seta present; in *Microbuthus* and *Picobuthus*, ECMS setae small, clavate, barely discernible; DEMC present as a dense, linear series (ca. 10–35 setae) in: *Aegaeobuthus*, *Androctonus*, *Apistobuthus*, *Buthacus*, *Buthus*, *Gint*, *Hottentotta*, *Kraepelinia*, *Leiurus*, *Liobuthus*, *Mesobuthus*, *Odontobuthus*, *Olivierus*, and *Trypanothacus*; two-tiered in *Hottentotta hottentotta*, *Mesobuthus afghanus*. *M. thersites* and *Odontobuthus bidentatus* (Figs. 33, 53–58), with sparser secondary series of macrosetae below denser main series; DEMC present as a sparse linear series (ca. 2–9 setae) in: *Anomalobuthus*, *Butheolus*, *Compsobuthus*, *Neobuthus*, *Orthochirus*, *Razianus*, *Somalibuthus*, and *Xenobuthus*; DEMC absent in *Microbuthus* and *Picobuthus*; DEMC setae usually shorter than ECMS setae, but of similar length in a few cases (e.g., *Anomalobuthus*, and some *Hottentotta*, *Mesobuthus* and *Odontobuthus*); other external surfaces lack macrosetae.

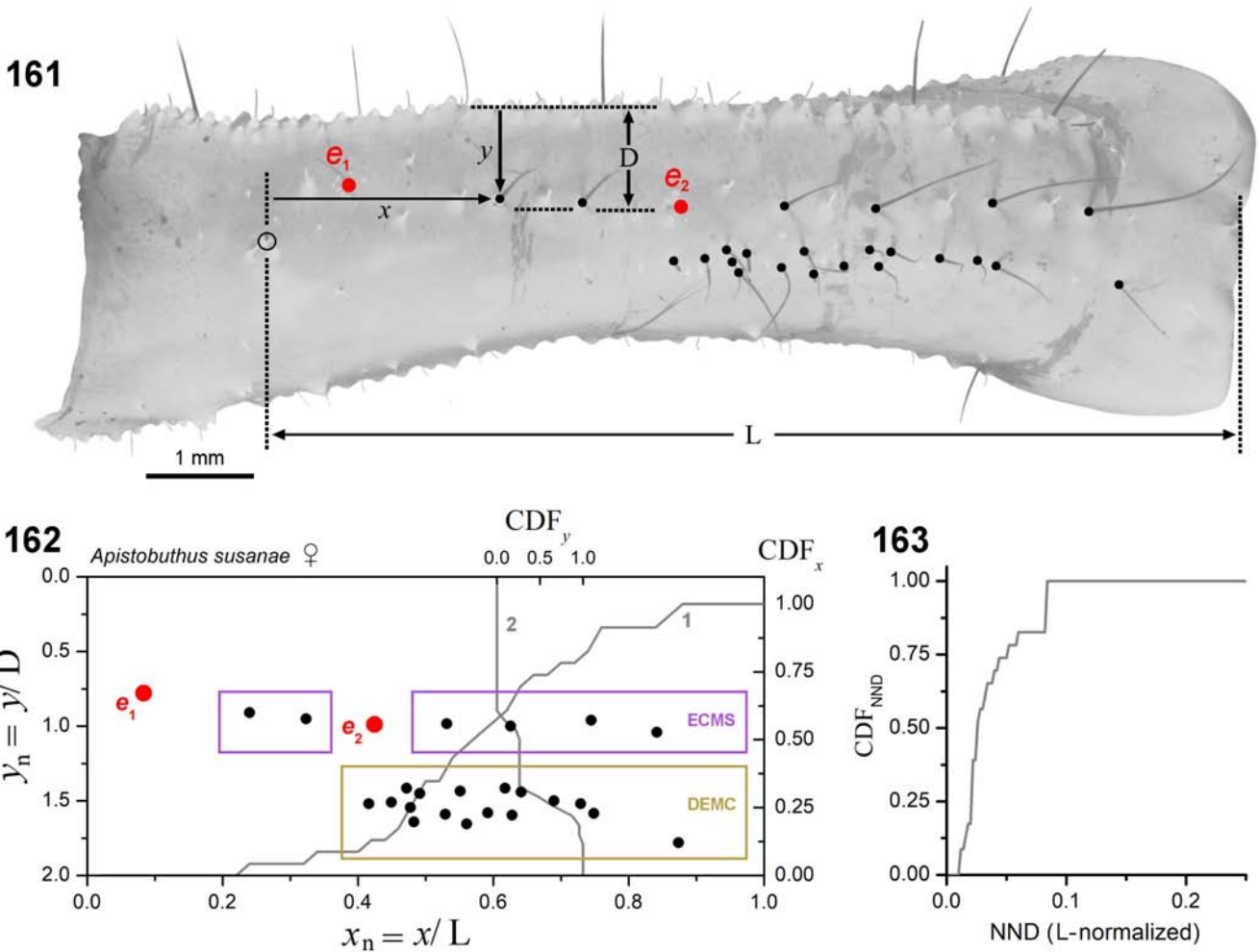
BUTHIDAE. ANANTERIS-ISOMETRUS GROUP (Figs. 89–94). *Babycurus centrurimorphus*, *Isometroides vesus*, *Isometrus maculatus*, *Langxie feti*, *Lychas mucronatus*, *Lychas scutillus*, and *Reddyanus bilyi*: external femur almost devoid of macrosetae; external median carina with only 1–2 macrosetae, including proximal landmark macroseta; DEMC absent.

BUTHIDAE. CHARMUS-UROPLECTES GROUP (Figs. 95–109). *Grosphus madagascariensis*, *Parabuthus abyssinicus*, *Parabuthus granulatus*, *Parabuthus transvaalicus*, *Teruelius ankarana*, *Teruelius flavopiceus*, *Teruelius grandidieri*, *Uroplectes flavoviridis*, *Uroplectes planimanus*, and *Uroplectes vittatus*: ECMS sparse, with < 10 macrosetae, setae longer in distal half of femur; DEMC sparse, not denser than ECMS, absent in *Grosphus madagascariensis* (Figs. 95–96); DEMC denser in *Parabuthus transvaalicus* (14 setae; Fig. 100); other external areas lack macrosetae.

BUTHIDAE. TITYUS GROUP (Figs. 110–124). *Alayotityus sierramaestrae*, *Centruroides bicolor*, *Centruroides edwardsii*, *Centruroides gracilis*, *Centruroides koesteri*, *Centruroides margaritatus*, *Centruroides nigrimanus*, *Heteroctenus junceus*, *Microtityus jaumei*, *Tityus championi*, *Tityus dedoslargos*, and *Tityus ecuadorensis*: ECMS sparse, with < 10 macrosetae; DEMC absent except in pilose *Centruroides*, i.e., *C. margaritatus* (male with 9 setae, female 4 setae; Figs. 111–112), *C. edwardsii* (5 setae; Fig. 117), and sparse in *Alayotityus* (3 setae, with truncate tips typical of the genus; Fig. 110); other external areas lack macrosetae, except in *C. margaritatus* and *C. edwardsii*, which bear additional distal, supracarinal macrosetae that may be viewed as extensions of macrosetal series on the dorsoexternal carina.

NON-BUTHIDS (Figs. 125–160). **CHAERILIDAE:** *Chaerilus hofereki*; **PSEUDOCHACTIDAE:** *Pseudochactas ovchinnikovi* and *Qianxie solegladi*; **BOTHRIURIDAE:** *Brachistosternus artigasi*, *Brachistosternus donosoi*, and *Brachistosternus mattonii*; **ANUROCTONIDAE:** *Anuroctonus phaiodactylus*; **BELISARIIDAE:** *Belisarius xambeui*; **CHACTIDAE:** *Brotheas gervaisii* and *Brotheas granimanus*; **EUSCORPIIDAE:** *Euscorpium deltshevi*; **CARABOCTONIDAE:** *Hadrurides maculatus*; **HADRURIDAE:** *Hadrurus obscurus*; **IURIDAE:** *Iurus dufourei*; **SCORPIOPIDAE:** *Scorpiops cf. tibetanus*; **VAEJOVIDAE:** *Catalinia andreas*, *Kochius hirsuticauda*, *Kovarikia angelena*, *Paravaejovis spinigerus*, *Paruroctonus gracilior*, *Paruroctonus hirsutipes*, *Pseudouroctonus apacheanus*, *Serradigitus torridus*, *Smeringurus mesaensis*, *Smeringurus vachoni*, *Stahnkeus subtilimanus*, and *Vejovoides longiunguis*; **HORMURIDAE:** *Hadogenes troglodytes* and *Hormurus waigiensis*; **DIPLOCENTRIDAE:** *Diplocentrus whitei*; **SCORPIONIDAE:** *Opisthophthalmus glabrifrons*, *Pandinoides cavimanus* and *Pandinus imperator*; **URODACIDAE:** *Urodacus hoplurus* and *Urodacus novaehollandiae*: external femoral setation generally sparse to very sparse in most taxa; external median carina variably developed, ranging from strong and granulate to obsolete; ECMS mostly sparse, with < 10 long, regular setae; DEMC absent, or distal infracarinal area with a few scattered setae (e.g., *Iurus dufourei*, Fig. 130; *Paruroctonus gracilior*, Figs. 143–144; *Pandinoides cavimanus*, Fig. 157); an exception was the heavily pilose species, *Hadogenes troglodytes*, with numerous long macrosetae arrayed on and around the external median carina, including distal infracarinal setae not classified as DEMC (Fig. 153).

In summary, the pattern of setation with DEMC was prevalent among buthids of the ‘Buthus’ group. The DEMC was generally denser and more compact in the larger species of the group, and sparser and more dispersed in the smaller species. In the very small picobuthoids (*Microbuthus* and *Picobuthus*), it was absent. Most species belonging to other major buthid lineages lacked a DEMC, with the exception of some *Parabuthus*, *Teruelius*, *Uroplectes* and *Centruroides*. In those genera, it was sparse and less compact than in the ‘Buthus’ group. In non-buthids, the DEMC was absent.



Figures 161–163. Measurement and analysis of spatial patterns of macrosetae and trichobothria distributed on the external surface of the pedipalp femur. **Figure 161.** External aspect of pedipalp femur of *Apistobuthus susanae* (Buthidae). Black-filled circles: position markers of macrosetal sockets; open circle: position marker of socket of proximal landmark macroseta at proximal terminus of external median carina; red-filled circles: position markers of external trichobothria. Segment oriented to level the distal half of the external median carina. L: femur length scale normalizing proximodistal coordinates (x) of setae; D: femur depth scale normalizing dorsoventral coordinates (y) of setae. Scale bar: 1 mm. UV fluorescence. **Figure 162.** Scatter plot of coordinates of macrosetae (black-filled circles) and trichobothria e_1 and e_2 (red-filled circles) in L/D-normalized morphospace ($x_n = x/L, y_n = y/D$). ECMS: external carinal macrosetal series (purple boxes); DEMC: distal external macrosetal cluster (yellow box). Gray curve 1: cumulative distribution function of macrosetal distribution along x -axis (CDF_x); gray curve 2: cumulative distribution function of macrosetal distribution along y -axis (CDF_y). **Figure 163.** Cumulative distribution function of nearest neighbor distances (NND) of macrosetae in L-normalized morphospace ($x/L, y/L$). Proximal landmark macroseta was not included in the analyses.

Morphometric analysis of macrosetal patterns on the external surface of the pedipalp femur

To quantify differences in setation, we performed statistical analyses of positions of macrosetae. Positions were recorded in a 2D orthogonal cartesian coordinate system superimposed on images of the external femur (Fig. 161). The femur was rotated to horizontally level the distal half of the external carina, and macrosetal sockets were marked for digitization. Proximodistal setal coordinates, x , were measured relative to the proximal limit of the carina, usually indicated by the proximal landmark seta; dorsoventral setal coordinates, y , were measured relative to the dorsoexternal carina. Values of x were normalized by length of femur, L, measured

with respect to the proximal landmark seta, and values of y by the vertical distance, D, between dorsoexternal carina and distal external median carina near the midpoint of the femur in the vicinity of trichobothrium e_2 in most buthids. These linear transformations map setation patterns into a dimensionless ‘L/D-normalized’ morphospace ($x_n = x/L, y_n = y/D$) (Fig. 162). Direct comparison of macrosetal positions between different femora is problematic because the number of macrosetae varies between specimens, even conspecifics. In theory, two patterns with different setal counts could be partially compared if each seta in the pattern with lower count could be matched to a unique, homologous seta in the pattern with higher count. In practice, identification of homologous setae is not feasible due to the lack of identifying features of

individual macrosetae, and the large variation in their numbers and positions. Perhaps only the proximal landmark seta of the external median carina could be presumed homologous across taxa, based on its highly conserved position. More generally, positional determination of homology in the analysis of variable positioning can quickly descend into circular arguments. Trichobothriotaxy has been contentious precisely for this reason. We therefore sought an alternative approach to describing setation patterns, one that is independent of setal counts. In L/D-normalized morphospace, we calculated marginal cumulative distribution functions of macrosetae, CDF_x and CDF_y (Fig. 162). The CDFs were computed on a fixed grid of points, enabling pointwise comparison of CDFs describing patterns with different setal counts. CDF_x and CDF_y are two independent functions capturing key aspects of setation patterns differing between scorpion groups. For instance, if setae are sparse in the proximal femur and the DEMC is present, then CDF_x ascends in the distal half of the femur. If the DEMC is absent and setae are uniformly distributed, then CDF_x ascends evenly along the length of the femur. If both DEMC and ECMS are present, then CDF_y includes two consecutive step rises (carinal and infracarinal) with relative magnitudes determined by setal counts of ECMS and DEMC. If DEMC is present and ECMS is sparse or absent, then CDF_y includes a single infracarinal step rise. If the DEMC is a narrower strip, then the step rise will be sharper.

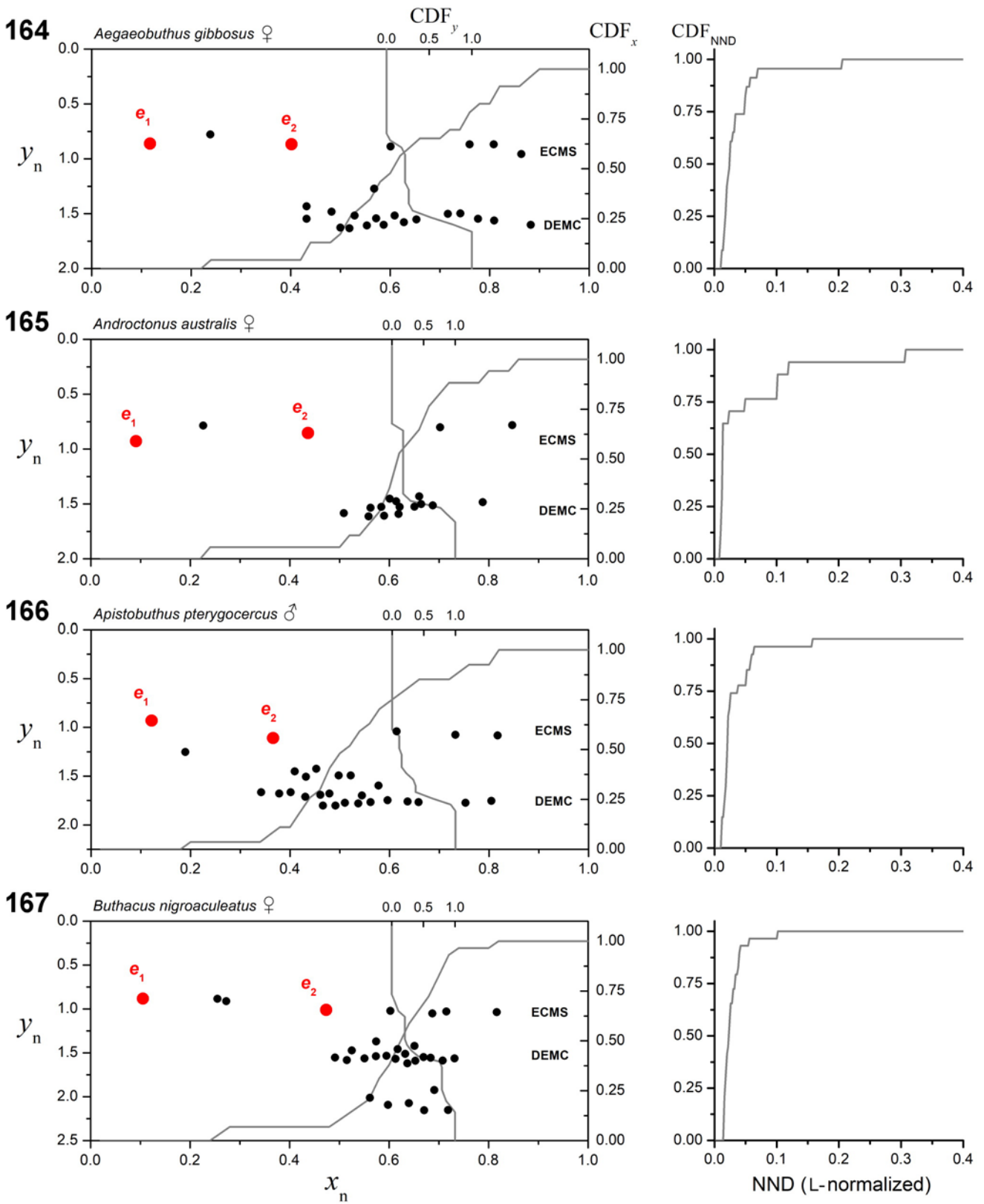
A third descriptive function, the cumulative distribution function of the nearest neighbor distance (NND) of each macroseta, CDF_{NND} , was computed for all setation patterns (Fig. 163). To compare relative clustering densities of different sized femora, NNDs were calculated in an isometric morphospace with x and y coordinates both L-normalized, preserving relative physical distances (the distances between points in Fig. 162 are not NNDs). The shape of CDF_{NND} is sensitive to clustering. Its ascent will be left-skewed for setation patterns that are more tightly clustered. The mean value of the L-normalized NNDs of all macrosetae on a femur is useful as a density index, describing relative clustering of the femoral setation pattern. It will be large if most of the setae are widely and evenly distributed; it will be small if most of the setae are tightly clustered. Multiplying the mean L-normalized NND (a dimensionless quantity) by L, the femur length, recovers the mean absolute NND, which is a measure of the average physical spacing of setae (with dimensional units of μm , or mm).

Figs. 164–187 show examples of digitized setation patterns from representative taxa, along with their CDF_x , CDF_y , and CDF_{NND} . In the ‘Buthus’ group (Figs. 164–175), most CDF_x ascended in the distal 40–70% of the femur where the DEMC is localized. Exceptions included *Hottentotta pellucidus* (Fig. 168) and *Orthochirus gromovi* (Fig. 174), which have a number of more proximal setae. Most CDF_y were double-stepped, with a smaller step at the ECMS and a larger step at the DEMC, corresponding to a sparse ECMS and a dense DEMC. The ECMS setae and step are located around $y_n = 1$, which corresponds to the location of the external median carina. In *Leiurus macroctenus*, CDF_y was steeply single-

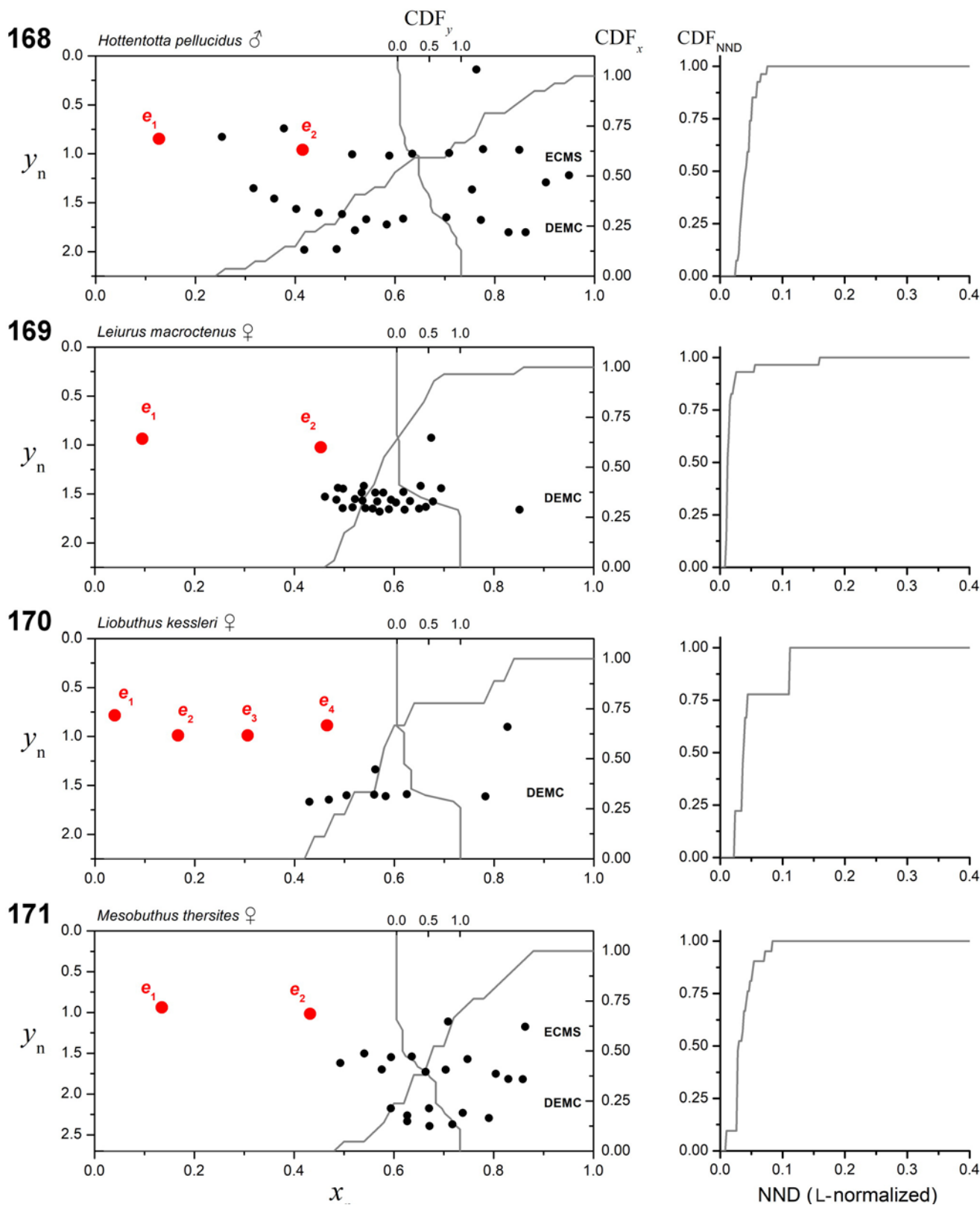
stepped, corresponding to the extreme scarcity of carinal setae and the presence of a dense, compact DEMC (Figs. 46, 69). In the ‘Buthus’ group, most CDF_{NND} rises were strongly left-skewed with 50% of L-normalized NNDs being less than 5% of L, corresponding to densely clustered DEMCs. In other buthids (Figs. 176–180), most CDF_x and CDF_y ascended more broadly, indicating more widely distributed setation. Most CDF_{NND} rises were not as strongly left-skewed, with 50% of L-normalized NNDs being less than 5–10% of L. An exception was *Centruroides margaritatus* with denser distal setation (Fig. 180). In non-buthids (Figs. 181–187), CDF_x ascended more broadly, indicating that setation was spread more evenly along the length of the femur. Ascent of CDF_y was either graded if setae were vertically scattered (e.g., *Hadogenes troglodytes*, Fig. 186), or occurred in two discrete steps if setae were organized into carinal and infracarinal series (e.g., *Hadrurus obscurus*, Fig. 183). Most CDF_{NND} rises were not strongly left-skewed, with 50% of L-normalized NNDs being approximately 10% of L (except for densely setose cases, e.g., Fig. 186).

Differences between the external femoral setation patterns of three major taxonomic groups are compared and contrasted in Figs. 188–199. Cumulative scatter plots (top row) of all macrosetal coordinates in L/D-normalized morphospace revealed overall setation patterns of sampled species in each group. In the ‘Buthus’ group, the overall pattern was dominated by a broad, dense elliptical concentration of setae corresponding to the DEMC, localized in the region $0.4 < x_n < 0.9$, $1.4 < y_n < 1.7$. Above the DEMC was a narrower, less dense, linear band of setae corresponding to the ECMS, with a smaller, proximally separated cluster ($0.2 < x_n < 0.3$, $0.7 < y_n < 1$) (Fig. 188). In other buthids, the horizontal bands of setae were sparser, particularly the DEMC, and the ECMS was somewhat denser than the DEMC. In non-buthids (Fig. 196), an ECMS band was visible, but infracarinal setation was more widely spread. These group differences could be visualized by group-averaged CDF curves (Figs. 189–199). In the ‘Buthus’ group, the average CDF_x ascended mainly in the distal region, with only ~5% of rise in the proximal zone $x_n < 0.4$ (Fig. 189). In contrast, the corresponding fractions of proximal zone setae were ~10% in other buthids (Fig. 193), and ~25% in non-buthids (Fig. 197). In the ‘Buthus’ group, the average CDF_y ascended steeply in two steps, a smaller step at $y_n \sim 1$ (ECMS) and a larger step in $1.5 < y_n < 2.0$ (DEMC) (Fig. 190). The DEMC step was smaller than the ECMS step in other buthids (Fig. 194), and in non-buthids a DEMC step was absent (Fig. 198).

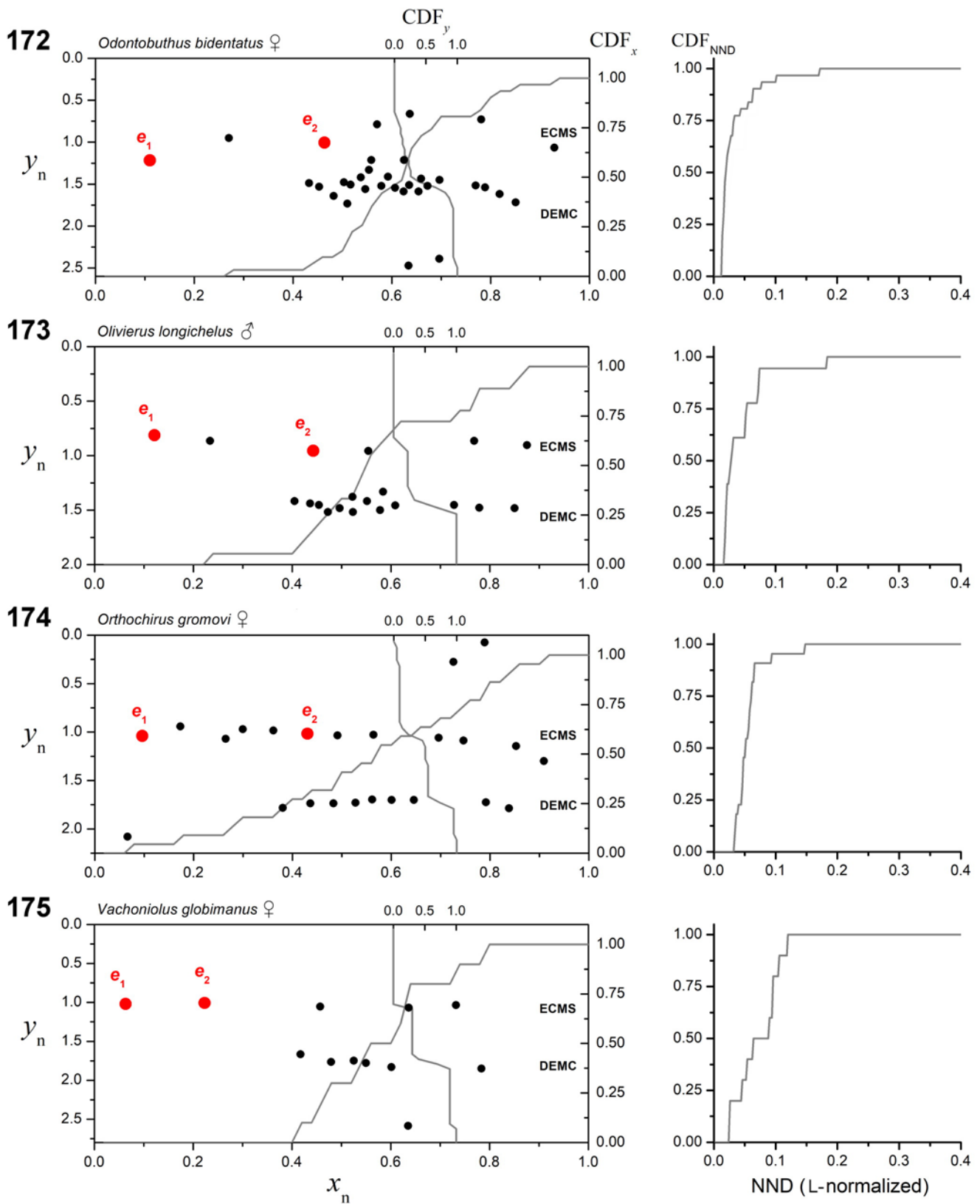
The group-averaged spatial profiles of CDF_x and CDF_y confirmed that the distinctive setation pattern with the majority of macrosetae localized in a compact DEMC is prevalent within the ‘Buthus’ group, but not in other buthid groups and non-buthids. If the DEMC is the main feature of the setation pattern, then femoral clustering is predicted to be denser overall, with smaller L-normalized NNDs. To compare clustering of groups, we calculated the group-averaged CDF_{NND} . This was found to be left-skewed with 50% rise at ~5% of L in the ‘Buthus’ group (Fig. 191), contrasting with



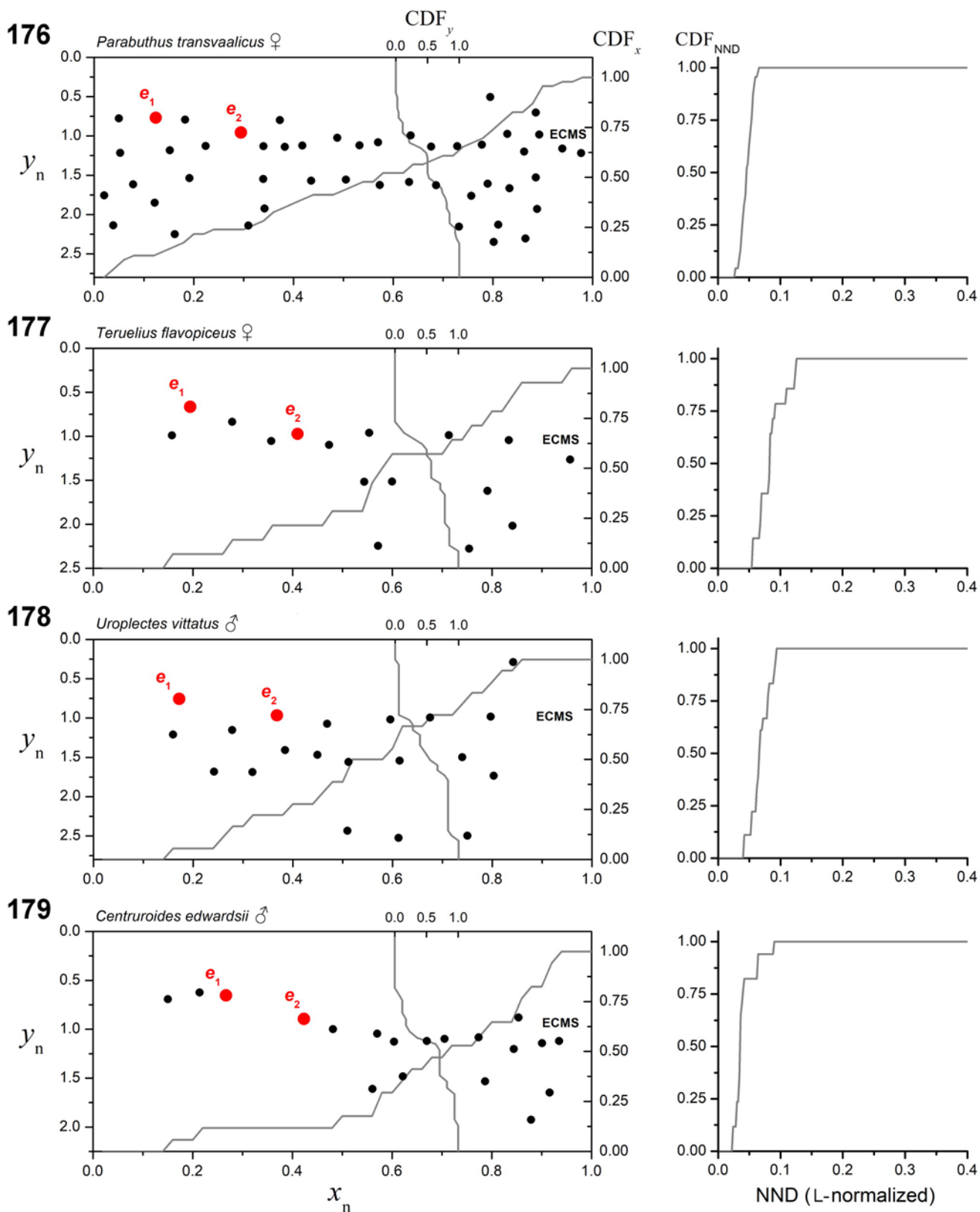
Figures 164–167. Patterns of setation on external pedipalp femur. Buthidae, ‘Buthus’ group. **Figure 164.** *Aegaeobuthus gibbosus*, female. **Figure 165.** *Androctonus australis*, female. **Figure 166.** *Apistobuthus pterygocercus*, male. **Figure 167.** *Buthacus nigroaculeatus*, female. Left panels: Scatter plots and cumulative distribution functions of setae in L/D-normalized morphospace; right panels: cumulative distribution functions of nearest neighbor distances (NND) of macrosetae in L-normalized morphospace.



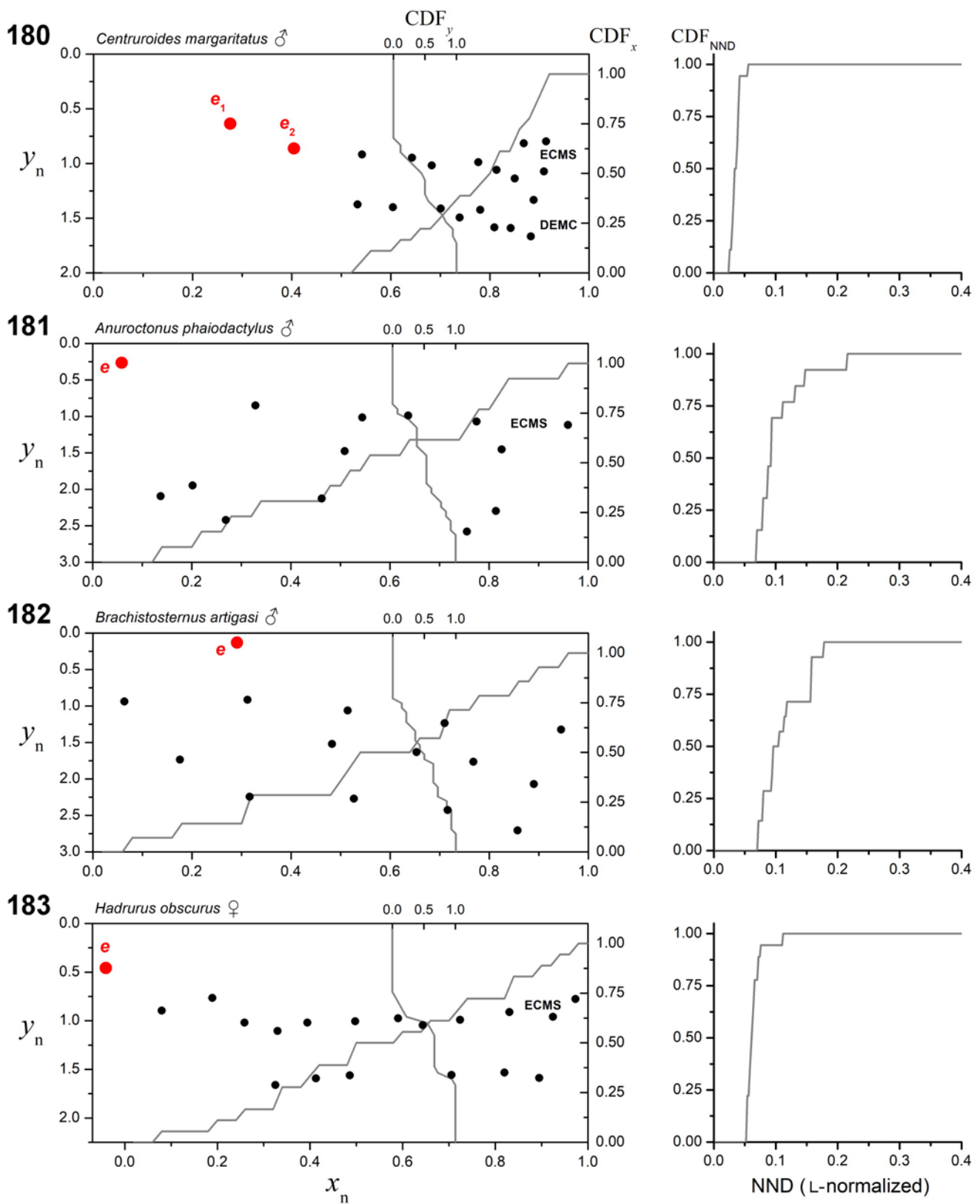
Figures 168–171. Patterns of setation on external pedipalp femur. Buthidae, ‘Buthus’ group. **Figure 168.** *Hottentotta pellucidus*, male. **Figure 169.** *Leiurus macroctenus*, female. **Figure 170.** *Liobuthus kessleri*, female. **Figure 171.** *Mesobuthus thersites*, female. Left panels: Scatter plots and cumulative distribution functions of setae in L/D-normalized morphospace; right panels: cumulative distribution functions of nearest neighbor distances (NND) of macrosetae in L-normalized morphospace.



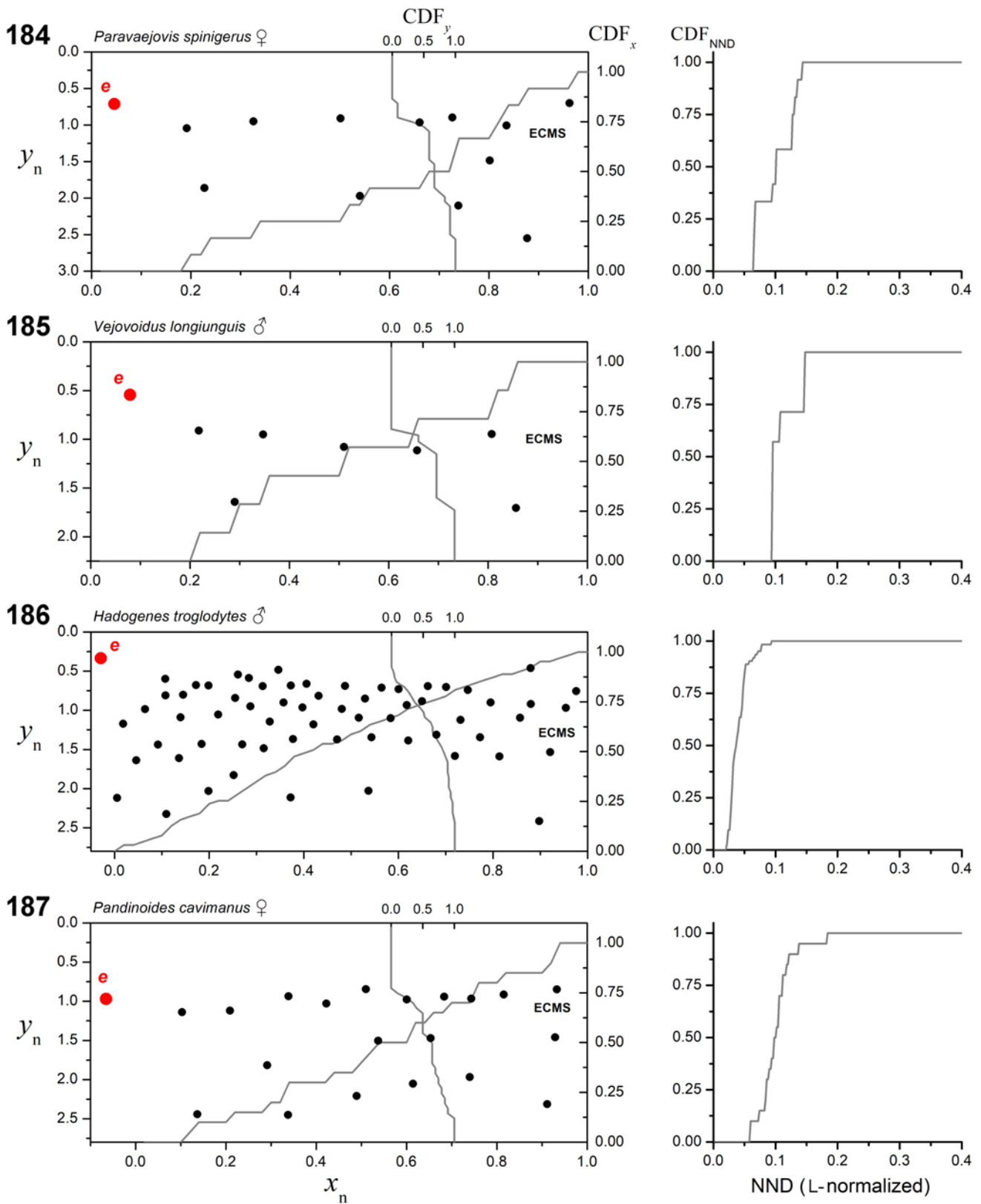
Figures 172–175. Patterns of setation on external pedipalp femur. Buthidae, ‘Buthus’ group. **Figure 172.** *Odontobuthus bidentatus*, female. **Figure 173.** *Olivierus longichelus*, male. **Figure 174.** *Orthochirus gromovi*, female. **Figure 175.** *Vachoniolus globimanus*, female. Left panels: Scatter plots and cumulative distribution functions of setae in L/D-normalized morphospace; right panels: cumulative distribution functions of nearest neighbor distances (NND) of macrosetae in L-normalized morphospace.



Figures 176–179. Patterns of setation on external pedipalp femur. Buthidae, ‘Charmus–Uroplectes’ group (176–178) and ‘Tityus’ group (179). **Figure 176.** *Parabuthus transvaalicus*, female. **Figure 177.** *Teruelius flavopiceus*, female. **Figure 178.** *Uroplectes vittatus*, male. **Figure 179.** *Centruroides edwardsii*, male. Left panels: Scatter plots and cumulative distribution functions of setae in L/D-normalized morphospace; right panels: cumulative distribution functions of nearest neighbor distances (NND) of macrosetae in L-normalized morphospace.



Figures 180–183. Patterns of setation on external pedipalp femur. Buthidae, ‘Tityus’ group (180); Anuroctonidae (181); Bothriuridae (182); and Hadruridae (183). **Figure 180.** *Centruroides margaritatus*, male. **Figure 181.** *Anuroctonus phaiodactylus*, male. **Figure 182.** *Brachistosternus artigasi*, male. **Figure 183.** *Hadrurus obscurus*, female. Left panels: Scatter plots and cumulative distribution functions of setae in L/D-normalized morphospace; right panels: cumulative distribution functions of nearest neighbor distances (NND) of macrosetae in L-normalized morphospace.



Figures 184–187. Patterns of setation on external pedipalp femur. Vaejovidae (184–185); Hormuridae (186); and Scorpionidae (187). **Figure 184.** *Paravaejovis spinigerus*, female. **Figure 185.** *Vejovoidus longiunguis*, male. **Figure 186.** *Hadogenes troglodytes*, male. **Figure 187.** *Pandinoides cavimanus*, female. Left panels: Scatter plots and cumulative distribution functions of setae in L/D-normalized morphospace; right panels: cumulative distribution functions of nearest neighbor distances (NND) of macrosetae in L-normalized morphospace.

~8% of L in other buthids (Fig. 195), and ~12% of L in non-buthids (Fig. 199). A ranked histogram of mean L-normalized NNDs of all examined femora emphasizes the preponderance of smaller NNDs in the 'Buthus' group, a consequence of committing a larger fraction of setae to tightly clustered DEMCs (Fig. 201).

The total number of macrosetae on the external femur varied widely, ranging from 2 setae (e.g., *Centruroides gracilis*, *Tityus*) up to 63 setae (*Hadogenes troglodytes*) (counts exclude proximal landmark seta). In the 'Buthus' group, high counts were 37–38 (*Hottentotta jayakari*, *Leiurus quinquestriatus*, *Odontobuthus bidentatus*). Does clustering vary as the number of setae is increased? A logarithmic plot of L-normalized mean NND vs. number of macrosetae (Fig. 202) reveals a negative trend. There was a progressive decrease in the mean NND with increasing number of setae in both the 'Buthus' group, and non-buthids. The decrease was steeper in the 'Buthus' group, with a log slope of -0.68. If the number were increasing by uniform addition of setae to a fixed spatial pattern, the spacing between setae will be inversely proportional to the number, and the log slope will be -1. The shallower slope implies that spatial patterns of setation are not fixed, but vary between taxa with different numbers of setae. For example, if a fraction of added setae expanded the area of the DEMC, then the mean normalized NND could decrease more slowly with number.

In the 'Buthus' group, the DEMC appeared relatively denser in larger species and sparser in smaller species, suggesting that clustering varies with size. A logarithmic plot of L-normalized mean NND vs. length of femur, L, (Fig. 203, lower plot, left ordinate) confirms a negative correlation. There was a progressive decrease in mean normalized NND with increasing size in the 'Buthus' group (lower blue circles), showing that clustering is denser in larger species. In other buthids and non-buthids, which lack a compact DEMC, mean normalized NND was uncorrelated with size. The log regression slope was -0.7698, i.e., shallower than -1, indicating that the rate of addition of setae was insufficient to maintain an inverse relation of spacing with increasing size. A plot of mean absolute NND (Fig. 203, upper plot, right ordinate) has positive log regression slope of 0.2302 (= 1-0.7698). The increase in the physical spacing of setae from smaller to larger species is relatively slow, only 1.5-fold over a 7-fold increase in size. The mean absolute NND over that range was $196 \pm 69 \mu\text{m}$ (mean \pm SD).

To test for sexual dimorphism in clustering, we compared mean L-normalized NNDs of males and females across species. In Fig. 204, the mean NNDs of males and females are plotted against each other for 30 species from the 'Buthus' group (blue circles), and 5 species from the 'Charmus-Uroplectes' group (red squares). Off-diagonal points reveal sexual dimorphism in individual species. Most NNDs were similar in the two sexes because the majority of points are near diagonal. There are more widely scattered points both above and below diagonal, showing that stronger clustering could occur in either sex. In a paired t-test, the average male mean

NND was not significantly different from that females ($P = 0.967$). Another measure of clustering is the number of setae in the DEMC. Higher setal counts are associated with denser clustering. In Fig. 205, the number of DEMC setae in males is plotted against the number in females for the same species sample as in Fig. 204. Relative positions of data points from the 'Buthus' group (blue circles), and 'Charmus-Uroplectes' group (red squares), are inverted compared to those in Fig. 204, due to the inverse relationship between mean NND and setal count (Fig. 202, blue line). Data points were either mostly near the diagonal, or scattered above and below it, i.e., higher DEMC counts could occur in either sex. Although above-diagonal points outnumbered below-diagonal points, a one-tailed, paired t-test found that male counts were not significantly higher than female counts ($P = 0.162$). Thus, we did not find evidence of a systematic difference in clustering between the sexes.

Some of the scatter in the plots of Figs. 204–205 may arise from intraspecific variation of setation, as the data points represent single samples of males and females of each species. The histogram in Fig. 200 shows the intraspecific variation in DEMC count for a sample of 42 male *Olivierus martensii*. The mean count was 16.405 ± 3.291 (mean \pm SD). In comparison, the male count of 8 species in Fig. 205 having female counts in the range 14–18 was 18.125 ± 4.883 (mean \pm SD). The means did not differ significantly ($P = 0.217$; t-test), but equal variance was rejected at $\alpha = 0.2$ ($P = 0.107$; Levene test). The larger variance of the 8-species sample is expected if there is interspecific variation.

Figs. 206–207 chart the variation of mean L-normalized NNDs and DEMC counts in different buthid genera. Taxa with denser setation are positioned towards the left in Fig. 206, and more numerous setae towards the right in Fig. 207. Fig. 206 shows the trend in the 'Buthus' group (blue bars) of denser setation in genera with larger species, and sparser setation in genera with smaller species. In other buthids (gray bars), density of setation was not related to size. The mean NNDs of other buthids had more overlap with those of less setose genera with smaller species in the 'Buthus' group, and less overlap with those of genera with larger species having higher density DEMCs. In Fig. 207, the order of genera in the 'Buthus' group is the reverse of that in Fig. 206, reflecting the inverse relationship between mean NND and seta count. The DEMC counts of other buthids show greater overlap with 'Buthus' group genera having higher density DEMCs. Although their seta counts are high, their distal infracarinal setation is not as dense because it is not gathered into a compact DEMC (cf. Fig. 192 vs. Fig. 188).

Setation patterns were compared by multivariate analysis of cumulative spatial distribution functions in L/D-normalized morphospace, CDF_x and CDF_y . For input variables, we used values of the functions on a fixed grid of points. On the proximodistal axis, CDF_x was sampled in the range $0.20 < x_n < 0.80$ at intervals of 0.04 (maximum x_n , 1.0), yielding 16 variables; on the dorsoventral axis, CDF_y was sampled in the range $0.896 < y_n < 2.048$ at intervals of 0.128 (maximum y_n ,

3.2), yielding 10 variables. The sampled ranges bracketed most of the variation in rising phases of the two CDFs, while excluding end variables with near zero variances. Femora with five or fewer macrosetae were excluded from analysis, leaving a sample size of 148. Principal components analysis (PCA) yielded six components (PC1–PC6) explaining 89.30% of the total variance. Plots of component scores are shown in Figs. 208–210. The ‘Buthus’ group appears largely separated from other buthids and non-buthids along the PC1 axis, while the other buthids largely overlapped the non-buthids (Fig. 208). The CDF variable loadings on PC1–6 are shown as heat maps in Fig. 210. Along the proximodistal axis, high loadings of PC1 were located over proximal and distal parts of the range, and high loadings of PC2 were located over the DEMC. Along the dorsoventral axis, high loadings for PC1 were located over the ECMS, and high loadings for PC3 were located over the DEMC. To further analyze the morphometric separation of the ‘Buthus’ group, we performed a linear discriminant analysis (LDA) on the first six principal components. Linear discriminant functions were constructed for three groups: the ‘Buthus’ group, other-buthids, and non-buthids. Correct classification was achieved for 137/148 samples (92.57% accuracy). Of the 11 misclassified samples, 4 were ‘Buthus’ group (2 each misclassified as other buthid, and non-buthid), 3 were other buthids (misclassified as non-buthids) and 4 were non-buthids (misclassified as other buthids). PC1 had the strongest influence (smallest Wilks’ lambda, 0.267), and the largest coefficient in the discriminant functions. Two canonical variates, CV1 and CV2, were constructed. A scatter plot of canonical scores (Fig. 211) shows improved separation of the three groups (Wilks’ lambda 0.149) compared to the principal component plots. The misclassified samples were included in a minority of points in the intersections of convex hulls.

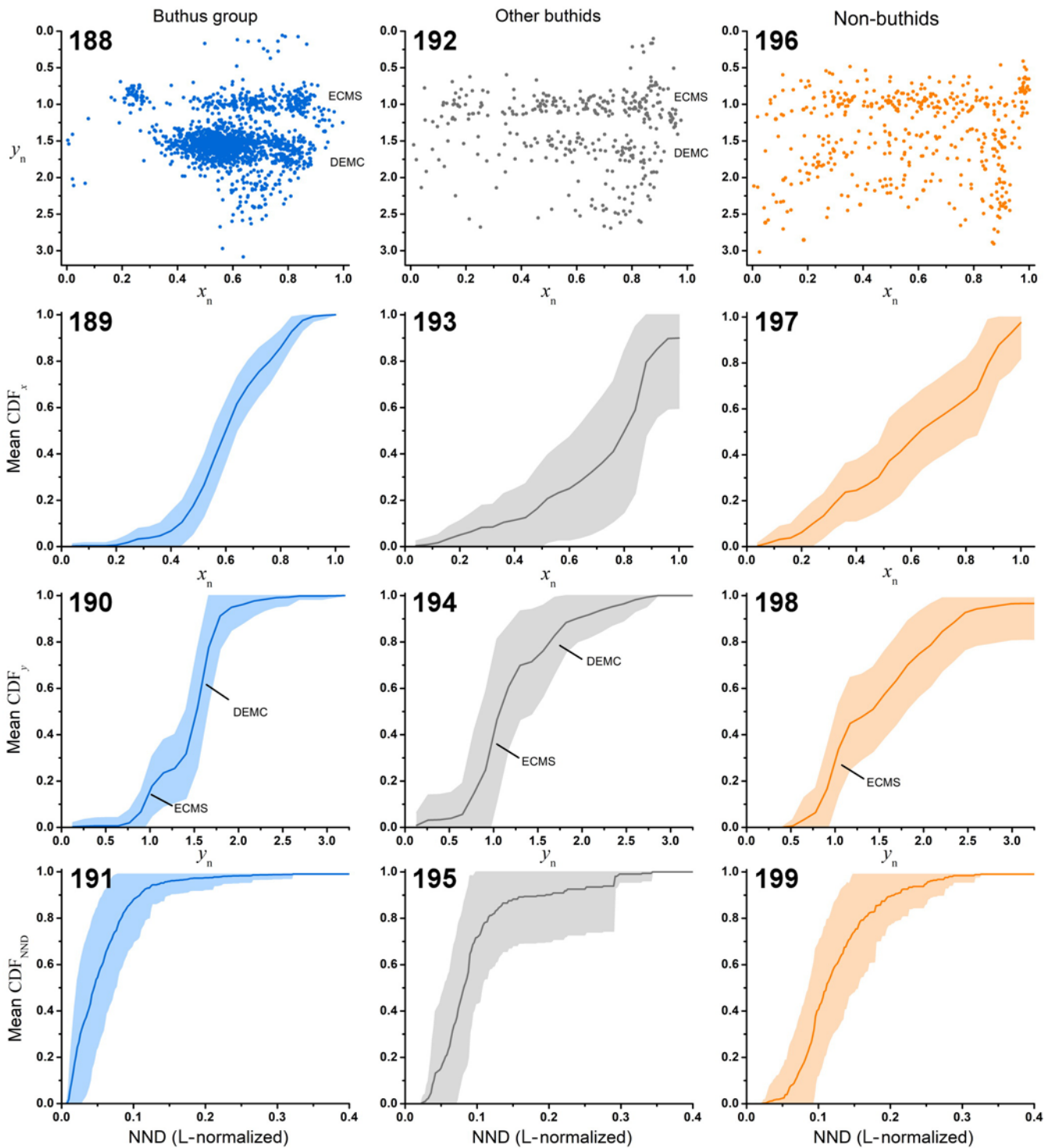
Inspection of ‘Buthus’ group setation patterns (Figs. 1–88) suggested systematic differences between genera. To test this, we focused our attention on four major genera (*Compsobuthus*, *Hottentotta*, *Leiurus* and *Olivierus*) each represented by at least 7 samples. Genera may share similar spatial patterns but differ in density of setation. To discriminate these, we augmented the spatial analysis by adding CDF_{NND} to represent density distributions. The L-normalized CDF_{NND} was sampled in the range $0.016 < NND < 0.16$ at intervals of 0.008, yielding 19 additional variables. The sampled range bracketed most variation in rising phases of CDF_{NND} . A female of *Compsobuthus polisi* was omitted as an outlier with a proximal macroseta close to trichobothrium e_1 , that was absent in all other samples of the genus. PCA yielded 6 components (PC1–PC6) explaining 79.55% of the total variance. These components were further analyzed by LDA and discriminant functions were constructed for the four genera. Correct generic classification was achieved for 38/41 samples (92.68% accuracy). The 3 misclassified samples, were: 1 *Hottentotta* and 1 *Leiurus* (both misclassified as *Olivierus*), and 1 *Olivierus* (misclassified as *Hottentotta*). PC1 had the strongest influence (smallest Wilks’ lambda, 0.144), and the largest coefficient in the discriminant functions.

Three canonical variates were constructed. A scatter plot of scores for the first two canonical variates (Fig. 212) shows the separation of the four genera (Wilks’ lambda 0.045). The misclassified samples were included in a minority of points straddling the convex hulls.

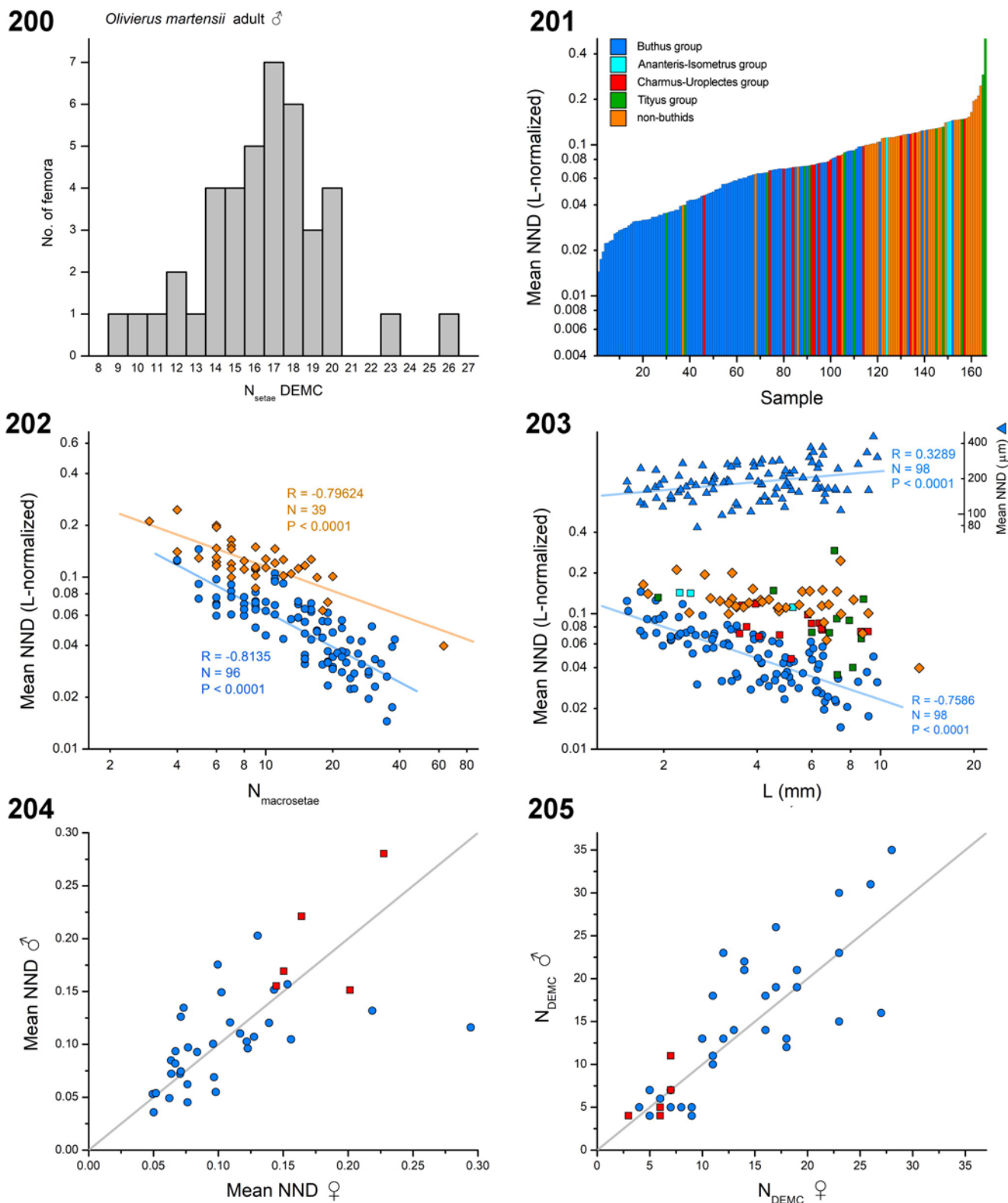
Differences between setation patterns were also analyzed by multidimensional scaling. A dissimilarity matrix was constructed from Euclidean distances between CDF_x and CDF_y of different femora. Each CDF was evaluated over its entire range on a fixed grid of 25 points, and the distances calculated between the 50-dimensional vectors. A metric solution was initially computed as a starting point for non-metric iteration. Fig. 213 shows the first two dimensions of a solution recovered in four dimensions with stress 0.0462. The ‘Buthus’ group was largely separable from the other groups, with only minor overlap. However, the other buthids were not well separated from the non-buthids. Euclidean distances between CDF curves carry enough information to resolve stereotypic patterns of DEMCs in the ‘Buthus’ group, but not enough to differentiate more variable patterns of other buthids from those of non-buthids. The latter were better resolved when information about CDF shapes was encoded by the input variables (Fig. 211). ‘Buthus’ group patterns are separable with less morphometric information because they share a similar configuration with a compact DEMC that is absent in other scorpions.

Hierarchical clustering offers another method for analyzing differences described by a dissimilarity matrix. We applied the UPGMA algorithm to standardized Euclidean distances between CDF_x and CDF_y vectors to construct ultrametric trees of buthids and non-buthids. Trees were constructed separately for males and females (Figs. 214–215; some species represented by only one sex). In males, the ‘Buthus’ group clustered almost exclusively in a single major branch, apart from other scorpions, the only exception being *Orthochirus gromovi*. In females, the ‘Buthus’ group also clustered mostly apart from other scorpions, although there were a few more exceptions. On the other hand, clusters of other buthids and non-buthids were mingled in both sexes. These results are similar to that obtained from multidimensional scaling.

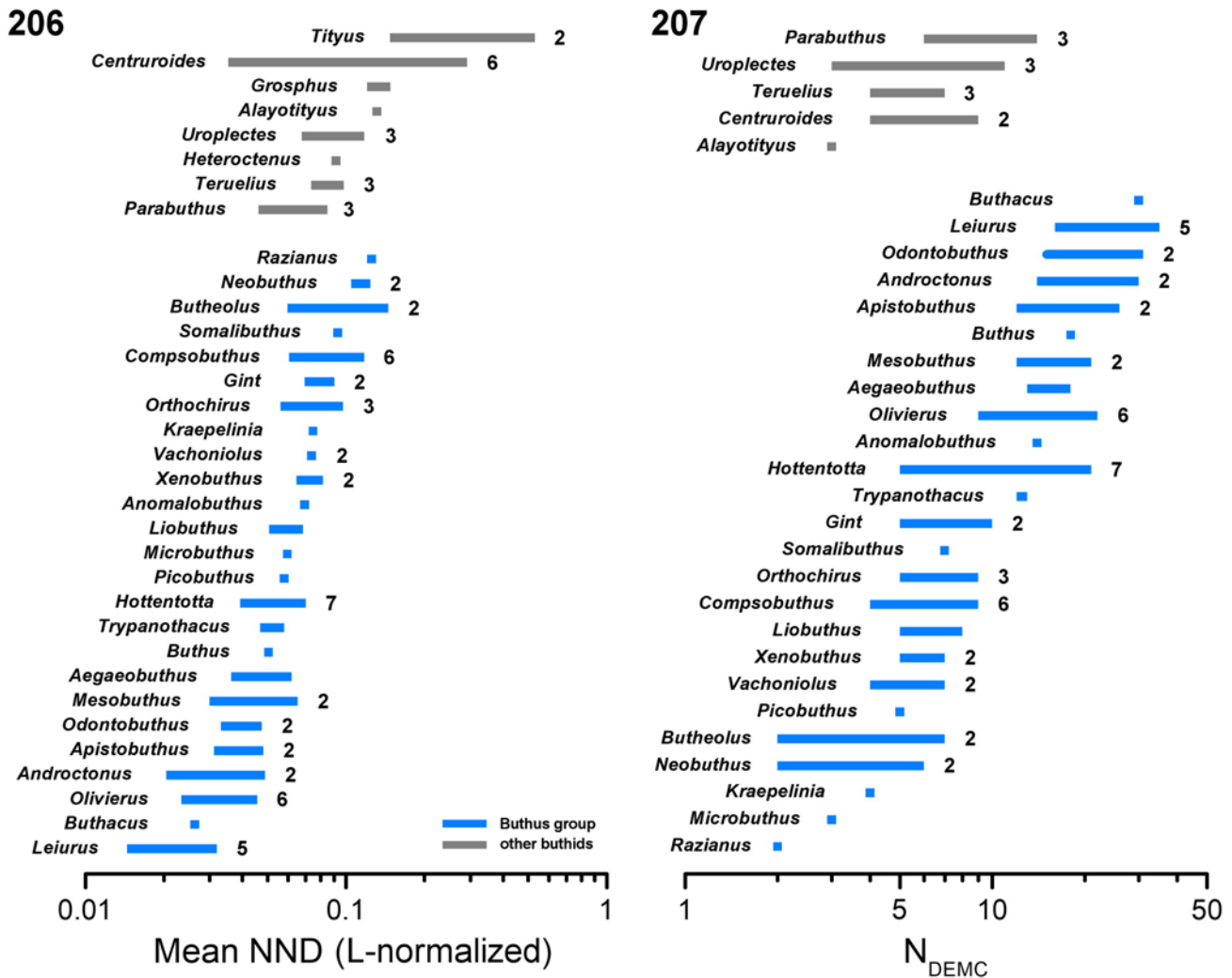
To analyze differences in setal clustering of buthids, UPGMA was applied to the CDF_{NND} curves of different species. This provided more a more detailed picture of the taxonomic trends in mean NNDs of different genera shown in Fig. 206. CDF_{NND} values were computed over the range [0, 0.2] at intervals of 0.004, yielding 50 variables, and standardized Euclidean distances were calculated between the 50-dimensional vectors. Separate trees were constructed for males (Fig. 216) and for females (Fig. 217). In both sexes, members of the ‘Buthus’ group with compact DEMCs aggregated into larger clusters. Buthids belonging to other groups were scattered through the trees alongside ‘Buthus’ group members with sparser setation. These results are in agreement with the broad overlap of the ‘Buthus’ group with other buthids seen with mean normalized NNDs (Fig. 206).



Figures 188–199. Macrosetal patterns on external pedipalp femur in three major scorpion lineages: Buthidae, ‘Buthus’ group (188–191) and other buthids (192–195); and non-buthids (196–199). **Figures 188, 192, 196 (top row).** Cumulative scatter plots of macrosetal coordinates in L/D-normalized morphospace from ‘Buthus’ group (188: 1,601 setae, 99 femora, 56 species, 25 genera, 43 ♂, 56 ♀), other buthids (192: 353 setae, 40 femora, 29 species, 15 genera, 21 ♂, 19 ♀), and non-buthids (196: 427 setae, 41 femora, 35 species, 29 genera, 17 ♂, 24 ♀). **Figures 189, 193, 197 (second row).** Group-averaged proximidistal cumulative distribution functions (CDF_x) of macrosetae of ‘Buthus’ group (189), other buthids (193) and non-buthids (197). **Figures 190, 194, 198 (third row).** Group-averaged dorsoventral cumulative distribution functions (CDF_y) of macrosetae of ‘Buthus’ group (190), other buthids (194) and non-buthids (198). **Figures 191, 195, 199 (bottom row).** Group-averaged cumulative distribution functions of nearest neighbor distances (NND) of macrosetae in L-normalized morphospace (CDF_{NND}) of macrosetae of ‘Buthus’ group (191), other buthids (192) and non-buthids (199). Group-averaged CDFs calculated from samples listed for Figs. 188, 192 and 196. Bands around each mean curve show standard deviations. The bands were truncated above CDF = 1.0. Abbreviations: ECMS, external carinal macrosetal series; DEMC, distal external macrosetal cluster.



Figures 200–205. Variation in the density of setation on external pedipalp femur. **Figure 200.** Histogram of macrosetal counts for distal external macrosetal cluster (DEMC) in *Olivierus martensii* (42 ♂). **Figure 201.** Ranked vertical logarithmic bar plot of mean L-normalized nearest neighbor distances (NND) of external macrosetae for 166 femora. Blue bars: ‘Buthus’ group (N = 96); cyan bars: ‘Ananteris-Isometrus’ group (N = 3), red bars: ‘Charmus-Uroplectes’ group (N = 16); green bars: ‘Tityus’ group (N = 12); orange bars: non-buthids (N = 39). **Figure 202.** Logarithmic scatter plot of mean L-normalized NND vs. number of macrosetae in ‘Buthus’ group (blue circles) and non-buthids (orange diamonds). Blue and orange regression lines and Pearson’s correlation coefficients (R) from linear least squares fits to respective data sets. **Figure 203.** Lower plot (left ordinate): logarithmic scatter plot of mean L-normalized NND vs. L (= femur length) in ‘Buthus’ group (blue circles), ‘Ananteris-Isometrus’ group (cyan squares), ‘Charmus-Uroplectes’ group (red squares), ‘Tityus’ group (green squares), and non-buthids (orange diamonds). Upper plot (right ordinate): mean absolute NND in μm of ‘Buthus’ group (blue triangles), plotted on the same abscissa. Blue regression lines and Pearson’s correlation coefficients (R) from linear least squares fit to ‘Buthus’ group data (blue circles). **Figures 204–205.** Scatter plots of male vs. female mean L-normalized NND (204) and number of DEMC macrosetae (205) in ‘Buthus’ group (blue circles) and ‘Charmus-Uroplectes’ group (red squares). Data points represent single samples of male and female femora from different species.



Figures 206–207. Variation in density of setation on external pedipalp femur in buthid genera. Logarithmic horizontal bar plots of mean L-normalized NND (206) and number of DEMC macrosetae (207) recorded from ‘Buthus’ group (25 genera; blue bars) and other buthids (8 genera; gray bars). Bars indicate observed ranges. Numeric labels on right of bars indicate number of exemplar species; unlabeled bars with single exemplar species. In Fig. 207, the genera *Grosphus*, *Heteroctenus* and *Tityus* are omitted because examined species lacked DEMC setae.

Ontogenetic variation of the DEMC

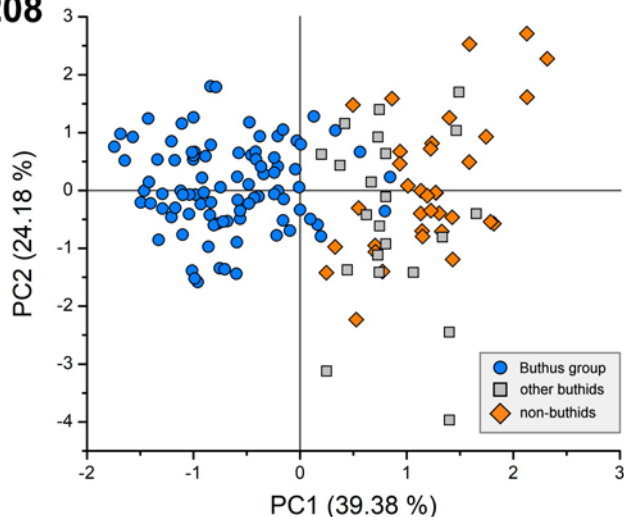
In the ‘Buthus’ group, spatial patterns of femoral setation were more or less stable across adults of different sized species, whereas the density of setation relative to femur length varied with size, being sparser in smaller species, and denser in larger species (Fig. 203). Size also varies intraspecifically during growth and development. Do the patterns and density of setation change across instars? Figs. 218–225 show the ontogenetic variation in external femoral setation of *Androctonus* cf. *crassicauda*. In adults (Figs. 218–219), most setae are concentrated in a dense, compact DEMC, with a few scattered ECMS setae. The patterns were similar to those seen in other adult *Androctonus* (Figs. 9–12). In immatures, the pattern was also similar, but the density of setation decreased progressively in smaller instars (Fig. 220–224); in the smallest juvenile, a DEMC was not formed (Fig. 225). The plots in Figs. 226–228 show ontogenetic scaling of

number and density of DEMC setae: (i) the number of setae in the DEMC was positively correlated with size (measured by carapace length) (Fig. 226); (ii) the L-normalized mean NND (inverse measure of relative density) was negatively correlated with size (Fig. 227); and (iii) the mean absolute NND was not significantly correlated with size ($P > 0.050$, mean \pm SD $163.3 \pm 22.0 \mu\text{m}$) (Fig. 228). As the scorpion grows and molts, the position and relative size of the DEMC remain stable, while setae are added to maintain nearly constant physical spacing of setae.

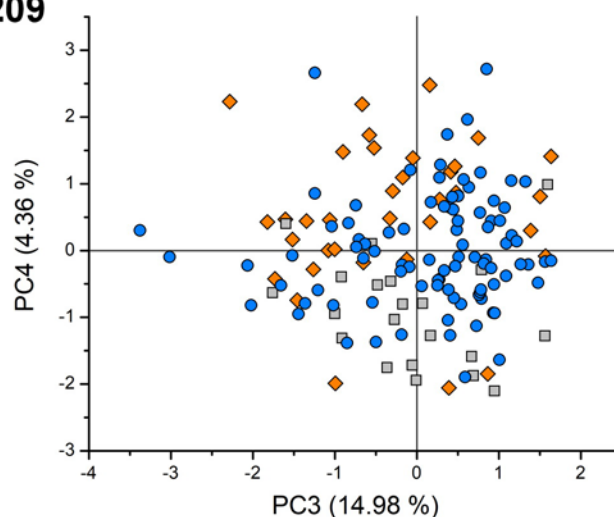
Patterns of trichobothria on the external surface of the pedipalp femur of buthids

Trichobothria were clearly visible in UV images, allowing us to record their positions for systematic comparison across buthid groups (Fig. 161). Proximodistal and dorsoventral coordinates of e_1 and e_2 in L/D-normalized morphospace

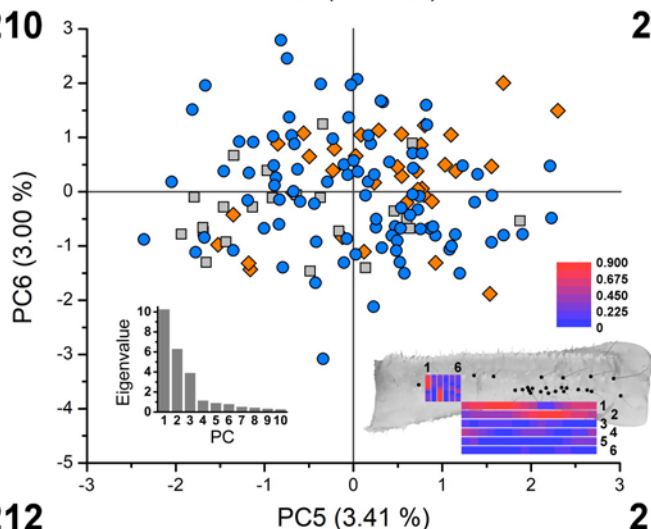
208



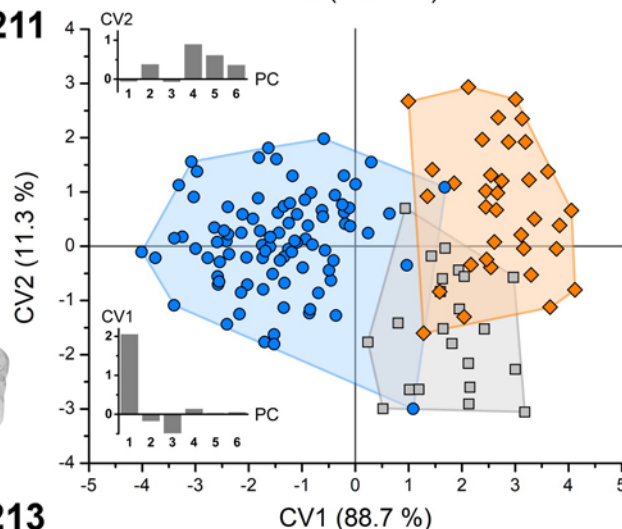
209



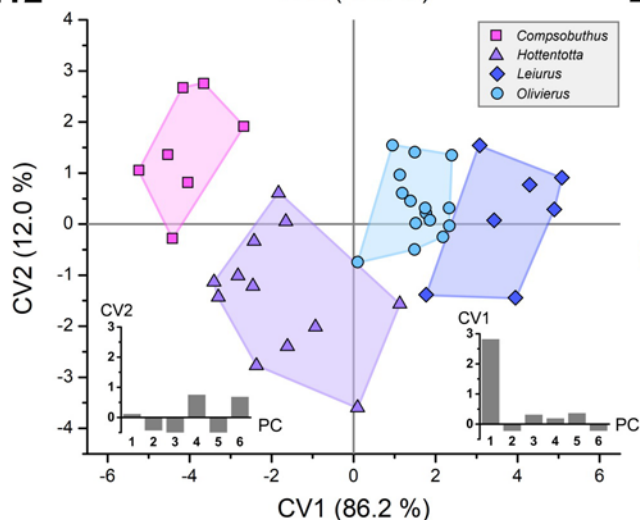
210



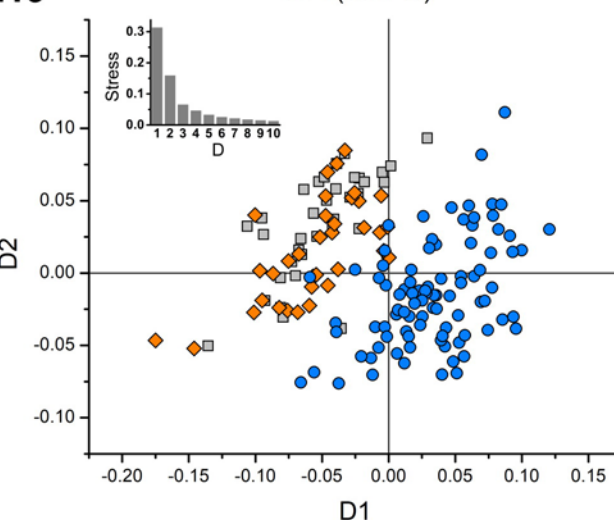
211



212



213



Figures 208–213. Multivariate analysis of macrosetal patterns on external pedipalp femur. **Figures 208–210.** Principal components analysis (PCA) of CDF_x and CDF_y . Scatter plots of scores for first six components, explaining 89.32% of the variance: PC1 vs. PC2 (208), PC3 vs. PC4 (209), and PC5 vs. PC6 (210). Percentages of variance explained by each component listed on axis labels. **Figure 210.** Lower left inset: scree plot of eigenvalues for first 10 components; lower right inset: heat maps of loadings of CDF_x variables (horizontal bars) and CDF_y variables (vertical bars) on PC1–PC6, positioned on femur. **Figure 211.** Linear discriminant analysis (LDA) of first 6 principal components, PC1–PC6, in Figs. 208–210. Scatter plot of scores for canonical variates, CV2 vs. CV1. Percentages of variance explained by each variate listed on axis labels. Insets: canonical coefficients of CV1 (lower left) and CV2 (upper left). **Figure 212.** LDA of first 6 principal components from PCA of CDF_x , CDF_y , and CDF_{NND} of six genera in the ‘Buthus’ group. Scatter plot of scores for canonical variates, CV2 vs. CV1. Percentages of variance explained by each variate listed on axis labels. Insets: canonical coefficients of CV1 (lower left) and CV2 (lower right). **Figure 213.** Non-metric multidimensional scaling analysis of CDF_x and CDF_y . Scatter plots of coordinates in first two dimensions, D1 vs. D2. Inset: scree plot of stress for first 10 dimensions. Symbols in Figs. 208–211, 213: blue circles, ‘Buthus’ group (91 femora, 52 species, 23 genera, 38 ♂, 53 ♀); gray squares, other buthids (22 femora, 15 species, 6 genera, 13 ♂, 9 ♀); orange diamonds, non-buthids (35 femora, 29 species, 23 genera, 13 families, 15 ♂, 20 ♀). Symbols in Fig. 212: violet squares, *Compsobuthus* (7 femora, 6 species, 4 ♂, 3 ♀); lavender triangles, *Hottentotta* (12 femora, 7 species, 4 ♂, 8 ♀), cobalt diamonds, *Leirus* (7 femora, 5 species, 2 ♂, 5 ♀), teal circles, *Olivierus* (15 femora, 6 species, 5 ♂, 10 ♀).

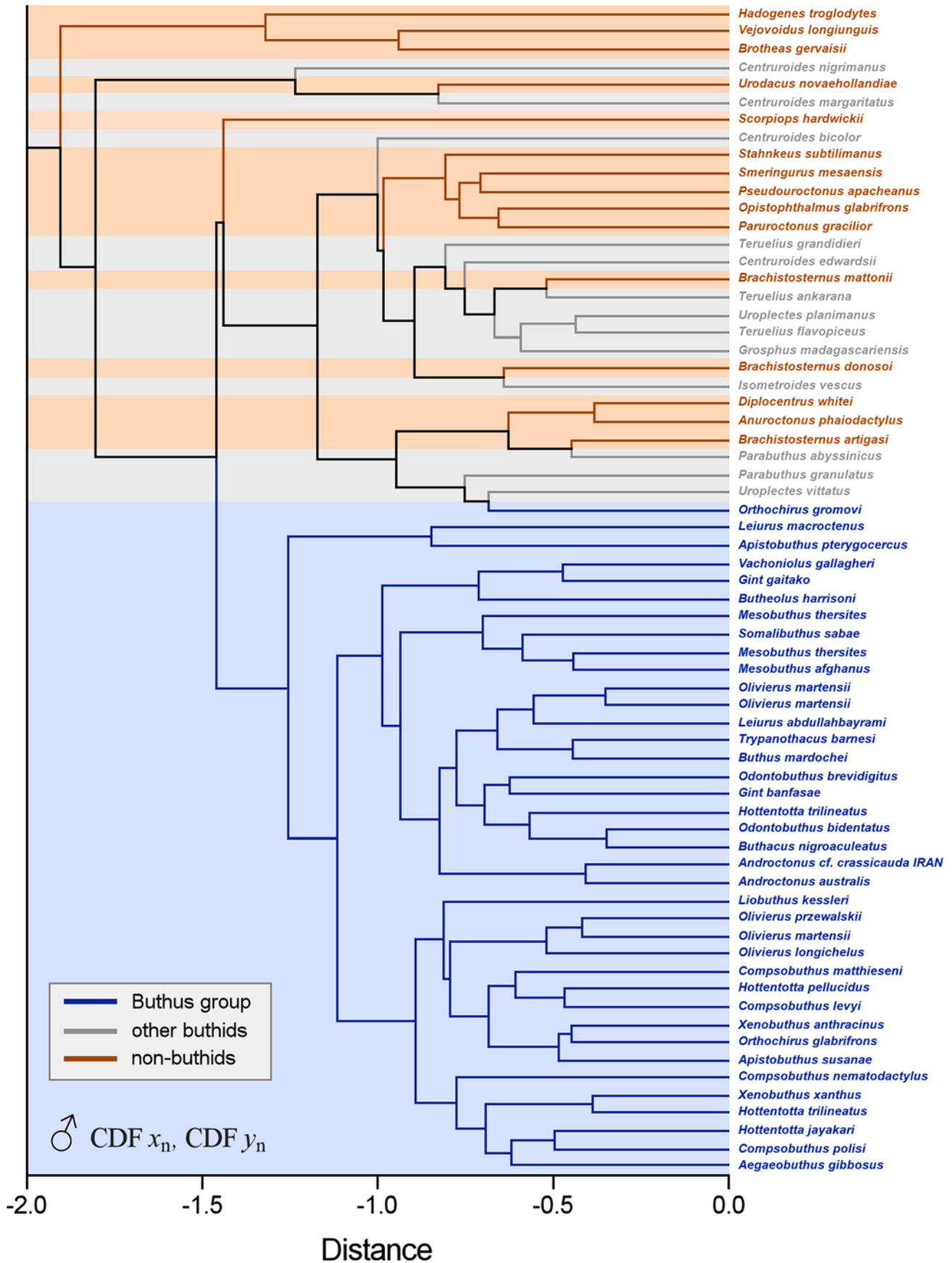


Figure 214. Hierarchical cluster analysis of macrosetal patterns on external pedipalp femur of males. Ultrametric tree obtained from by application of UPGMA algorithm to Euclidean distances between cumulative proximodistal and dorsoventral distribution functions in L/D-normalized morphospace of femoral setation patterns. Blue terminals, ‘Buthus’ group; gray terminals, other buthids; orange terminals, non-buthids. Each terminal represents one femur.

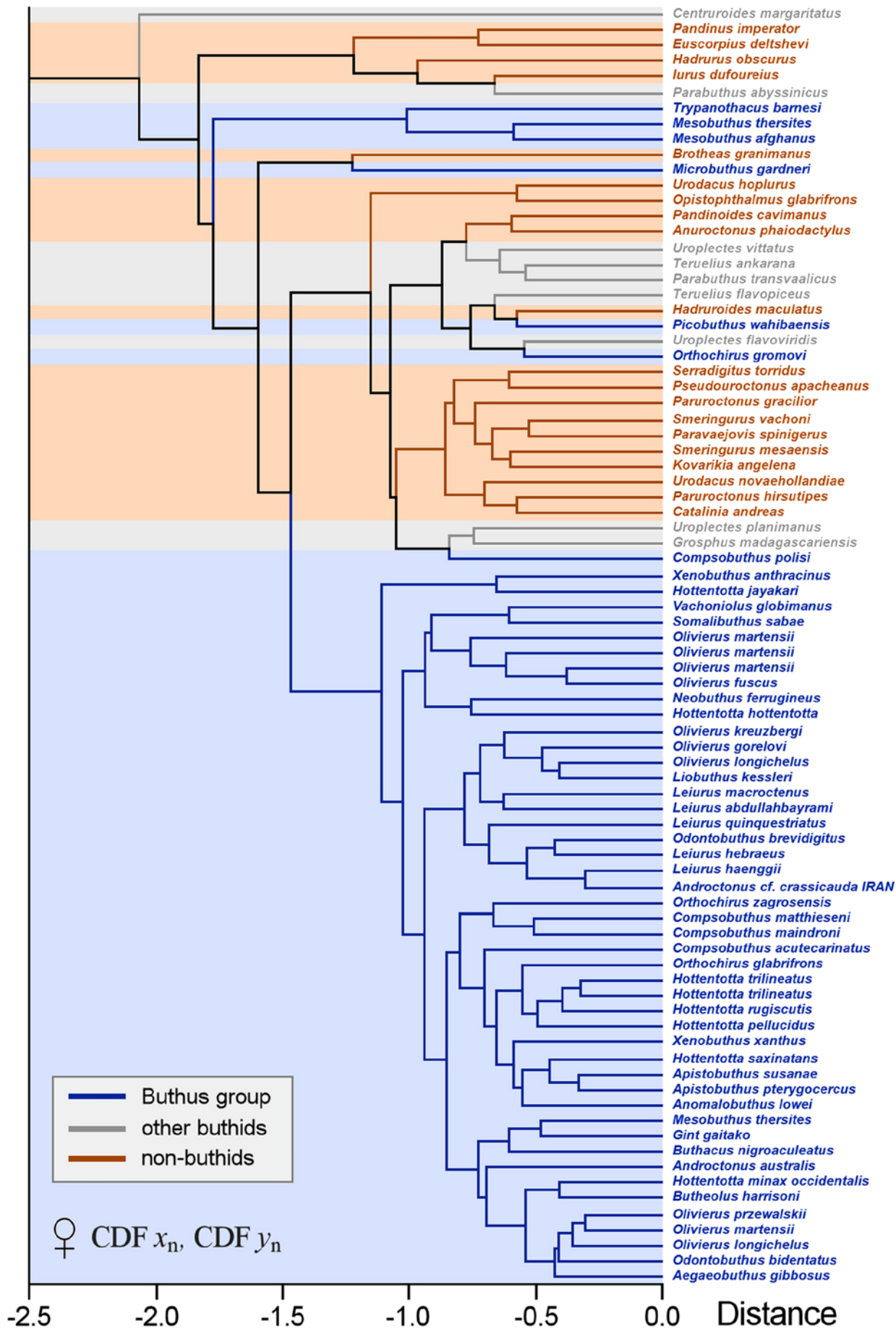


Figure 215. Hierarchical cluster analysis of macrosetal patterns on external pedipalp femur of females. Ultrametric tree obtained from by application of UPGMA algorithm to Euclidean distances between cumulative proximodistal and dorsoventral distribution functions in L/D-normalized morphospace of femoral setation patterns. Blue terminals, ‘Buthus’ group; gray terminals, other buthids; orange terminals, non-buthids. Each terminal represents one femur.

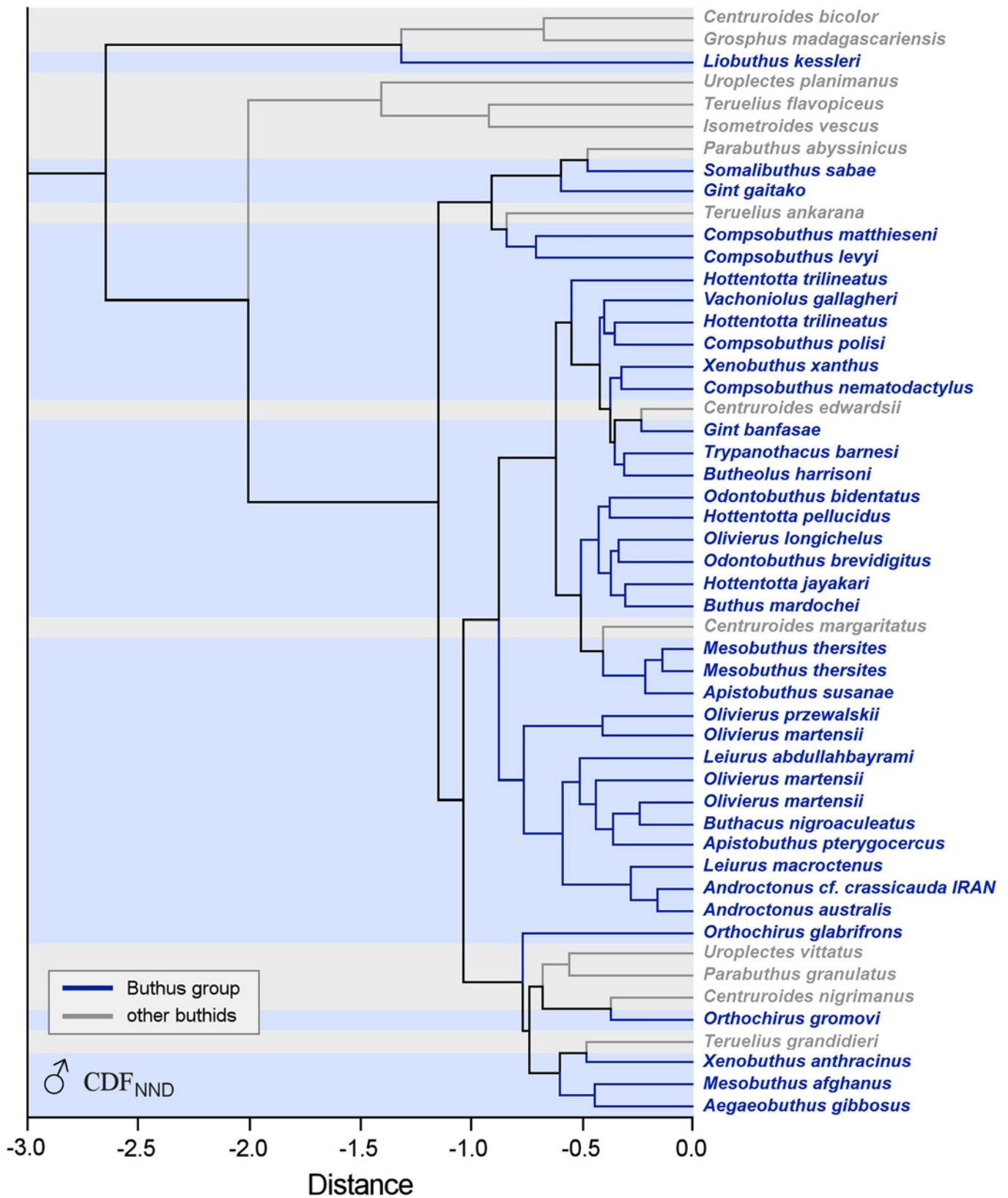


Figure 216. Hierarchical cluster analysis of nearest neighbor distances (NND) between macrosetae on external pedipalp femur of buthids. Ultrametric tree obtained from by application of UPGMA algorithm to Euclidean distances between cumulative distribution functions of nearest neighbor distances of macrosetae of males. Blue terminals, ‘Buthus’ group; gray terminals, other buthids. Each terminal represents one femur.

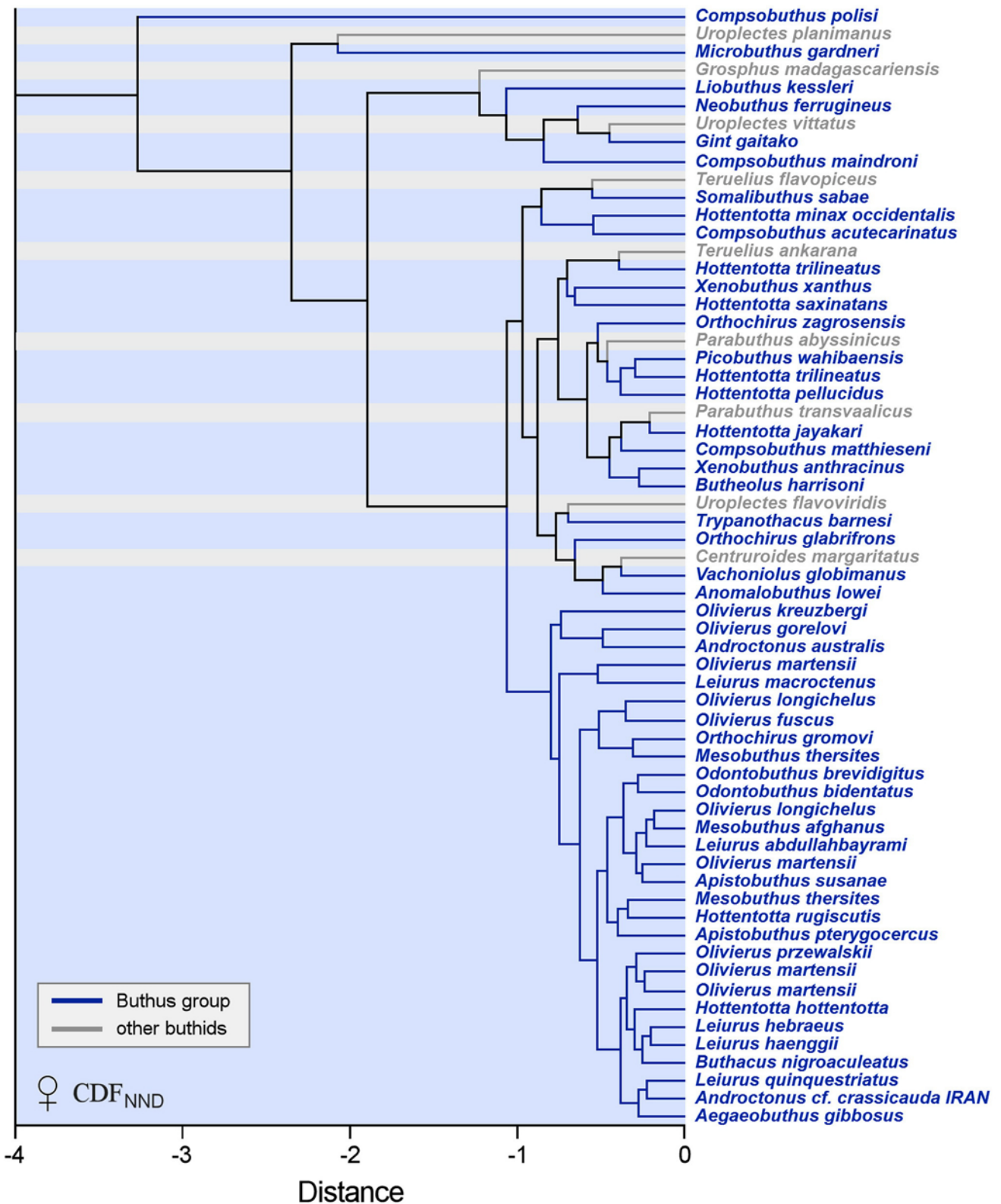
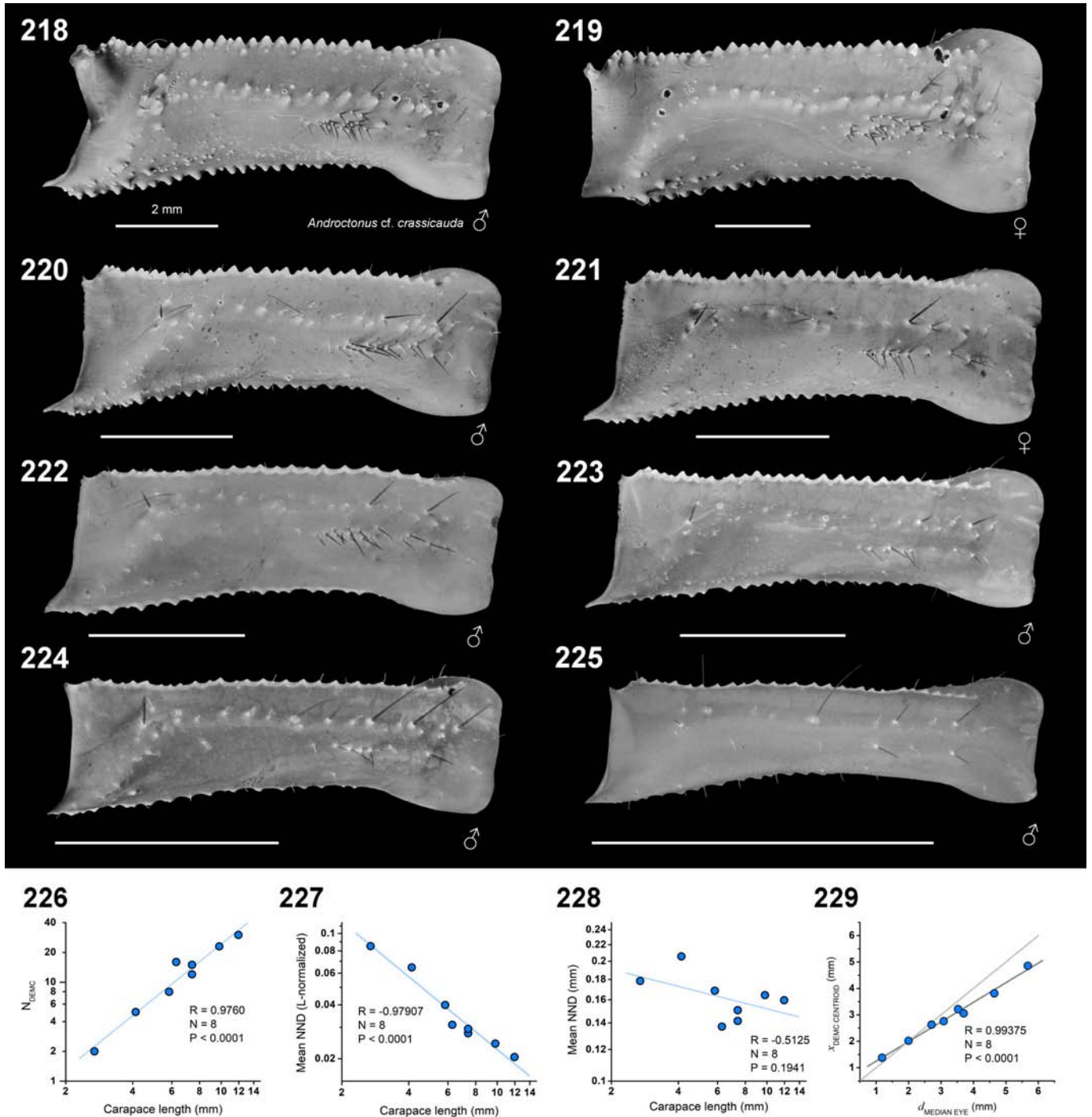


Figure 217. Hierarchical cluster analysis of nearest neighbor distances (NND) between macrosetae on external pedipalp femur of buthids. Ultrametric tree obtained by application of UPGMA algorithm to Euclidean distances between cumulative distribution functions of nearest neighbor distances of macrosetae of females. Blue terminals, ‘Buthus’ group; gray terminals, other buthids. Each terminal represents one femur.

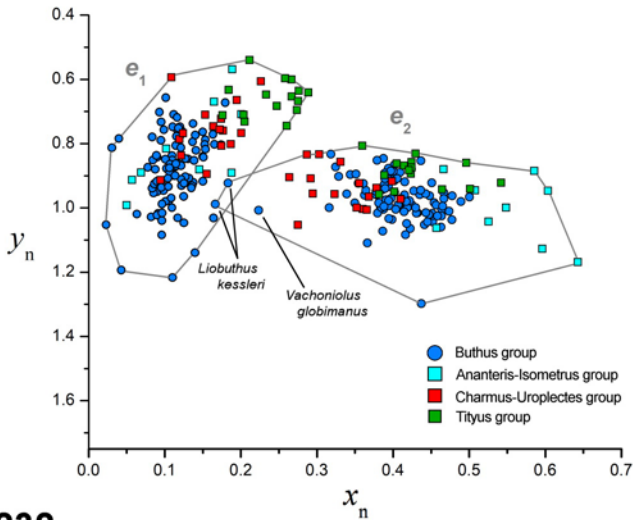


Figures 218–229. Ontogenetic variation of distal external macrosetal cluster (DEMC) in *Androctonus cf. crassicauda* (Oman). **Figures 218–225.** External aspect of pedipalp femur of adult male (218), adult female (219), subadult male (220), subadult female (221), and juvenile male (222–225) instars. Scale bars: 2 mm. UV fluorescence. **Figures 226–228.** Ontogenetic scaling of number and density of DEMC macrosetae. **Figure 226.** Number of DEMC macrosetae vs. carapace length. **Figure 227.** L-normalized mean nearest neighbor distance (NND) vs. carapace length. **Figure 228.** Mean absolute nearest neighbor distance (NND) vs. carapace length. **Figure 229.** Scatter plot showing matching of proximodistal coordinate of DEMC centroid ($x_{\text{DEMC CENTROID}}$) to distance of median eye from ipsilateral anterolateral vertex of carapace ($d_{\text{MEDIAN EYE}}$). R: Pearson’s correlation coefficient.

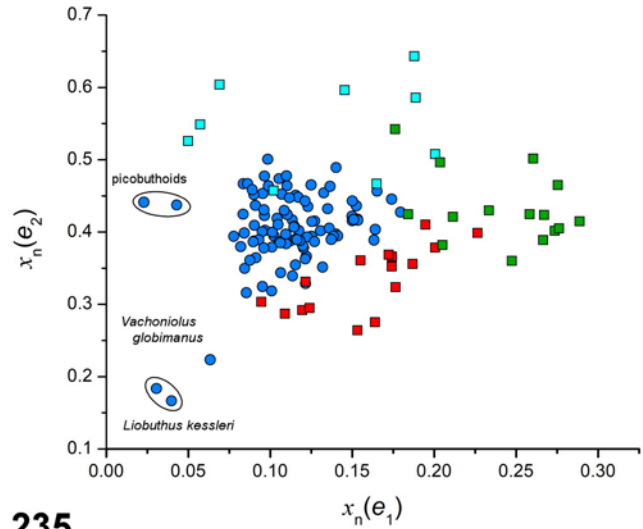
are plotted in Fig. 230. Their territories of distribution in 139 femora from 85 species of buthid were almost non-overlapping, except for e_2 intruding into e_1 territory in the two samples of *Liobuthus kessleri*. This species is neobothriotaxic,

with four external trichobothria (Figs. 50, 170), and the one designated as e_2 by taxonomists may not be homologous with orthobothriotaxic e_2 . If *Liobuthus e_2* is an ‘accessory’ (i.e., supernumerary) trichobothrium, and either e_3 or e_4 are

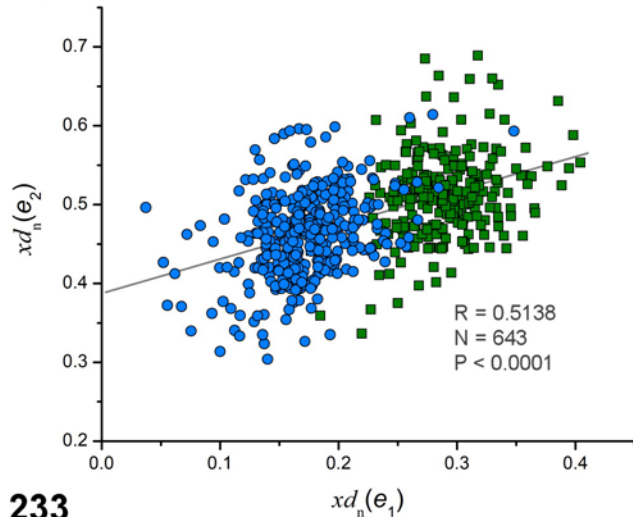
230



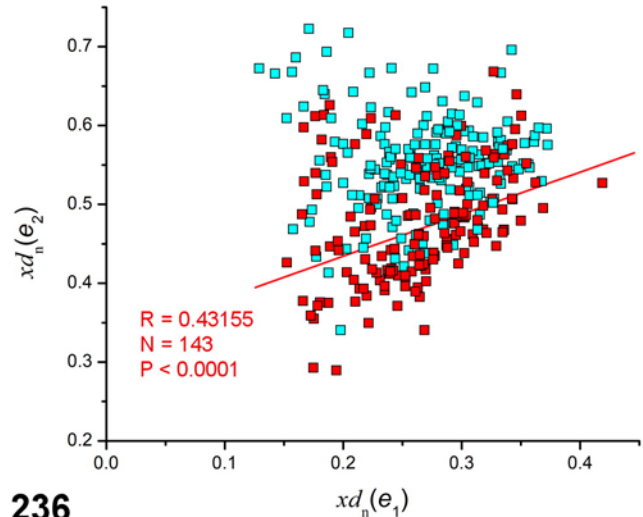
231



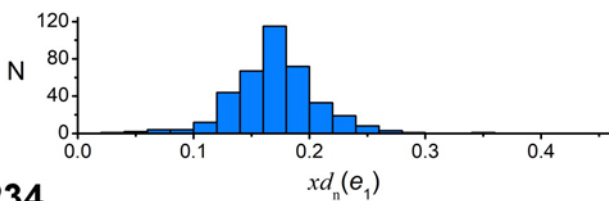
232



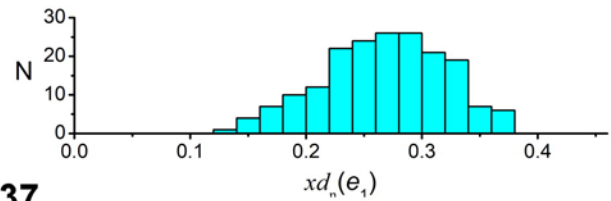
235



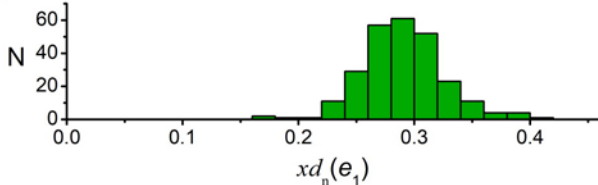
233



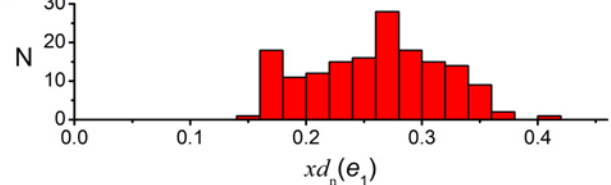
236



234



237



Figures 230–237. Variation in positions of trichobothria e_1 and e_2 on external pedipalp femur of buthids. **Figures 230–231.** Scatter plots of normalized e_1 and e_2 positions extracted from UV fluorescence images of 139 examined femora (same sample as in Figs. 188 and 192). **Figure 230.** Cumulative scatter plot of proximidistal and dorsoventral positions of e_1 and e_2 in L/D-normalized morphospace ($x_n = x/L$, $y_n = y/D$). **Figure 231.** Cumulative scatter plot of proximidistal positions of e_1 and e_2 in L-normalized morphospace ($x_n = x/L$). Taxa with extreme proximal e_1 or e_2 are labeled. **Figures 232–237.** Plots of proximidistal positions of e_1 and e_2 extracted from 988 published trichobothrial configurations of buthid femora (850 species, 267 photographs, 721 illustrations). Coordinates xd_n measured relative to dorsal trichobothrium d_1 , and normalized by distance between d_1 and distal limit of femur. **Figures 232–234.** ‘Buthus’ group (N = 386; 349 species, 44 genera; 219 ♂, 147 ♀, 6 sex unspecified) and ‘Tityus’ group (N = 257; 196 species, 13 genera; 132 ♂, 119 ♀, 6 sex unspecified): cumulative scatter plot of positions of e_1 and e_2 (232), and histograms showing proximidistal distributions in ‘Buthus’ group (233) and ‘Tityus’ group (234). **Figures 235–237.** ‘Ananteris–Isometrus’ group (N = 202; 180 species, 18 genera; 93 ♂, 103 ♀, 5 sex unspecified) and ‘Charmus–Uroplectes’ group (N = 143; 125 species, 18 genera; 65 ♂, 73 ♀, 5 sex unspecified), cumulative scatter plot of positions of e_1 and e_2 (235), and histograms showing proximidistal distributions in ‘Ananteris–Isometrus’ group (236) and ‘Charmus–Uroplectes’ group (237). Scatter plot symbol and histogram bar colors: blue circles, ‘Buthus’ group; cyan squares, ‘Ananteris–Isometrus’ group; red squares, ‘Charmus–Uroplectes’; green squares, ‘Tityus’ group. In the histograms, the ordinate N = number of femora in each abscissa bin.

homologous with orthobothriotaxic e_2 , then the two regions of distribution would be completely non-overlapping. In that case, the species with e_2 closest to e_1 territory would become *Vachoniolus globimanus*, a member of an unusual genus with a strongly abbreviated femur in which e_2 is proximal to d_5 (Lowe, 2010b; Vachon, 1979). The distributions of e_1 and e_2 within their territories appear to be non-uniform with respect to the major buthid lineages. For example, the ‘Buthus’ and ‘Tityus’ groups show partial separation of e_1 along x_n - and y_n -axes, and the ‘Ananteris-Isometrus’ and ‘Charmus-Uroplectes’ groups show partial separation of e_2 along the x_n -axis. Separation of the groups becomes more apparent in a scatter plot of x_n coordinates of e_2 vs. e_1 (Fig. 231). Positions of e_1 are more distal in the ‘Tityus’ group, than in the ‘Buthus’ group; and positions of e_2 are more distal in the ‘Ananteris-Isometrus’ group, than in the ‘Charmus-Uroplectes’ group. *Liobuthus* and *Vachoniolus* are again outliers, as are the picobuthoids, *Microbuthus* and *Picobuthus*.

In Fig. 231, the number of samples of buthids not belonging to the ‘Buthus’ group is relatively small, raising the risk of sampling bias. To obtain a more significant test of group separation, we analyzed a more extensive dataset of proximodistal positions of e_1 and e_2 compiled from published trichobothrial maps. Since maps of the femur are usually shown in dorsal view, the proximal limit of the external carina was not a reliable reference point for distance measurements. Instead, we set the origin of the x -axis at trichobothrium d_1 , and defined coordinate $xd_n(e_i)$ as the proximodistal separation of e_i and d_1 ($i=1,2$), normalized by the distance between the distal end of the femur and d_1 . We compiled e_1 and e_2 coordinates from 988 illustrated or photographed femora of 850 species of buthid. This larger dataset confirmed the major separation of e_1 positions and minor separation of e_2 positions of ‘Buthus’ vs. ‘Tityus’ groups with minor overlap (xd_n mean \pm SD: e_1 : 0.171 ± 0.037 vs. 0.290 ± 0.036 ; e_2 : 0.462 ± 0.053 vs. 0.512 ± 0.052) (Figs. 232–234). Collectively, the position of e_1 was positively correlated with that of e_2 (slope = 0.4329, $R = 0.5138$). On the other hand, there was complete overlap of e_1 positions and only minor separation of e_2 positions of ‘Ananteris-Isometrus’ vs. ‘Charmus-Uroplectes’ groups (xd_n mean \pm SD: e_1 : 0.265 ± 0.053 vs. 0.262 ± 0.055 , $P = 0.609$, Mann-Whitney U test; e_2 : 0.552 ± 0.061 vs. 0.467 ± 0.069) (Figs. 235–237). Position of e_1 was positively correlated with that of e_2 (slope = 0.53342, $R = 0.43155$) in the ‘Charmus-Uroplectes’ group, but not in the ‘Ananteris-Isometrus’ group ($P = 0.93294$).

The strength of a meta-analysis depends on the accuracy of the published data used as input. It is vulnerable to corruption of data by errors or fraud, which may invalidate the results. To test the integrity of the data, we compared statistical estimates derived from trichobothrial maps published as illustrations, against those published as photographs. We reasoned that errors are more likely in illustrations, which depend on observation and recording by authors, than in photographs recorded by a camera. In the ‘Buthus’ group, mean values of xd_n from illustrations ($N = 212$) and photographs ($N = 174$) did not differ significantly for either e_1 or e_2 ($P = 0.069$ and 0.050 ,

Mann-Whitney U test). In the ‘Tityus’ group there was also no significant difference between illustrations ($N = 288$) and photographs ($N = 29$) for either e_1 or e_2 ($P = 0.697$ and 0.264 , Mann-Whitney U test). Similar positive collective correlations of e_2 vs. e_1 for the two groups were estimated from illustrations and photographs (slope = 0.40983, $R = 0.4981$, $N = 440$, $P < 0.0001$; and slope = 0.45926, $R = 0.4550$, $N = 203$, $P = 0.00054$, respectively). In the ‘Ananteris-Isometrus’ group, there was a significant difference between illustrations ($N = 152$) and photographs ($N = 33$) for e_1 but not e_2 ($P = 0.00002$ and 0.415 , Mann-Whitney U test). In the ‘Charmus-Uroplectes’ group there was a significant difference between illustrations ($N = 129$) and photographs ($N = 31$) for both e_1 and e_2 ($P = 0.003$ and 0.00001 , Mann-Whitney U test). Different positive correlations of e_2 vs. e_1 were found for illustrations and photographs (Pearson’s $R = 0.245$, and 0.586). We attributed the differences between illustrations and photographs seen in the ‘Ananteris-Isometrus’ and ‘Charmus-Uroplectes’ groups to the relatively small sample sizes of photographs which strongly skewed the sampling of genera. Taking this into consideration, we have no evidence of widespread systematic errors in published data that would invalidate our general conclusions, although errors cannot be ruled out. For example, two errors in illustrated trichobothrial maps were detected in the descriptions of *Ananteris dacostai* and *A. tresor* (Ythier et al., 2020: 27, figs. 11A, 11H). In the figures, e_1 and e_2 appear in the proximal 1/3 of the femur, an anomalous pattern that deviates from that of other known members of the genus, and indeed of the entire buthid family. We initially flagged these as extreme outliers in a preliminary version of Fig. 235. Photographs in the same paper (Ythier et al., 2020: 9, 24, figs. 2, 10) show trichobothrial patterns of the two species visible as pale spots on base fuscidity, in which e_1 and e_2 appear to be located in more distal positions standard for the genus. These photographic positions were substituted into our compiled data, purging the extreme outliers.

Patterns of macrosetae on the distal ventral surface of the pedipalp movable finger

We studied setation on the ventral movable finger by UV fluorescence imaging. Figs. 238–239 show ventral views of the movable finger of the buthid, *Apistobuthus pterygocercus*. Numerous macrosetae are visible, distinguishable from microsetae by their lack of fluorescence (Lowe & Fet, 2024). At the base of the finger, macrosetae are long, sparse and irregular; along the length of the finger, they are short, dense and more regular, being arranged in roughly two longitudinal rows. The finger tapers gradually along most of its length, but is transversely dilated near the tip. The density of ventral macrosetae increases abruptly on the distal dilation, and we refer to this patch of dense setation as the ‘distal ventral macrosetal cluster’ (DVMC). Immediately proximal to the tip of the finger, the DVMC bends inward, wrapping around the ventrointernal surface of the finger, and is tapered at its apex (Figs. 239–240). Figs. 241–242 show ventral views of the movable finger of another buthid, *Androctonus australis*.

Numerous short macrosetae are arranged in two rows along the length of the finger. As the rows approach the tip, they coalesce into a single row whose density increases abruptly in the distal zone, forming an elongated patch, the DVMC. This DVMC also wraps around the ventrointernal surface at the tip of the finger, but without tapering (Fig. 243).

Although differing in some details, the DVMCs of *Apistobuthus* and *Androctonus* share a common basic layout, suggesting homologous structures. Does this distinctive setation pattern, with DVMC, occur in other buthids, or other scorpion families? To address this question, we examined the distal ventral movable finger of 82 species (39 genera) of buthids, and 36 species (31 genera) of non-buthids. We sampled all four major buthid lineages and 15 non-buthid families.

BUTHIDAE. BUTHUS GROUP (Figs. 238–335, 348–350). *Aegaobuthus gibbosus*, *Androctonus australis*, *Androctonus* cf. *crassicauda* (Iran), *Anomalobuthus lowei*, *Apistobuthus pterygocercus*, *Apistobuthus susanae*, *Buthacus nigroaculeatus*, *Butheolus gallagheri*, *Butheolus harrisoni*, *Buthus mardochei*, *Compsobuthus acutecarinatus*, *Compsobuthus levyi*, *Compsobuthus maindroni*, *Compsobuthus matthiesseni*, *Compsobuthus nematodactylus*, *Compsobuthus polisi*, *Gint gaitako*, *Hottentotta hottentotta*, *Hottentotta jakyari*, *Hottentotta minax occidentalis*, *Hottentotta pellucidus*, *Hottentotta saxinatans*, *Hottentotta trilineatus*, *Kraepelinia palpator*, *Leiurus abdullahbayrami*, *Leiurus haenggii*, *Leiurus hebraeus*, *Leiurus macroctenus*, *Liobuthus kessleri*, *Mesobuthus afghanus*, *Mesobuthus thersites*, *Microbuthus gardneri*, *Neobuthus amoudensis*, *Neobuthus ferrugineus*, *Odontobuthus bidentatus*, *Odontobuthus brevidigitus*, *Olivierus fuscus*, *Olivierus gorelovi*, *Olivierus kreuzbergi*, *Olivierus longichelus*, *Olivierus martensii*, *Olivierus przewalskii*, *Orthochirus glabrifrons*, *Orthochirus gromovi*, *Picobuthus wahibaensis*, *Razianus zarudnyi*, *Somalibuthus sabae*, *Trypanothacus barnesi*, and *Vachoniolus globimanus*: subdistal ventral surface of movable finger with macrosetae arranged either (i) more or less regularly in two longitudinal rows, or (ii) irregularly in longitudinal strip 2–4 setae wide, of approximately constant density along the finger; distal ventral surface with patch of higher density of setation, the DVMC; immediately proximal to tip of finger, DVMC bent inward, wrapping around ventrointernal surface, with ventroexternal carina of finger also bent inwards apically, thickening and capping the finger; DVMC associated with distal dilation only in *Apistobuthus* (Figs. 239, 252, 256, 258), relatively sparse in *Kraepelinia*, not much denser than subapical setation (Fig. 348), absent in picobuthoids, *Microbuthus* and *Picobuthus* (Figs. 349–350); apical and subapical setae with truncate, digitate tips in *Razianus* (Figs. 328–329); apical setae with truncate, bifid tips in *Compsobuthus maindroni* (Figs. 270–271) and *C. polisi* (Figs. 278–279).

BUTHIDAE. ANANTERIS-ISOMETRUS GROUP (Figs. 351–357). *Babycurus centrurimorphus*, *Isometroides vesus*, *Isometrus maculatus*, *Langxie feti*, *Lychas mucronatus*, *Lychas scutillus*, and *Reddyanus bilyi*: subdistal ventral surface of movable finger with macrosetae arranged regularly in single

row in *Lychas* and *Reddyanus* (Figs. 355–357), regularly in two rows in *Isometroides* and *Langxie* (Figs. 353–354), or irregularly in *Babycurus* (Fig. 351); macrosetae sparse or absent in *Isometrus* (Fig. 353); distal setation not significantly denser than subdistal, i.e., DVMC absent; apical setae with truncate, bifid tips in *Langxie feti*, *Lychas mucronatus*, *Lychas scutillus*, and *Reddyanus bilyi* (Figs. 354–357).

BUTHIDAE. CHARMUS-UROPLECTES GROUP (Figs. 336–343, 358–359). *Grosphus madagascariensis*, *Parabuthus abyssinicus*, *Parabuthus granulatus*, *Parabuthus transvaalicus*, *Teruelius ankarana*, *Teruelius flavopiceus*, *Teruelius grandidieri*, *Uroplectes flavoviridis*, *Uroplectes planimanus*, and *Uroplectes vittatus*: subdistal ventral surface of movable finger with macrosetae arranged in two dense longitudinal strips separated by ventromedian carina in *Parabuthus* (Figs. 336–339), or dense and irregular in *Teruelius*, *Grosphus*, and *Uroplectes* (Figs. 340–343, 358–359); distally, two longitudinal strips remaining separated in *Parabuthus*, ventromedian carina thickening and capping finger; DVMC ventrointernal when present; DVMC present in *Parabuthus* and *Teruelius* (Figs. 336–343), weak in *Uroplectes* (Fig. 359), absent in *Grosphus* (Fig. 358).

BUTHIDAE. TITYUS GROUP (Figs. 344–347, 360–365). *Alayotityus sierramaestrae*, *Centruroides bicolor*, *Centruroides edwardsii*, *Centruroides gracilis*, *Centruroides koesteri*, *Centruroides margaritatus*, *Centruroides nigrimanus*, *Heteroctenus junceus*, *Microtityus jaumei*, *Tityus championi*, *Tityus dedoslargos*, and *Tityus ecuadorensis*: subdistal ventral surface of movable finger with macrosetae arranged more or less regularly in two rows, separated by a weak ventromedian carina, in *Alayotityus*, *Centruroides*, *Heteroctenus* and *Tityus ecuadorensis* (Figs. 344–347, 360–362; *T. ecuadorensis* not shown); macrosetae sparse or absent in *Tityus championi* and *T. dedoslargos* (Figs. 364–365); fluorescent microsetae (Type ‘F’; Lowe & Fet, 2024) much more numerous than non-fluorescent (Type ‘N’) macrosetae in *Tityus* vs. *Centruroides* and *Heteroctenus*; DVMC ventrointernal when present; DVMC present in *Centruroides edwardsii* and *C. koesteri* (Figs. 344–347), weak in *C. bicolor* (Fig. 361), absent in *Heteroctenus* (Fig. 362).

NON-BUTHIDS (Figs. 366–398). *Chaerilus hofereki*; **PSEUDOCHACTIDAE**: *Pseudochactas ovchinnikovi* and *Qianxie solegladi*; **BOTHRIURIDAE**: *Brachistosternus artigasi*, *Brachistosternus donosoi*, and *Brachistosternus mattonii*; **ANUROCTONIDAE**: *Anuroctonus phaiodactylus*; **BELISARIIDAE**: *Belisarius xambeui*; **CHACTIDAE**: *Brotheas gervaisii* and *Brotheas granimanus*; **EUSCORPIIDAE**: *Euscorpium deltshevi*; **CARABOCTONIDAE**: *Hadrurides maculatus*; **HADRURIDAE**: *Hadrurus obscurus*; **IURIDAE**: *Iurus dufourei*; **SCORPIOPIIDAE**: *Scorpiops* cf. *tibetanus*; **VAEJOVIDAE**: *Catalinia andreas*, *Chihuahuanus crassimanus*, *Kochius hirsuticauda*, *Kovarikia angelena*, *Paravaejovis spinigerus*, *Paruroctonus gracilior*, *Paruroctonus hirsutipes*, *Pseudouroctonus apacheanus*, *Serradigitus torridus*, *Smeringurus mesaensis*, *Smeringurus vachoni*, *Stahnkeus subtilimanus*, and *Vejovoidus longiunguis*;

HORMURIDAE: *Hadogenes troglodytes* and *Hormurus waigiensis*; DIPLOCENTRIDAE: *Diplocentrus whitei*; SCORPIONIDAE: *Opisthophthalmus glabrifrons*, *Pandinoides cavimanus* and *Pandinus imperator*; URODACIDAE: *Urodacus hoplurus* and *Urodacus novaehollandiae*: subdistal ventral surface of movable finger with macrosetae sparse or absent in *Chaerilus*, *Pseudochactas*, *Qianxie*, *Brachistosternus*, *Anuroctonus*, *Belisarius*, *Brotheas*, and *Hadrurides* (Figs. 366–373, 375), arranged in two sparse rows in *Euscorpis*, *Scorpiops*, *Hadrurus*, *Iurus*, vaejovids, hormurids, *Opisthophthalmus* and *Urodacus* (Figs. 374, 376–394, 396, 398), in three rows in *Pandinoides* (Fig. 397), or dense and irregular in *Diplocentrus* (Fig. 395); DVMC absent in all examined taxa except for *Vejovoidus*, in which it bends inward, over the ventrointernal surface (Figs. 391–392); ventroexternal carina of finger bent inwards apically, thickening and capping the finger in *Chihuahuanus*, *Kochius*, *Paravaejovis*, *Paruroctonus*, *Smeringurus*, and *Vejovoidus* (Figs. 380–384, 388–392).

In summary, the DVMC was prevalent among buthids of the ‘Buthus’ group. In *Kraepelinia* and the very small picobuthoids, it was sparse or absent. Among examined taxa from other buthid lineages, a DVMC was present in *Parabuthus*, *Teruelius* and some *Centruroides*, and was weakly developed in *Uroplectes*. In the examined non-buthids, a DVMC was absent except in *Vejovoidus*.

Morphometric analysis of macrosetal patterns on the distal ventral surface of the pedipalp movable finger

To quantify the clustering of macrosetae on the distal ventral movable finger, we recorded positions of setae in a 2D coordinate system superimposed on images of the distal finger (Figs. 399, 402). The finger was rotated to horizontally level the distal section of the finger in UV fluorescence images, and macrosetal sockets were marked for digitization. Proximodistal setal coordinates, x , were measured relative to the most proximal macroseta in the image; transverse setal coordinates, y , were measured relative to an arbitrary line on the internal side of the finger (on the bounding box of the image). Values of x and y were both normalized by length of finger section, L , measured with respect to the the most proximal macroseta in the image. A plot of L -normalized coordinates (x_n, y_n) was generated, and the marginal cumulative distribution function, CDF_x , was calculated and superimposed (Figs. 400, 403). A cutoff value was manually set along the x_n -axis to define and separate the DVMC from the subdistal section of the finger for analysis. Variability and complexity of setation patterns precluded a general automatic criterion to set the position of cutoff. We followed an empirical procedure, selecting the point where the longitudinal strip of setae on the more proximal section either (i) increased in width, or (ii) bent internally; or if neither (i) nor (ii), then the point where the slope of CDF_x abruptly increased, indicating a step increase in the density of setation. By this procedure, we were able to delimit the

DVMC in the ‘Buthus’ group, and in the other buthids with a DVMC. If a DVMC was not identifiable by the above procedure, we selected the distal 25% of the finger in the images (cutoff = 0.75 L) to obtain a sample of the distal setation for analysis. To quantify clustering, we calculated the cumulative distribution function of nearest neighbor distance, CDF_{NND} , normalized to the distal finger width, w . Measurements of w were taken midway along the DVMC or the distal section (25% L) (Fig. 402), except in *Apistobuthus*, in which w was taken to be the width of DVMC dilation (Fig. 399). The w -normalization method equalizes distal finger widths, facilitating comparison of distal setation densities in fingers with distal sections of varying lengths. CDF_{NND} was calculated for the DVMC, or distal section, and compared to that of the distal section. If the density of setation increased distally, the rising phase of distal CDF_{NND} was left-shifted relative to that of subdistal CDF_{NND} (Figs. 401, 404).

To compare distal clustering across taxa, we evaluated two different measures of clustering: (i) the ratio of macrosetal counts of the distal section, to counts of a subdistal section of equal length; this gauges the relative increase in setation density in the distal section relative to the subdistal section, independent of intrinsic density; and (ii) the mean w -normalized NND of the distal section; this gauges the density of setation relative to finger width, independent of section length. The ranked bar charts in Figs. 405–406 show the variation of these measures in different genera of the three major groups: ‘Buthus’ group, other buthids, and non-buthids. Within each group, genera are plotted in ascending order. Taxa with stronger clustering are positioned towards the right in Fig. 405, and towards the left in Fig. 406. Variation of both clustering measures spanned about one order of magnitude. The distal/ subdistal count ratios of the three groups were broadly overlapped (Fig. 405). Within each group, genera with dense and sparse distal setation were mingled in the ratio-ranked charts. Systematic trends in distal density were masked by independent variation in the denominator of the ratio (subdistal density). Distal mean NNDs of the three groups showed less overlap (Fig. 406) and better resolution of genera. Ordering of distal density was: non-buthids < other buthids < ‘Buthus’ group, with limited overlap between successive groups. Within each group, genera with dense and sparse distal setation were mostly separated. In the ‘Buthus’ group, genera with larger body size were skewed towards the lower left of the chart, suggesting a positive correlation between body size and DVMC density. A similar trend was noted in external femoral setation of the ‘Buthus’ group, with the DEMC being denser in larger genera, and sparser in smaller genera (Fig. 206). A ranked histogram of mean w -normalized NNDs of all examined movable fingers emphasizes the preponderance of smaller NNDs in the ‘Buthus’ group, attributable to presence of a tightly clustered DVMC (Fig. 409).

In the ‘Buthus’ group, the number of macrosetae in the DVMC varied widely, ranging from 11 setae (*Butheolus*, *Orthochirus*) up to 276 setae (*Apistobuthus*). A logarithmic

plot of mean w -normalized NND vs. distal count (Fig. 407) reveals a progressive decrease in the mean NND with increasing number of DVMC setae. The log regression slope was -0.3912 , i.e., much shallower than -1 , implying spatially non-uniform increase in the density of DVMC setation across species. The DVMC of different species can vary in shape, size and distribution of setae on the distal finger (Figs. 244–335). The DVMC appeared relatively denser in larger species and sparser in smaller species, suggesting that clustering varies with size. A logarithmic plot of mean w -normalized NND vs. distal finger width, w (Fig. 408, lower plot) reveals a negative correlation. There was a progressive decrease in mean normalized NND with increasing size, showing that clustering is indeed denser in larger species. The log regression slope was -0.6444 , i.e., shallower than -1 , indicating that the rate of addition of setae was insufficient to maintain an inverse relation of spacing with increasing size. A plot of mean absolute NND (Fig. 203, upper plot, right ordinate) has a positive log regression slope of 0.3556 ($= 1-0.6444$). The increase in the physical spacing of setae from smaller to larger species is relatively modest, 1.8-fold over a 5.4-fold increase in size as quantified by distal finger width. The mean absolute NND over that range was $40.1 \pm 9.4 \mu\text{m}$. The NND scaling relations of the DVMC were similar to those of the DEMC (cf. Figs. 407–408 vs. 202–203). The parallels between clustering of DVMC and DEMC are highlighted in a bivariate plot of their mean normalized NNDs, showing a strong positive correlation, and consistent separation of ‘Buthus’ group taxa from the other groups (Fig. 410).

Ontogenetic variation of the DVMC

Our data showed that both the DVMC and the DEMC tend to be sparser in smaller species. We also found DEMC to be sparser in earlier instars of the same species (*Androctonus* cf. *crassicauda*; Figs. 218–228). Does the DVMC show a similar ontogenetic gradient? Figs. 411–418 show the ontogenetic variation in the DVMC of *Apistobuthus pterygocercus*. The relative size and shape of the area of the distal ventral finger occupied by the DVMC remain roughly the same across immature instars, being similar to those of the adult (Figs. 411–412). The number and density of setae decreased progressively in smaller instars (Fig. 413–417); in the smallest juvenile, only 3 macrosetae were present (Fig. 418). The scatter plots in Figs. 419–421 show the ontogenetic scaling of number and density of DVMC setae (excluding the smallest juvenile): (i) the number of setae in the DVMC was positively correlated with size (measured by carapace length) (Fig. 419); (ii) the L-normalized mean NND (inverse measure of relative density) was negatively correlated with size (Fig. 420); and (iii) the mean absolute NND was uncorrelated with size ($P > 0.050$; mean \pm SD = $37.4 \pm 3.3 \mu\text{m}$) (Fig. 421). As the scorpion grows and molts, setae are added to maintain nearly constant physical spacing of setae.

Cuticular structure of the DVMC.

Figs. 422–423 show macrosetae in cross sections of the ventral cuticle of the DVMC of an adult *Apistobuthus pterygocercus* viewed under a light microscope. In Fig. 422, the chitinous macrosetal shafts and finger cuticle appear bright and refractile under differential interference contrast. The basal sockets of the setae connect to the finger lumen via darker canals or voids traversing the thick layers of mesocuticle or endocuticle. The canals are characteristic of sensory setae, allowing hair shafts to connect to sensory neurons (Foelix & Schabronath, 1983). Under UV illumination, an intensely fluorescent hyaline exocuticle (thickness $\sim 5 \mu\text{m}$) is visible on the surface (Fig. 423). Strong fluorescence is also present on the basal portions of the macrosetae, as described for sensilla classified as ‘Type N’ in Lowe & Fet (2024).

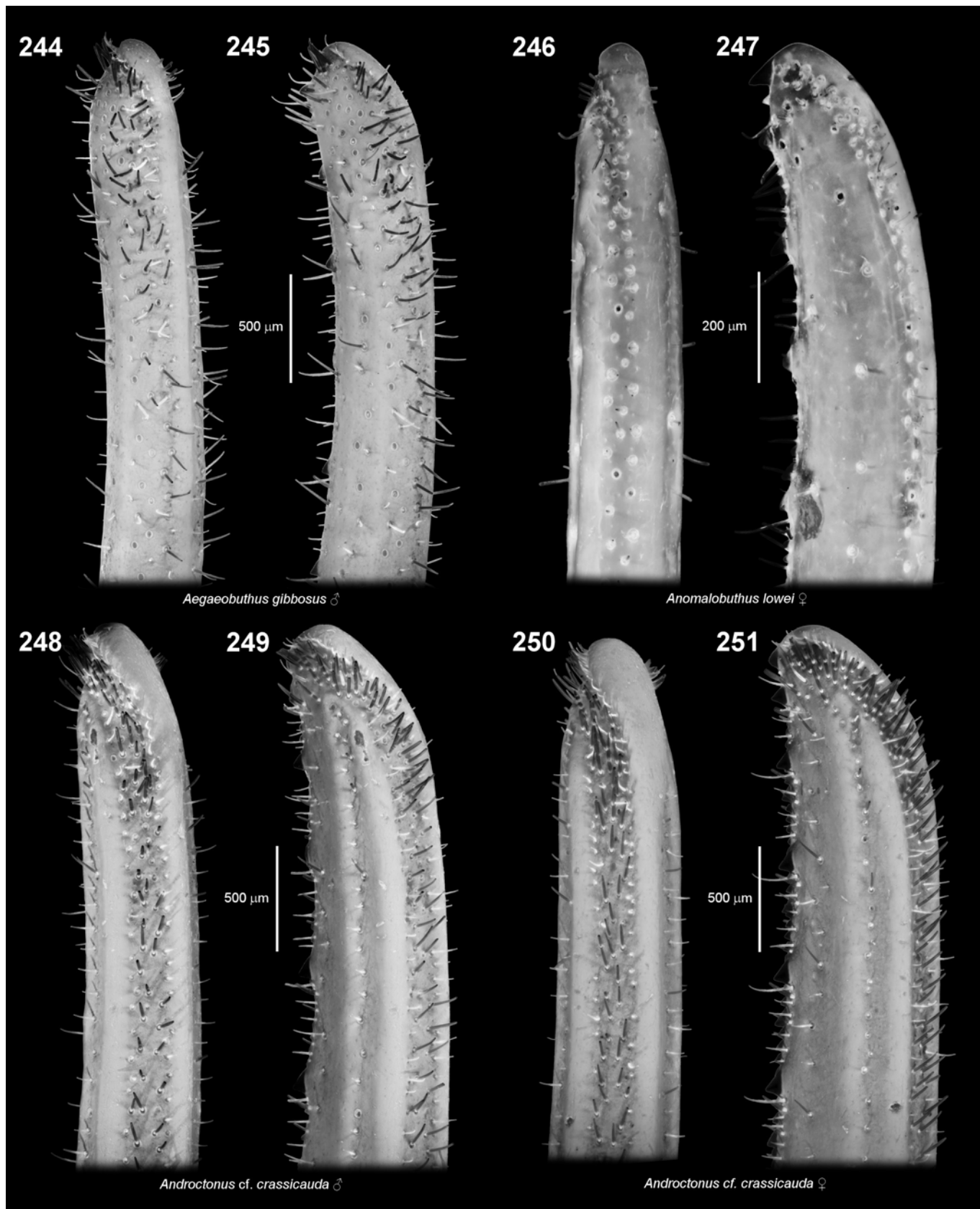
DEMC and DVMC in ocular grooming.

Socketed macrosetae of scorpions are presumed to be mechanoreceptive (Foelix & Schabronath, 1983; Kladt et al., 2007; Rao, 1964). The pedipalps of many species bear numerous macrosetae that could serve general tactile functions (Lowe & Fet, 2024). Particularly intriguing are dense local clusters of setae, such as DEMC and DVMC, that appear to be adapted for specialized functions. The location of the DVMC at the ventrodistal apex of the movable finger suggests that it may play an important role in probing the substrate ahead of the animal as it explores its environment. Sensory functions of the DEMC, located on the external femur, are less evident. Clues may lie in the non-sensory functions of clustered setae on appendages of other arthropods. Setal brushes, combs and spurs on appendages are widely used as tools to groom and clean sensory organs, other appendages, and body surfaces in insects (Basibuyuk & Quicke, 195; Hlavac, 1975; Reborá et al., 2019) and crustaceans (Bauer, 1981, 2013; Wortham & Kostecka, 2019). In arachnids, specialized grooming tools include the cleaning organ on the pedipalp tarsus of amblypygids (Chiriví-Joya et al., 2021; Lawrence, 1968) and the comb-like serrulae on the chelicerae of pseudoscorpions (Chamberlin, 1931; Endel, 2012). Scorpions engage in protracted grooming rituals termed ‘sponge-bathing’, in which the pedipalps, legs and telson spread an oral exudate over the appendages and body (Constantinou, 1985; Rosin & Shulov, 1962; Shulov & Amitai, 1960; Williams, 1966). Specialized cleaning organs were not mentioned in previous descriptions of scorpion sponge-bathing. However, Locket (2001) reported anecdotal observations of Fleissner & Fleissner describing a role for DEMC in ocular grooming:

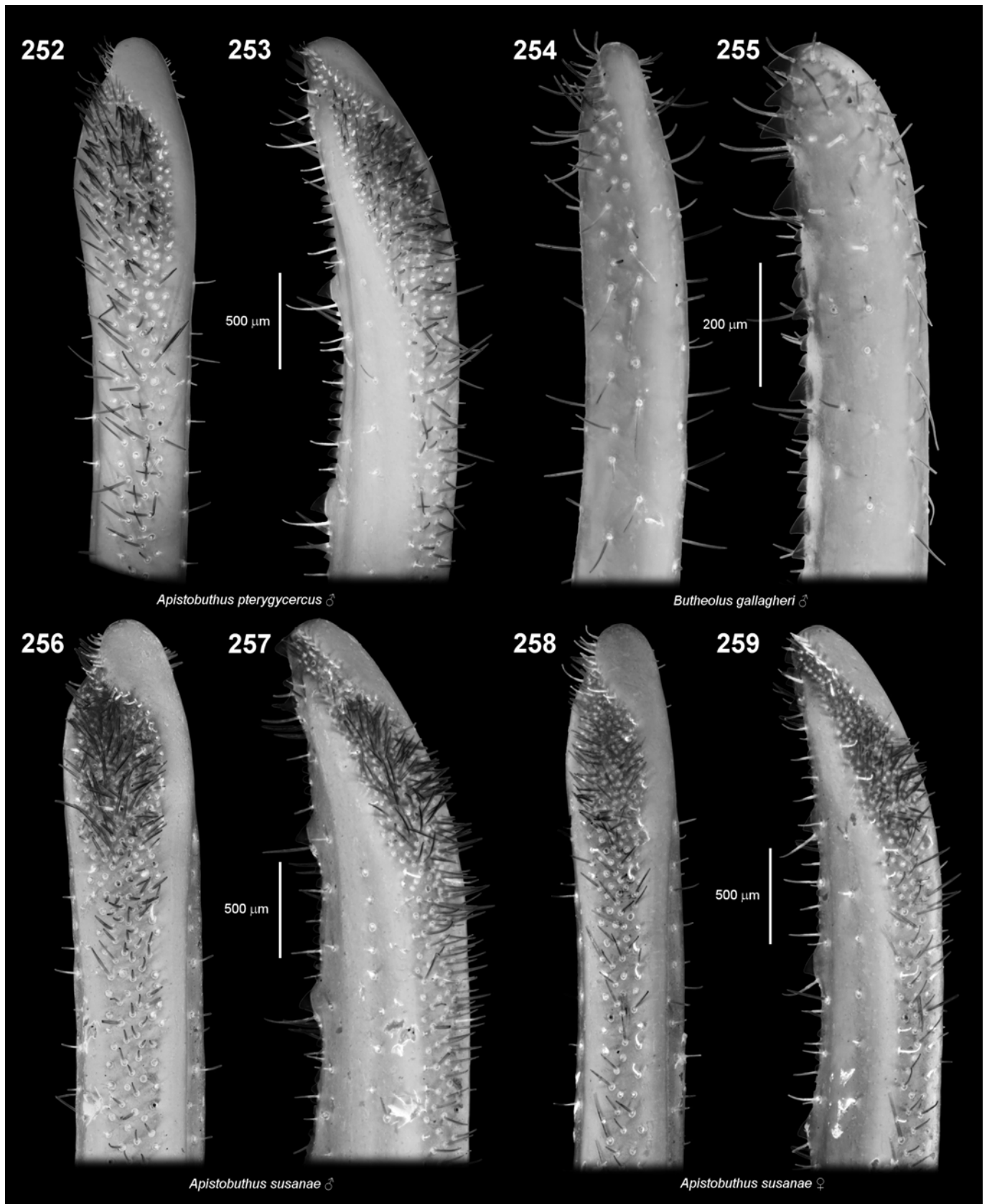
“Fleissner and Fleissner (personal communication) have observed that the lenses in the buthids *Androctonus australis* and *Buthus occitanus* remain clean even when the rest of the scorpion is dusty. They have found a small brush of setae beneath the femur of the pedipalp which works across the ocular eminence when scorpion assumes a resting position, brushing dust from the surface of the median eyes. This brush is present in many buthids and some other scorpions.” (Locket, 2001: 83).



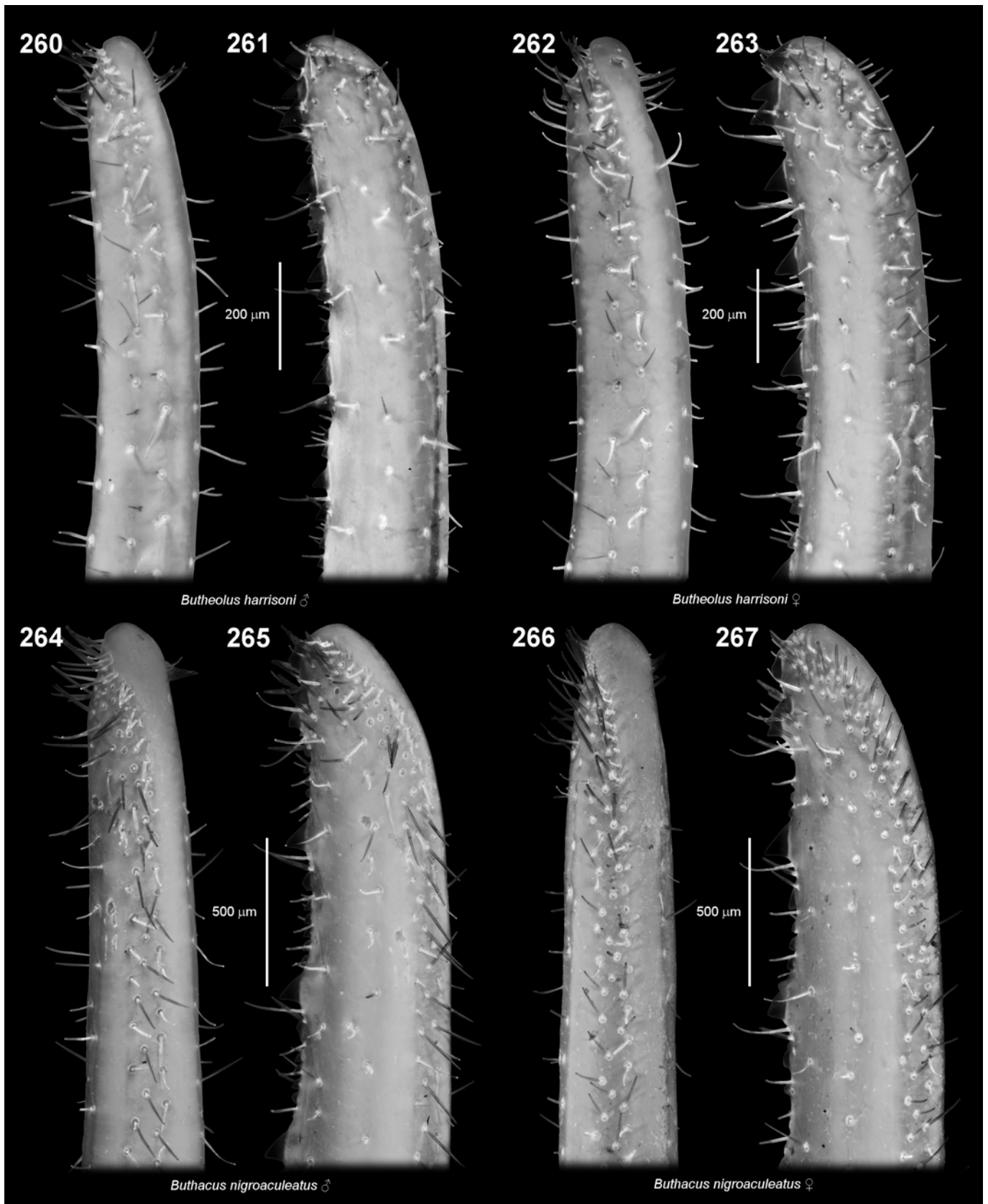
Figures 238–243. Setation on ventral surface of movable finger of pedipalp chela. Buthidae, ‘Buthus’ group. **Figures 238–240.** *Apistobuthus pterygocercus*, female, entire movable finger in ventral aspect (238), and distal movable finger in ventral (239) and ventrointernal aspect (240). **Figures 241–243.** *Androctonus australis*, male, entire movable finger in ventral aspect (241), and distal movable finger in ventral (242) and ventrointernal aspect (243). DVMC: distal ventral macrosetal cluster. Scale bars: 2 mm (238, 241), 1 mm (239–240, 242–243). UV fluorescence.



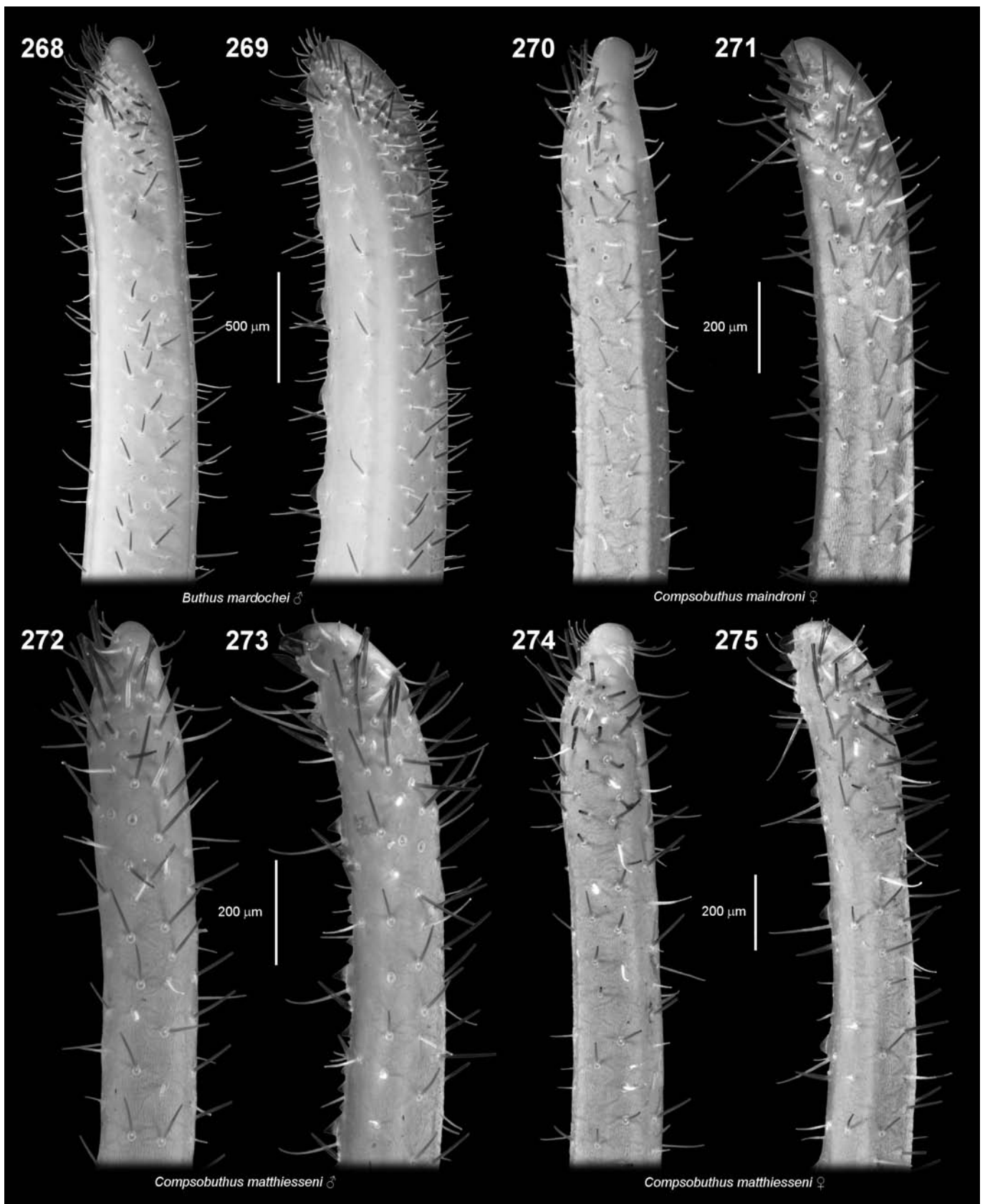
Figures 244–251. Distal movable finger of pedipalp chela. Buthidae, ‘Buthus’ group. **Figures 244–245.** *Aegaeobuthus gibbosus*, male. **Figures 246–247.** *Anomalobuthus lowei*, female. **Figures 248–251.** *Androctonus cf. crassicauda* (Iran), male (248–249) and female (250–251). Ventral (244, 246, 248, 250) and ventrointernal (245, 247, 249, 251) aspects. Scale bars: 500 µm (244–245, 248–251), 200 µm (246–247). UV fluorescence.



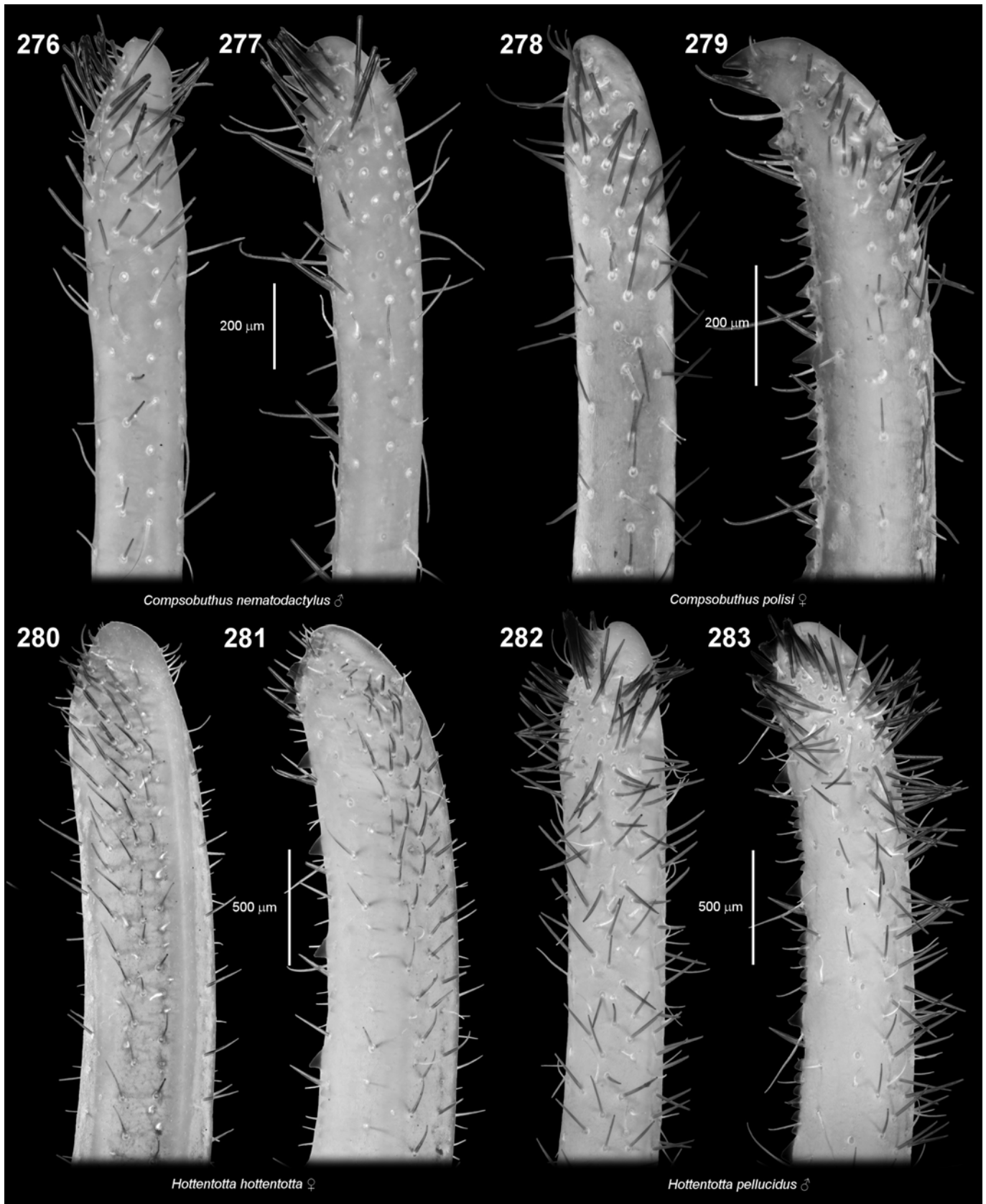
Figures 252–259. Distal movable finger of pedipalp chela. Buthidae, ‘Buthus’ group. **Figures 252–253.** *Apistobuthus pterygocercus*, male. **Figures 254–255.** *Butheolus gallagheri*, female. **Figures 256–259.** *Apistobuthus susanae*, male (256–257) and female (258–259). Ventral (252, 254, 256, 258) and ventrointernal (253, 255, 257, 259) aspects. Scale bars: 500 μm (252–253, 256–259), 200 μm (254–255). UV fluorescence.



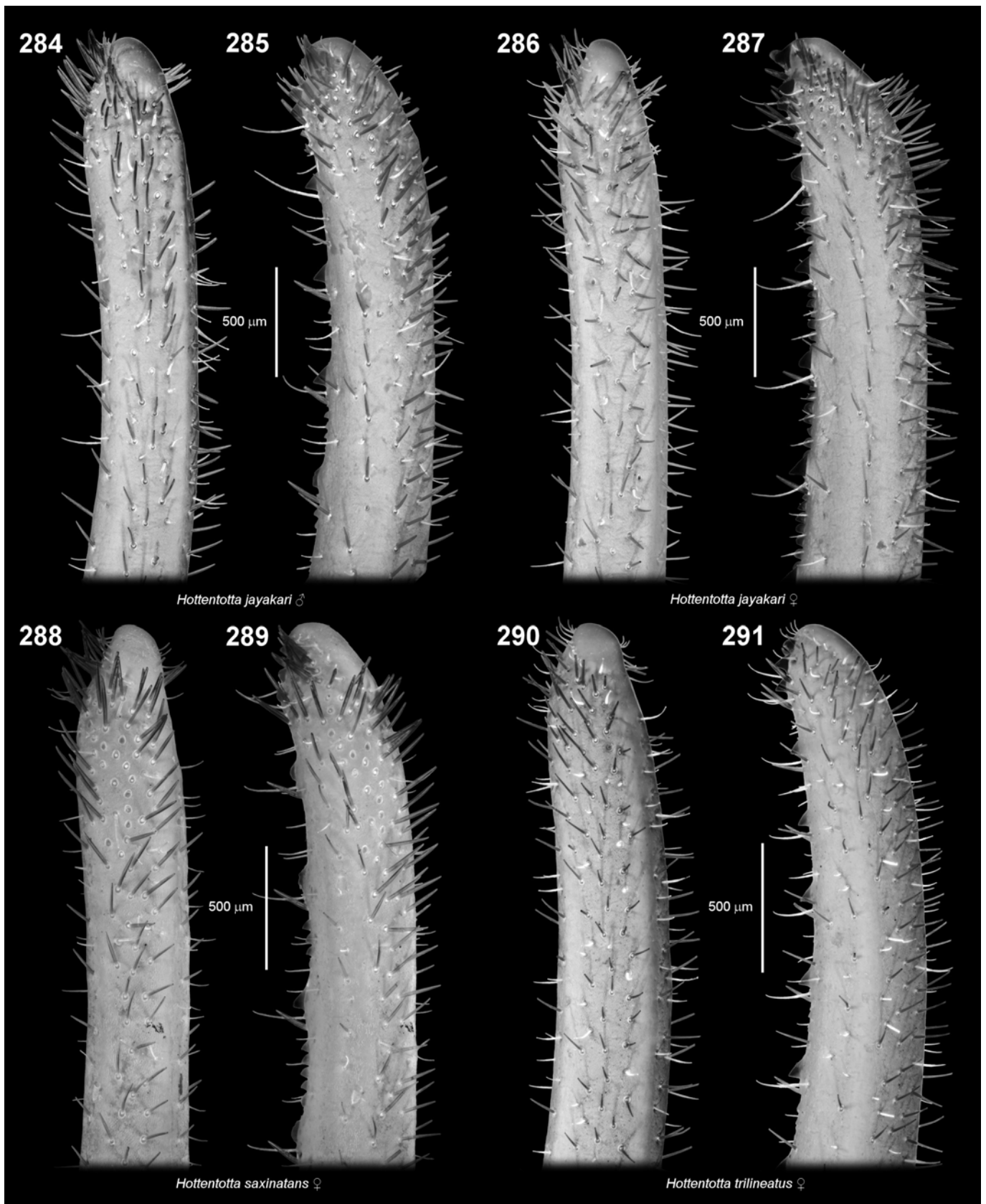
Figures 260–267. Distal movable finger of pedipalp chela. Buthidae, ‘Buthus’ group. **Figures 260–263.** *Butheolus harrisoni*, male (260–261) and female (262–263). **Figures 264–267.** *Buthacus nigroaculeatus*, male (264–265) and female (266–267). Ventral (260, 262, 264, 266) and ventrointernal (261, 263, 265, 267) aspects. Scale bars: 500 μm (264–267), 200 μm (260–263). UV fluorescence.



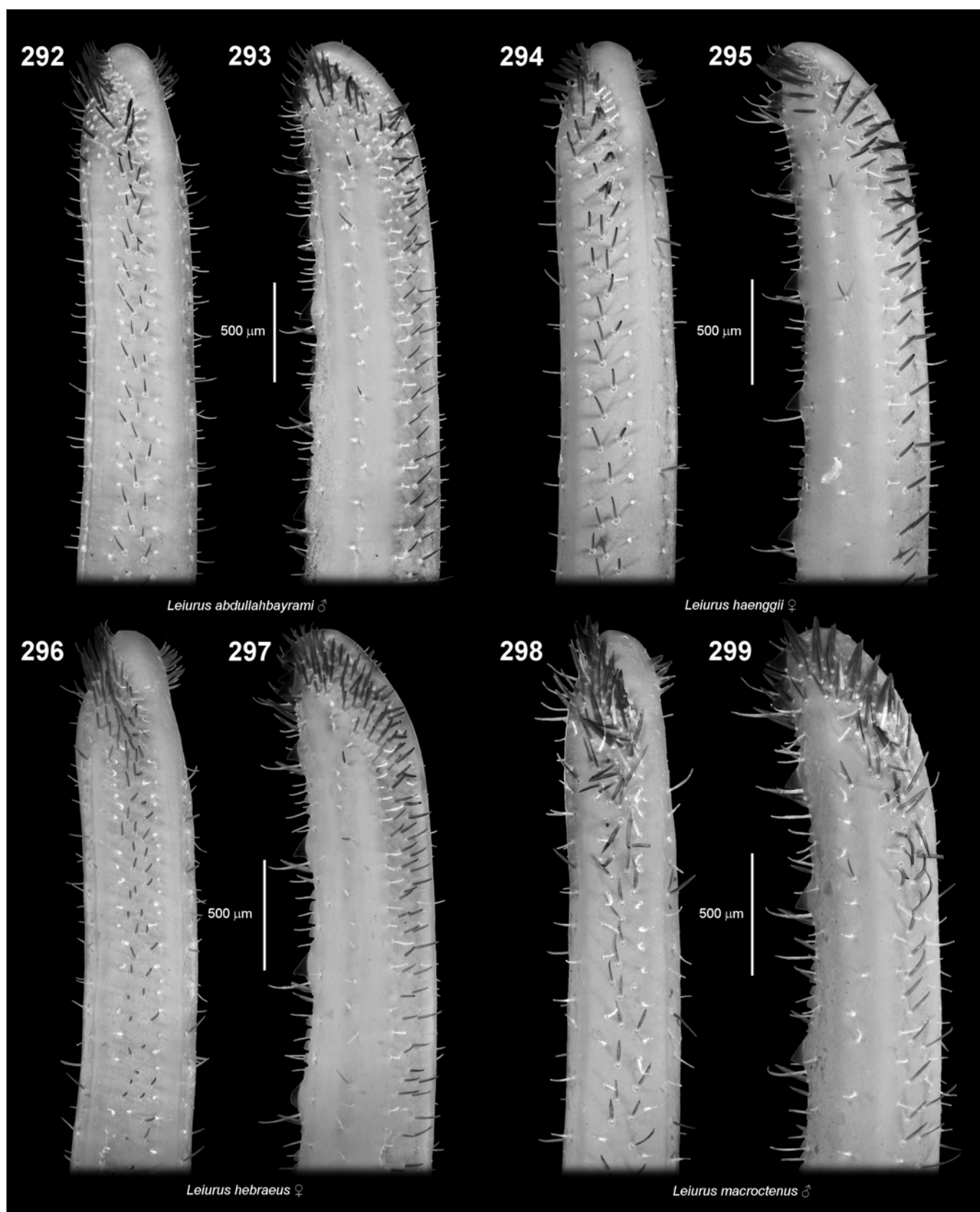
Figures 268–275. Distal movable finger of pedipalp chela. Buthidae, ‘Buthus’ group. **Figures 268–269.** *Buthus mardochei*, male. **270–271.** *Compsobuthus maindroni*, female. **Figures 272–275.** *Compsobuthus matthiesseni*, male (272–273) and female (274–275). Ventral (268, 270, 272, 274) and ventrointernal (269, 271, 273, 275) aspects. Scale bars: 500 μm (268–269), 200 μm (270–275). UV fluorescence.



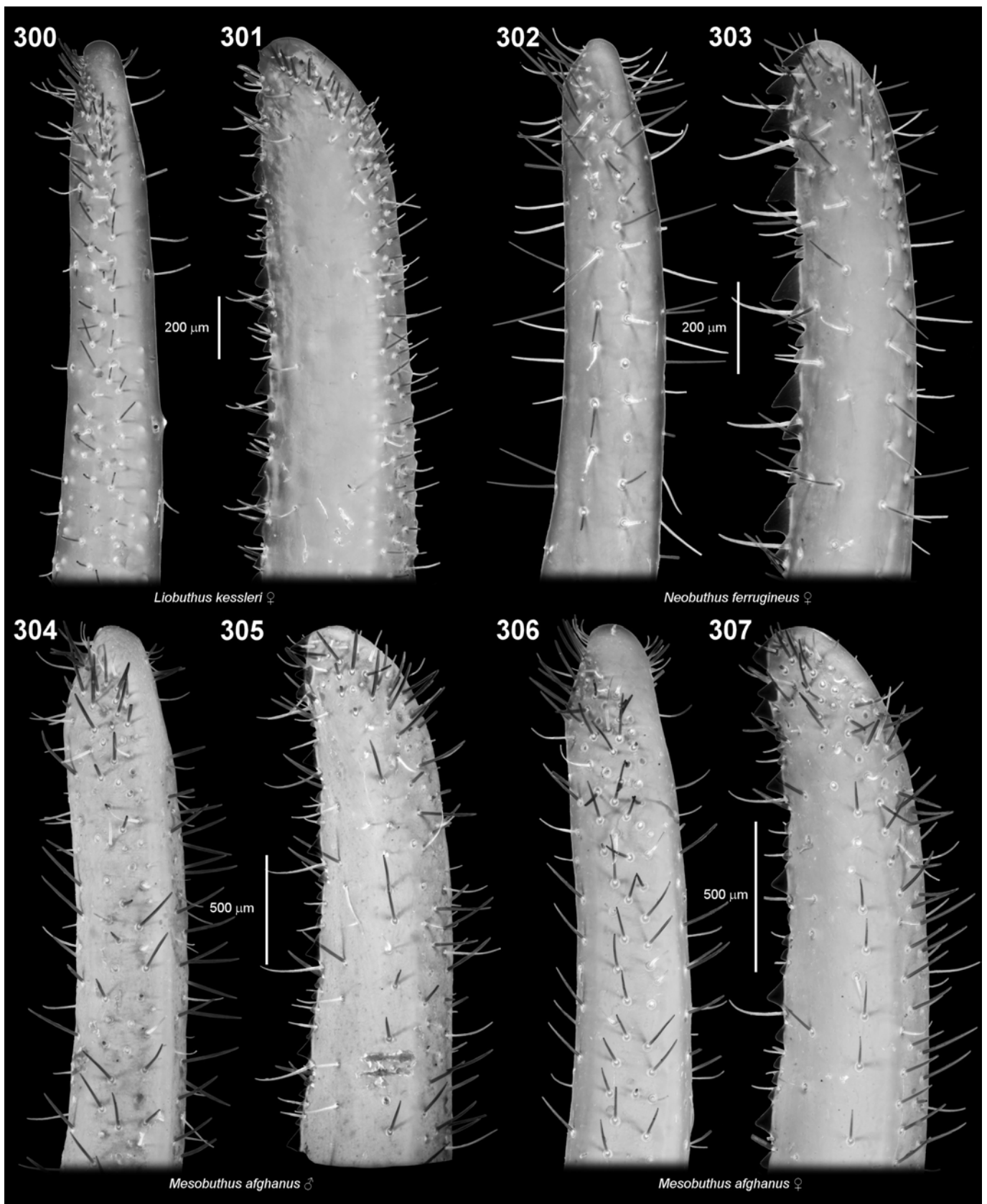
Figures 276–283. Distal movable finger of pedipalp chela. Buthidae, ‘Buthus’ group. **Figures 276–277.** *Compsobuthus nematodactylus*, male. **278–279.** *Compsobuthus polisi*, female. **Figures 280–281.** *Hottentotta hottentotta*, female. **Figures 282–283.** *Hottentotta pellucidus*, male. Ventral (276, 278, 280, 282) and ventrointernal (277, 279, 281, 283) aspects. Scale bars: 500 μm (280–283), 200 μm (276–279). UV fluorescence.



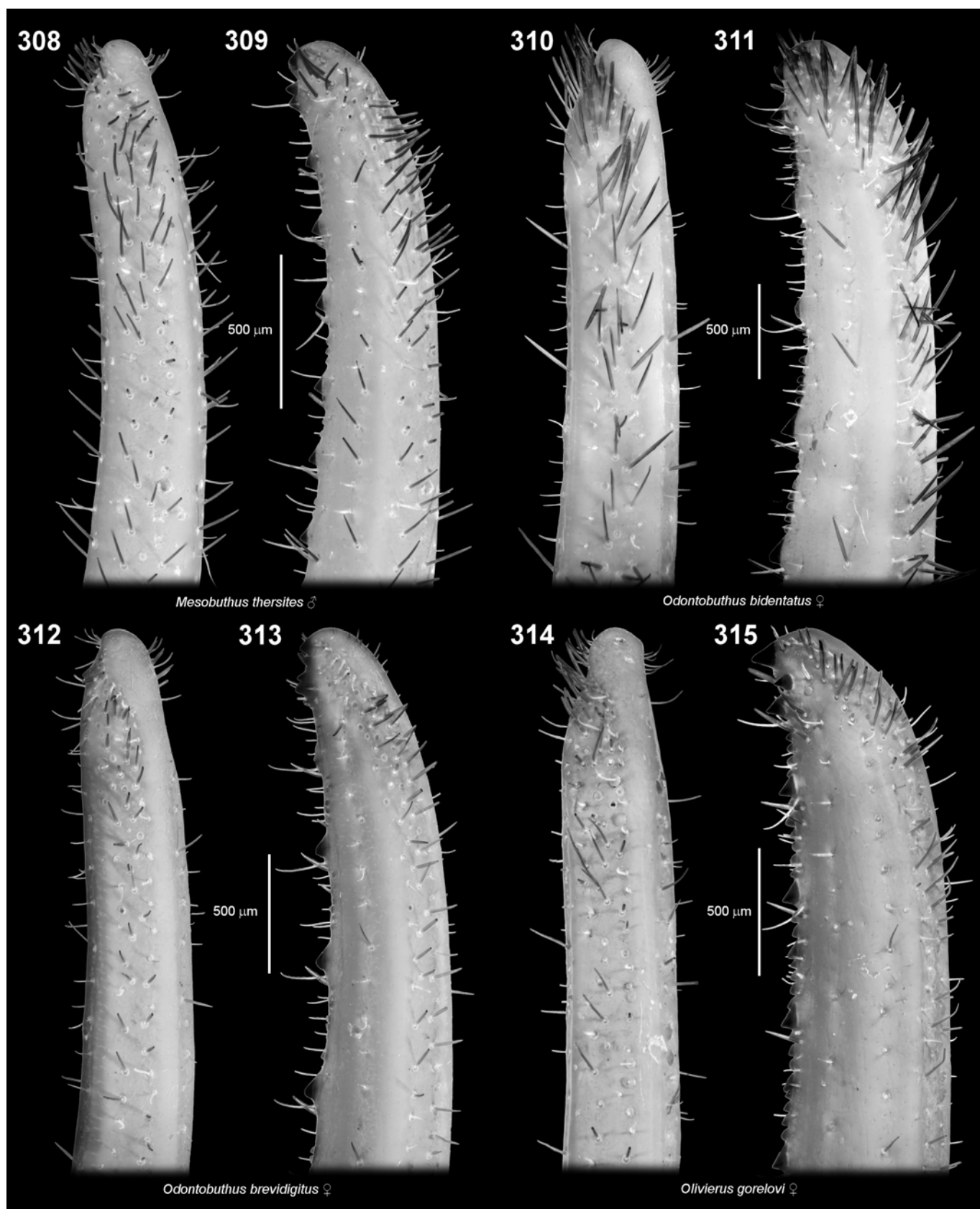
Figures 284–291. Distal movable finger of pedipalp chela. Buthidae, ‘Buthus’ group. **Figures 284–287.** *Hottentotta jayakari*, male (284–285) and female (286–287). **Figures 288–289.** *Hottentotta saxinatans*, female. **Figures 290–291.** *Hottentotta trilineatus*, female. Ventral (284, 286, 288, 290) and ventrointernal (285, 287, 289, 291) aspects. Scale bars: 500 µm. UV fluorescence.



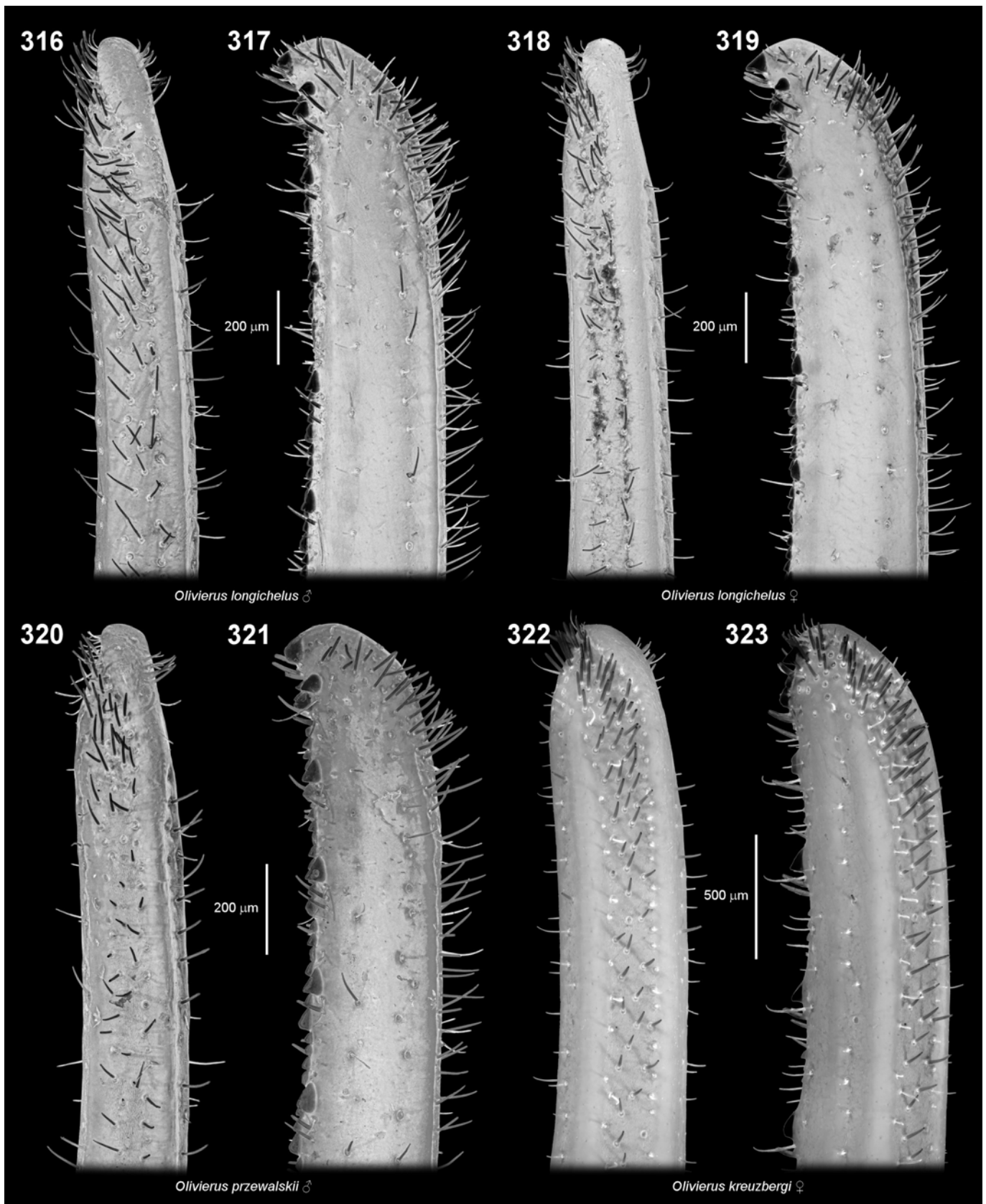
Figures 292–299. Distal movable finger of pedipalp chela. Buthidae, ‘Buthus’ group. **Figures 292–293.** *Leirus abdullahbayrami*, male. **Figures 294–295.** *Leirus haenggii*, female. **Figures 296–297.** *Leirus hebraeus*, female. **Figures 298–299.** *Leirus macroctenus*, male. Ventral (292, 294, 296, 298) and ventrointernal (293, 295, 297, 299) aspects. Scale bars: 500 µm. UV fluorescence.



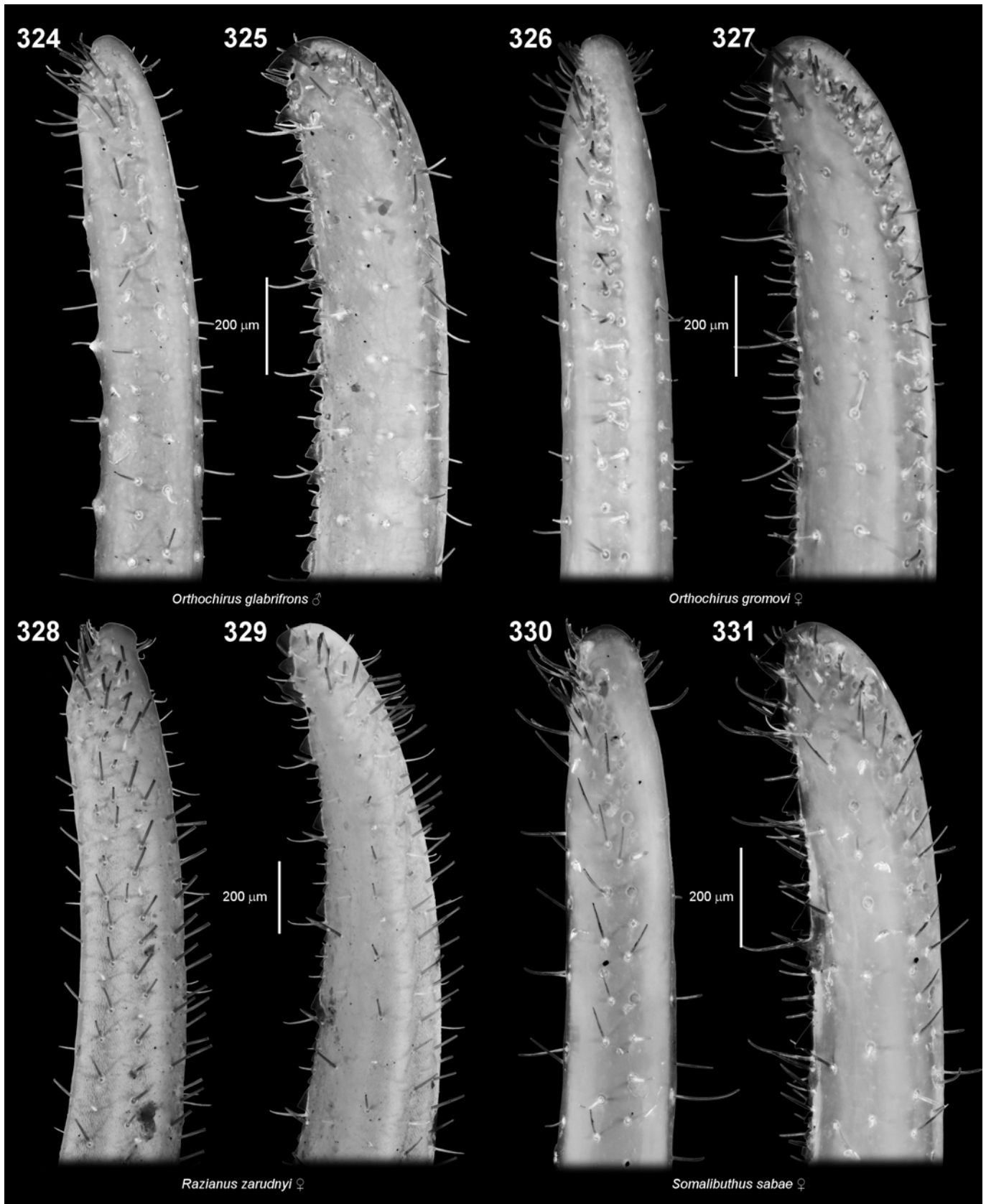
Figures 300–307. Distal movable finger of pedipalp chela. Buthidae, ‘Buthus’ group. **Figures 300–301.** *Liobuthus kessleri*, female. **Figures 302–303.** *Neobuthus ferrugineus*, female. **Figures 304–307.** *Mesobuthus afghanus*, male (304–305) and female (306–307). Ventral (300, 302, 304, 306) and ventrointernal (301, 303, 305, 307) aspects. Scale bars: 500 μm (304–307), 200 μm (300–303). UV fluorescence.



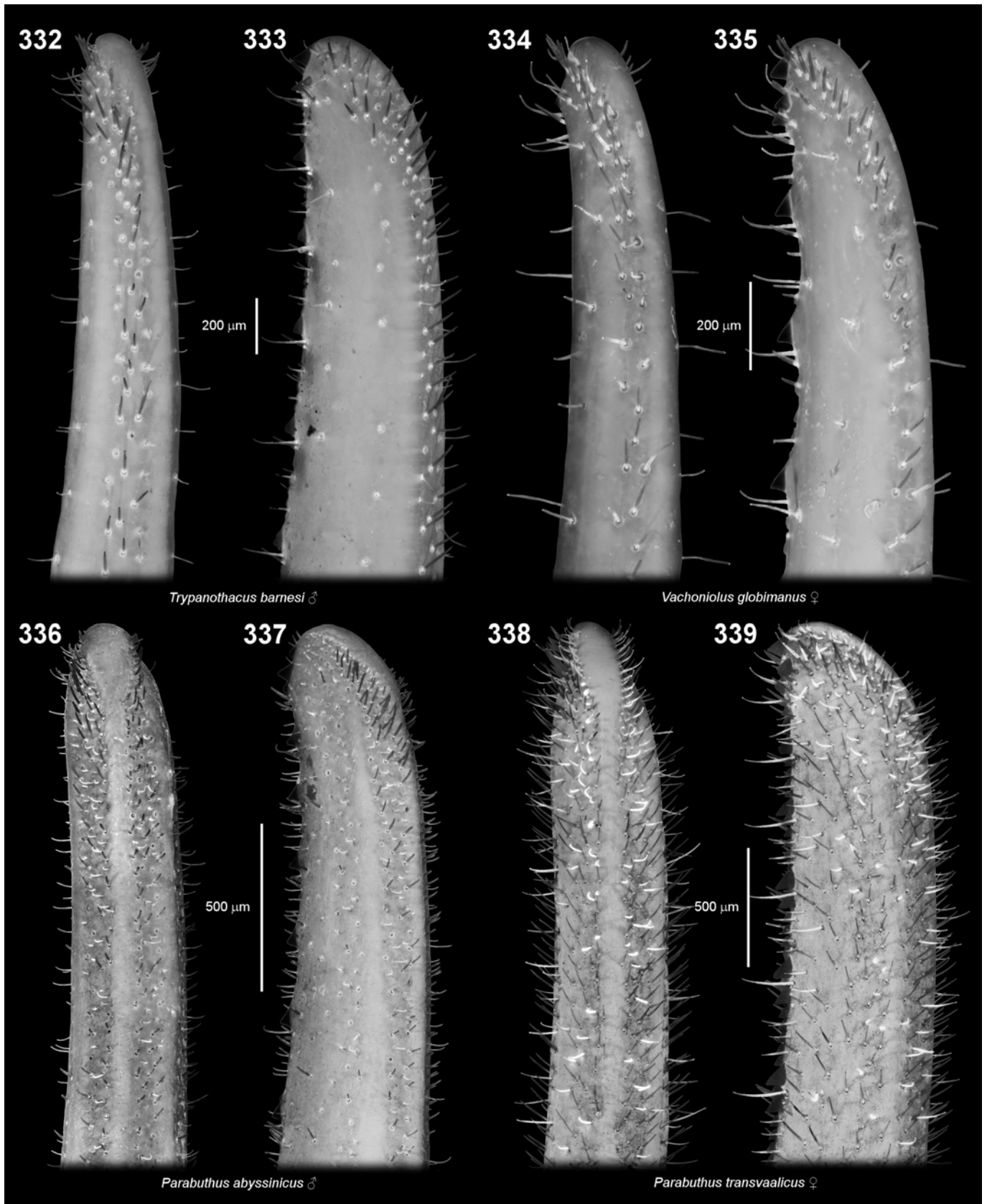
Figures 308–315. Distal movable finger of pedipalp chela. Buthidae, ‘Buthus’ group. **Figures 308–309.** *Mesobuthus thersites*, male. **Figures 310–311.** *Odontobuthus bidentatus*, female. **Figures 312–313.** *Odontobuthus brevidigitus*, female. **Figures 314–315.** *Olivierus gorelovi*, female. Ventral (308, 310, 312, 314) and ventrointernal (309, 311, 313, 315) aspects. Scale bars: 500 μm . UV fluorescence.



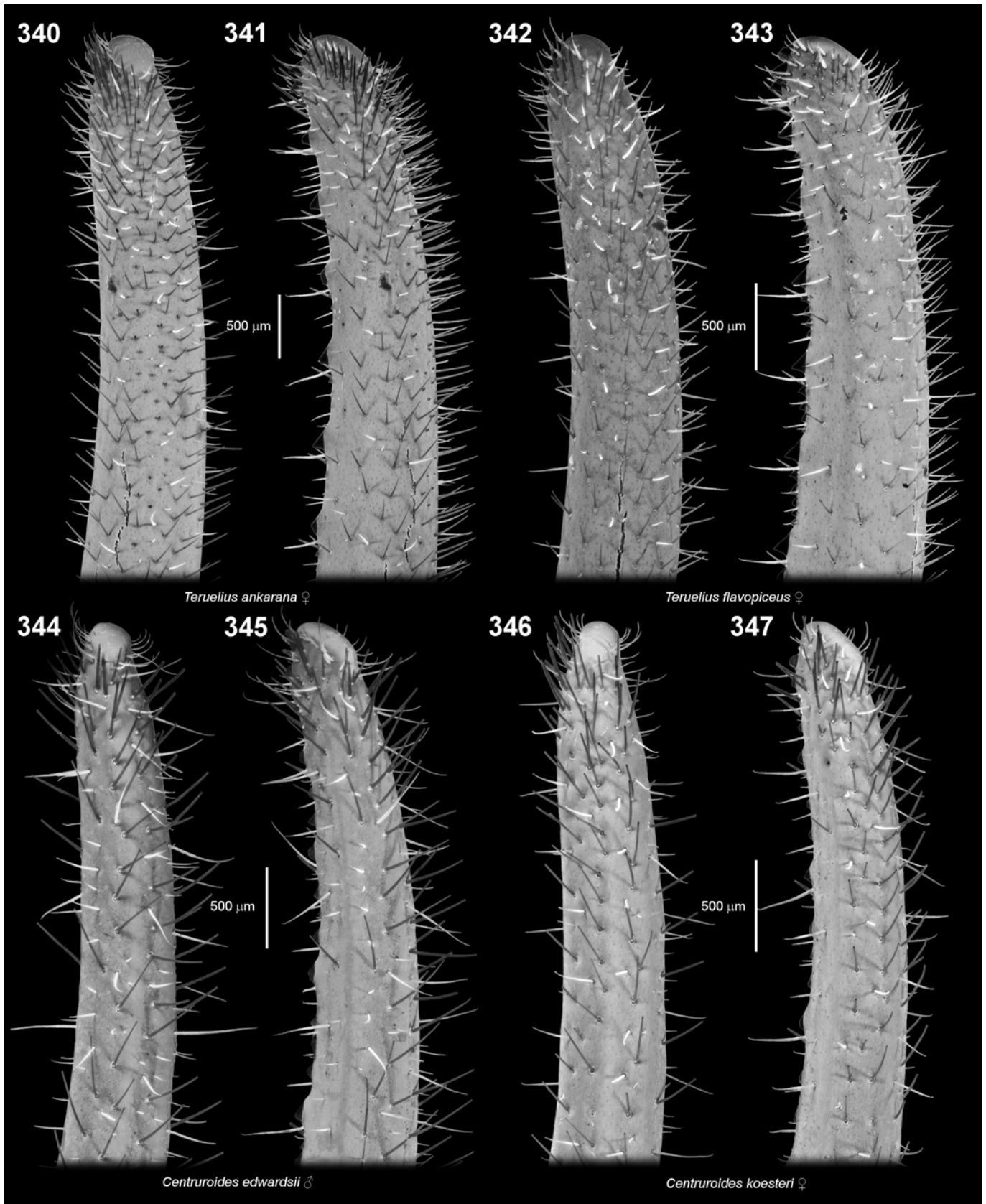
Figures 316–323. Distal movable finger of pedipalp chela. Buthidae, ‘Buthus’ group. **Figures 316–319.** *Olivierus longichelus*, male (316–317) and female (318–319). **Figures 320–321.** *Olivierus przewalskii*, male. **Figures 322–323.** *Olivierus kreuzbergi*, female. Ventral (316, 318, 320, 322) and ventrointernal (317, 319, 320, 323) aspects. Scale bars: 500 μm (322–323), 200 μm (316–321). UV fluorescence.



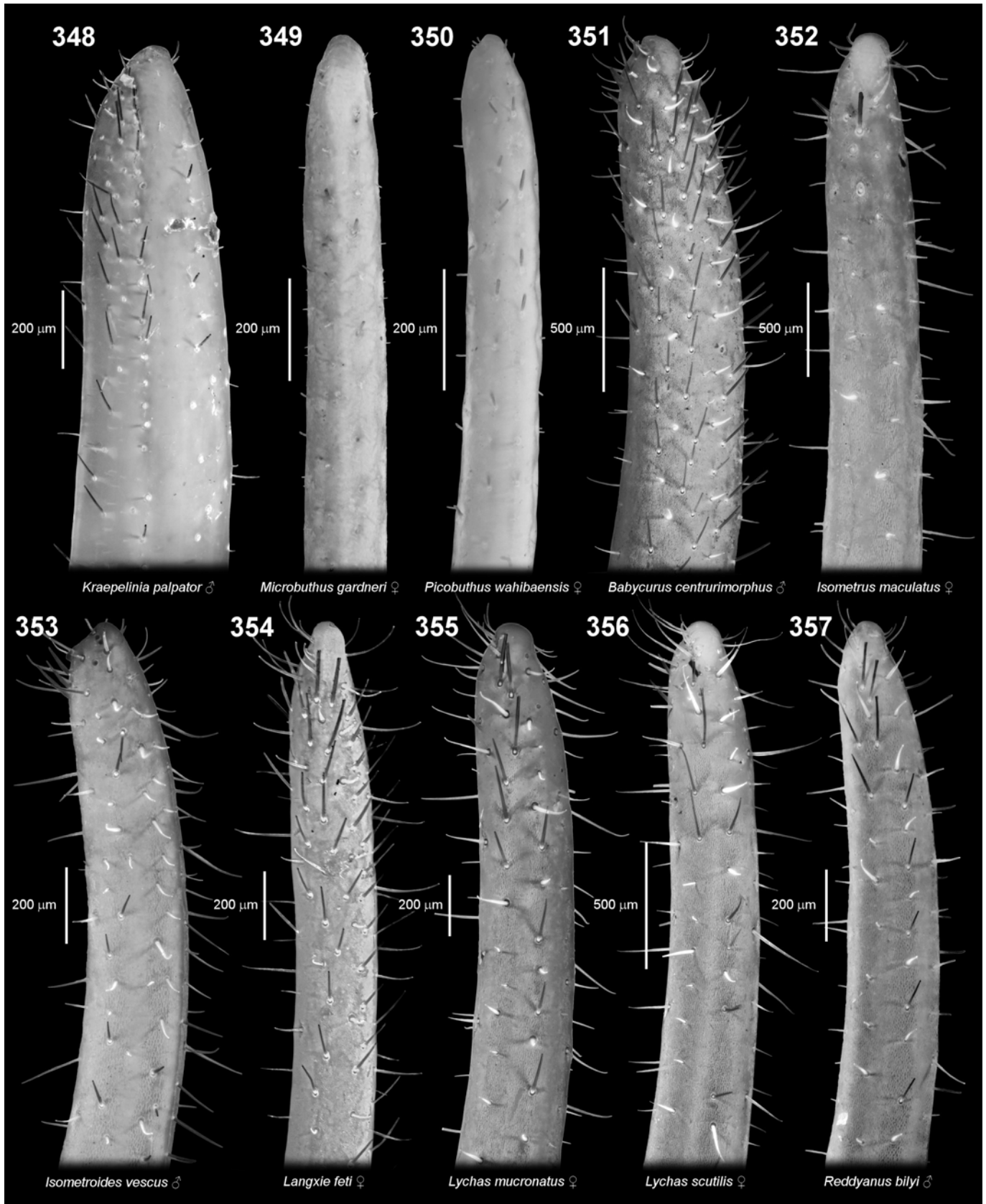
Figures 324–331. Distal movable finger of pedipalp chela. Buthidae, ‘Buthus’ group. **Figures 324–325.** *Orthochirus glabrifrons*, male. **Figures 326–327.** *Orthochirus gromovi*, female. **Figures 328–329.** *Razianus zarudnyi*, female. **Figures 330–331.** *Somalibuthus sabae*, female. Ventral (324, 326, 328, 330) and ventrointernal (325, 327, 329, 331) aspects. Scale bars: 200 μm . UV fluorescence.



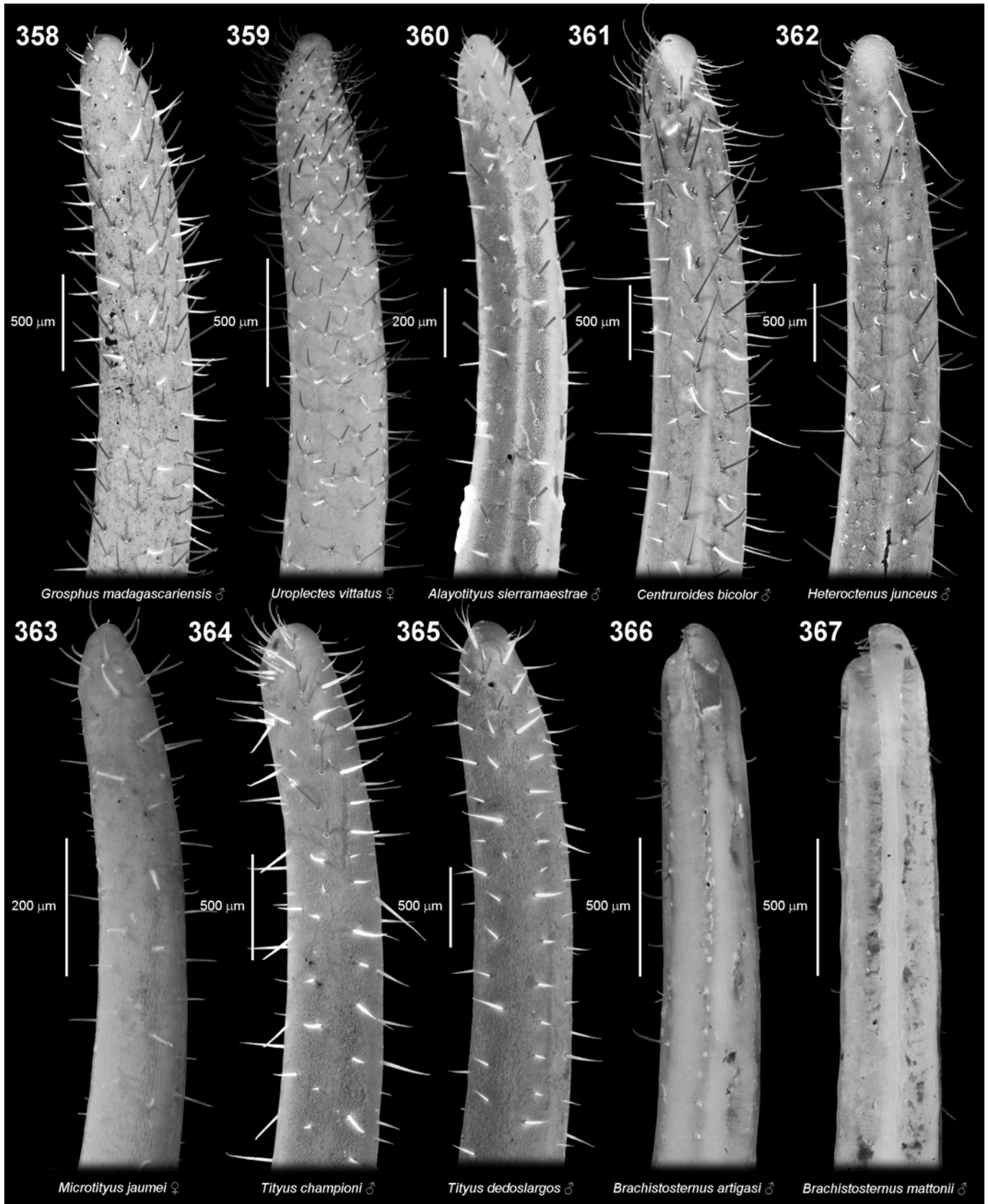
Figures 332–339. Distal movable finger of pedipalp chela. Buthidae, ‘Buthus’ group (332–335) and ‘Charmus–Uroplectes’ group (336–339). **Figures 332–333.** *Trypanothacus barnesi*, male. **Figures 334–335.** *Vachoniolus globimanus*, female. **Figures 336–337.** *Parabuthus abyssinicus*, male. **Figures 338–339.** *Parabuthus transvaalicus*, female. Ventral (332, 334, 336, 338) and ventrointernal (333, 335, 337, 339) aspects. Scale bars: 500 μm (336–339), 200 μm (332–335). UV fluorescence.



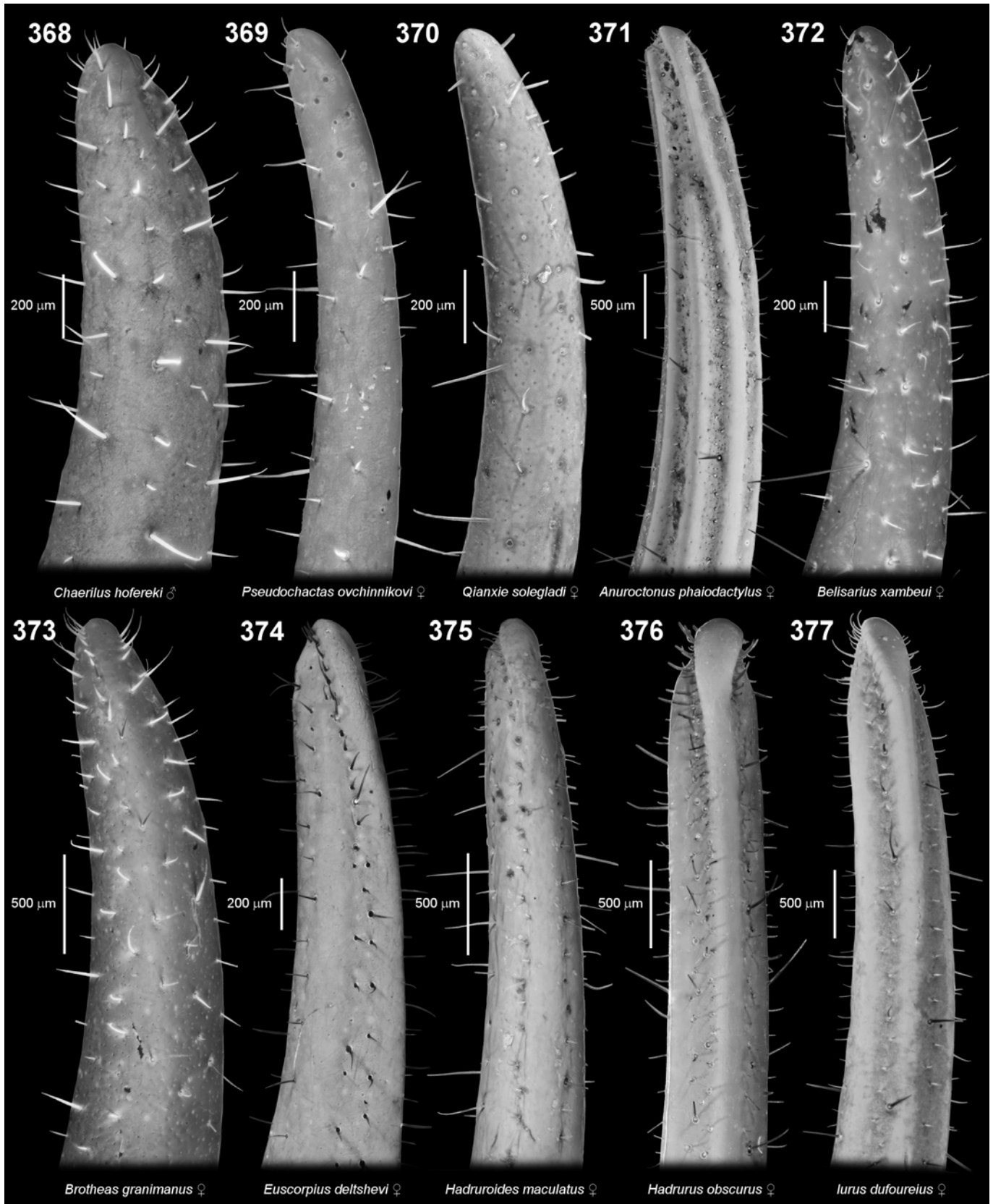
Figures 340–347. Distal movable finger of pedipalp chela. Buthidae, ‘Charmus–Uroplectes’ group (340–343) and ‘Tityus’ group (344–347). **Figures 340–341.** *Teruelius ankarana*, female. **Figures 342–343.** *Teruelius flavopiceus*, female. **Figures 344–345.** *Centruroides edwardsii*, male. **Figures 346–347.** *Centruroides koesteri*, female. Ventral (340, 342, 344, 346) and ventrointernal (341, 343, 345, 347) aspects. Scale bars: 500 µm. UV fluorescence.



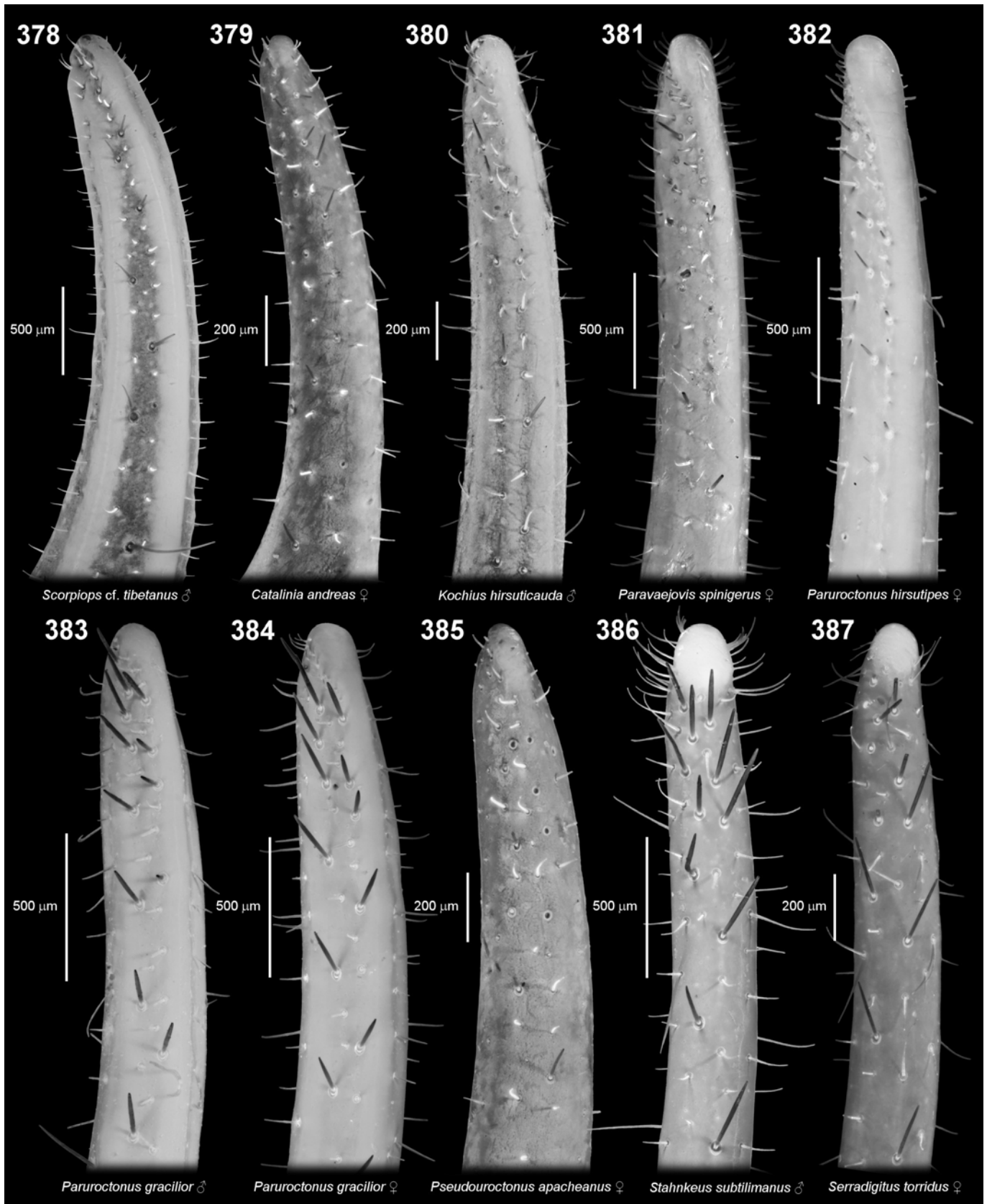
Figures 348–357. Distal movable finger of pedipalp chela. Buthidae, ‘Buthus’ group (348–350) and ‘Ananteris–Isometrus’ group (351–357). **Figure 348.** *Kraepelinia palpator*, male. **Figure 349.** *Microbuthus gardneri*, female. **Figure 350.** *Picobuthus wahibaensis*, female. **Figure 351.** *Babycurus centrurimorphus*, male. **Figure 352.** *Isometrus maculatus*, female. **Figure 353.** *Isometroides vescus*, male. **Figure 354.** *Langxie feti*, female. **Figure 355.** *Lychas mucronatus*, female. **Figure 356.** *Lychas scutillus*, female. **Figure 357.** *Reddyanus bilyi*, male. Ventral aspects. Scale bars: 500 μm (351–352, 356), 200 μm (348–350, 353–355, 357). UV fluorescence.



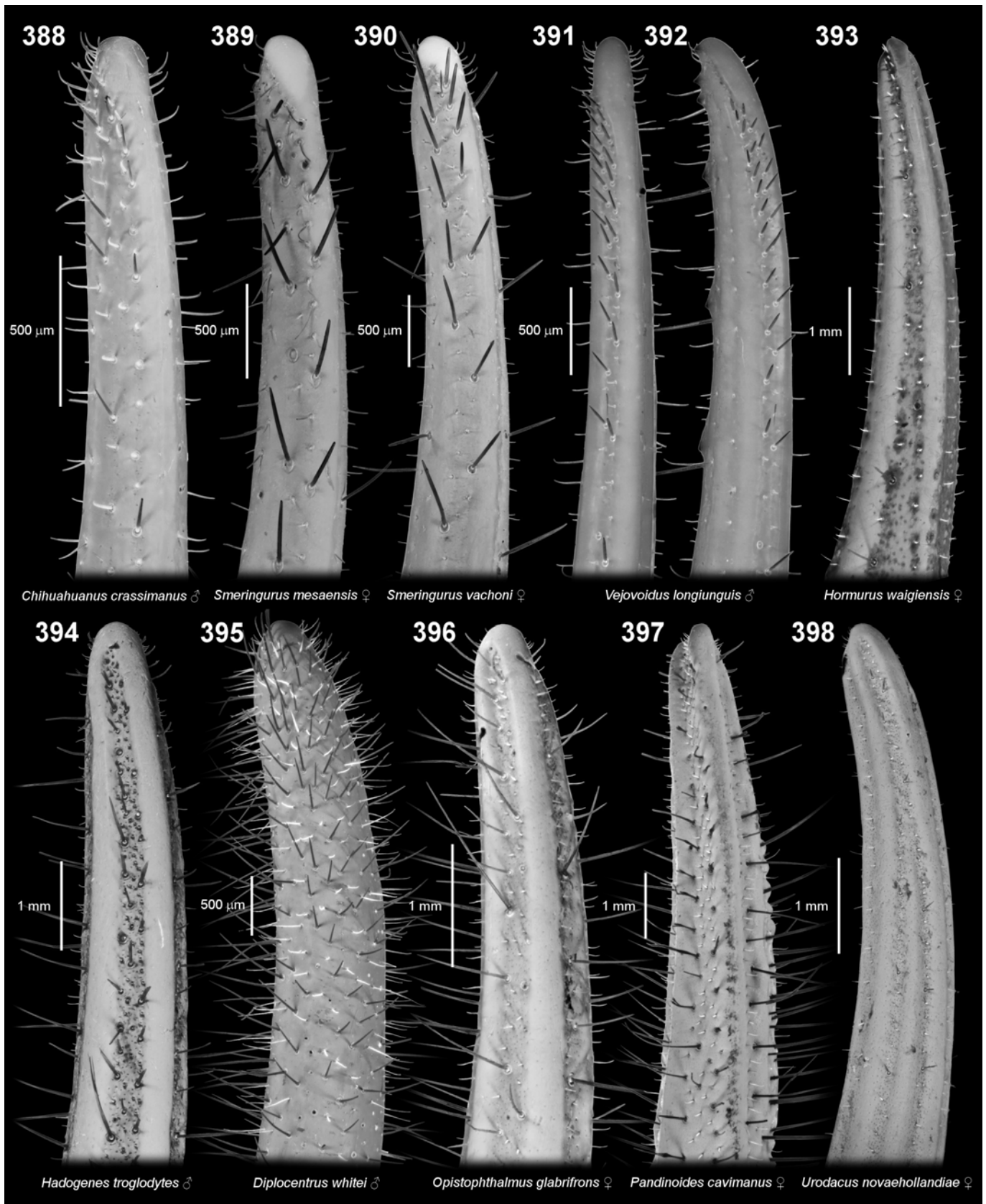
Figures 358–367. Distal movable finger of pedipalp chela. Buthidae, ‘Charmus–Uroplectes’ group (358–359) and ‘Tityus’ group (360–365). **Figure 358.** *Grosphus madagascariensis*, male. **Figure 359.** *Uroplectes vittatus*, female. **Figure 360.** *Alayotityus sierramaestrae*, male. **Figure 361.** *Centruroides bicolor*, male. **Figure 362.** *Heteroctenus junceus*, male. **Figure 363.** *Microtityus jaumei*, female. **Figure 364.** *Tityus championi*, male. **Figure 365.** *Tityus dedoslargos*, male. Bothriuridae. **Figure 366.** *Brachistosternus artigasi*, male. **Figure 367.** *Brachistosternus mattonii*, male. Ventral aspects. Scale bars: 500 μm (358–359, 361, 364–367), 200 μm (360, 363). UV fluorescence.



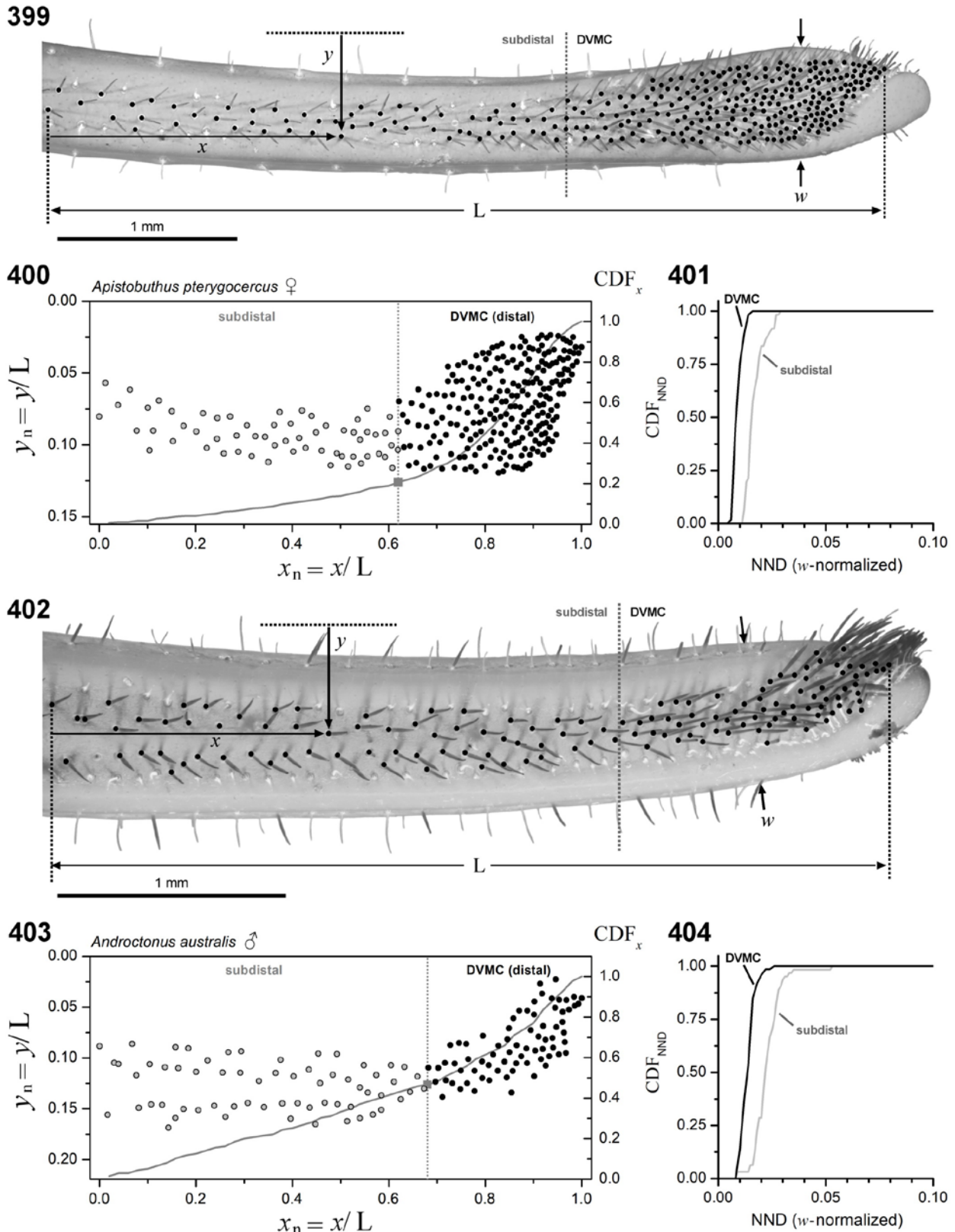
Figures 368–377. Distal movable finger of pedipalp chela. Chaerilidae. **Figure 368.** *Chaerilus hofereki*, male. Pseudochactidae. **Figure 369.** *Pseudochactas ovchinnikovi*, female. **Figure 370.** *Qianxie solegladi*, female. Anuroctonidae. **Figure 371.** *Anuroctonus phaiodactylus*, female. Belisariidae. **Figure 372.** *Belisarius xambeui*, female. Chactidae. **Figure 373.** *Brotheas granimanus*, female. Euscorpidae. **Figure 374.** *Euscorpium deltshevi*, female. Caraboctonidae. **Figure 375.** *Hadruioides maculatus*, female. Hadruridae. **Figure 376.** *Hadrurus obscurus*, female. Iuridae. **Figure 377.** *Iurus dufourei*, female. Ventral aspects. Scale bars: 500 μm (371, 373, 375–377), 200 μm (368–370, 372, 374). UV fluorescence.



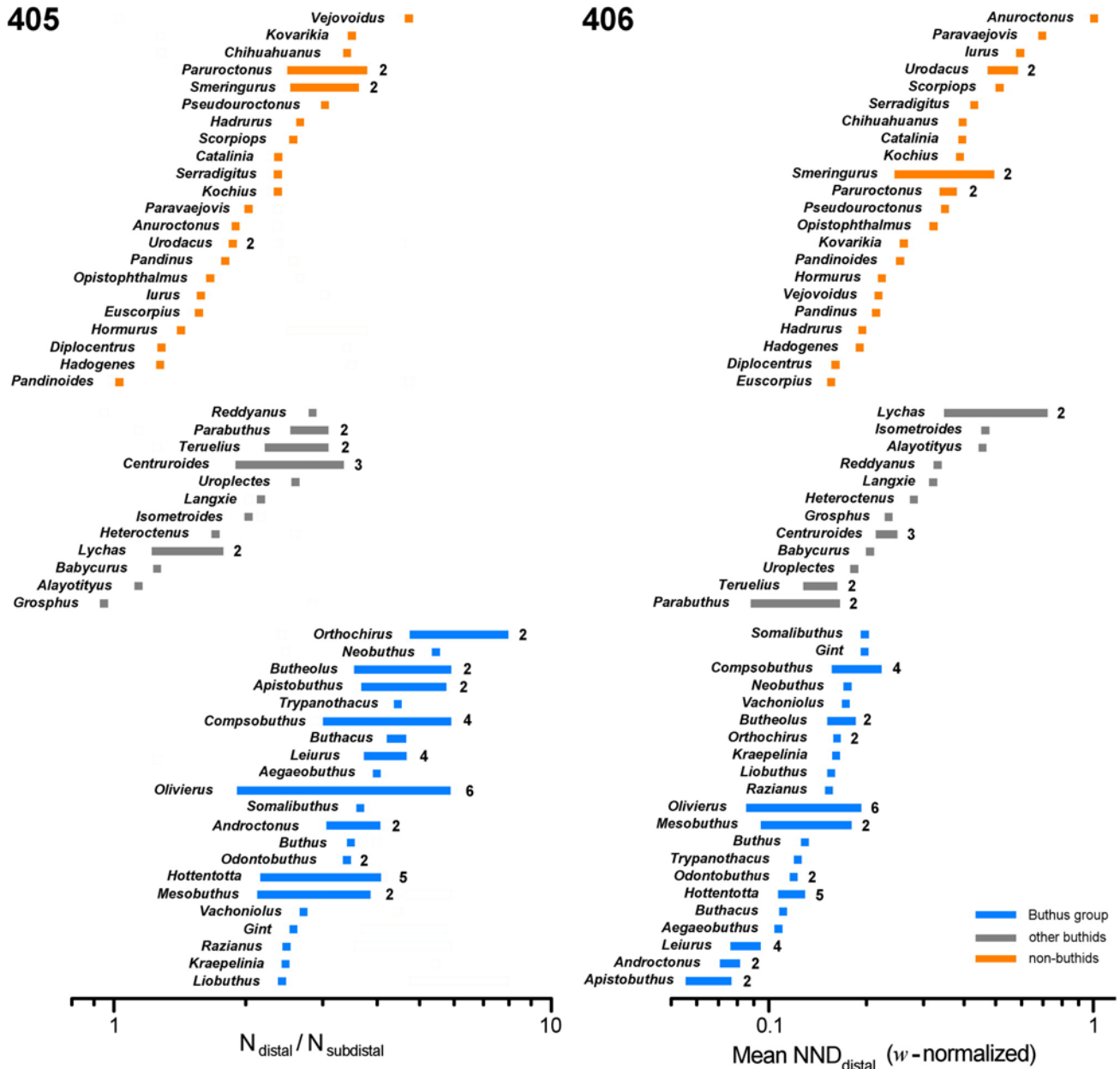
Figures 378–387. Distal movable finger of pedipalp chela. Scorpiopidae. **Figure 378.** *Scorpiops cf. tibetanus*, male. Vaejovidae. **Figure 379.** *Catalinia andreas*, female. **Figure 380.** *Kochius hirsuticauda*, male. **Figure 381.** *Paravaejovis spinigerus*, female. **Figure 382.** *Paruroctonus hirsutipes*, female. **Figure 383–384.** *Paruroctonus gracillior*, male (383) and female (384). **Figure 385.** *Pseudouroctonus apacheanus*, female. **Figure 386.** *Stahnkeus subtilimanus*, male. **Figure 387.** *Serradigitus torridus*, female. Ventral aspects. Scale bars: 500 μm (378, 381–384, 386), 200 μm (379–380, 385, 387). UV fluorescence.



Figures 388–398. Distal movable finger of pedipalp chela. Vaejovidae. **Figure 388.** *Chihuahuanus crassimanus*, male. **Figure 389.** *Smeringurus mesaensis*, female. **Figure 390.** *Smeringurus vachoni*, female. **Figure 391–392.** *Vejovoidus longiunguis*, male. **Figure 393.** *Hormurus waigiensis*, female. **Figure 394.** *Hadogenes troglodytes*, male. **Figure 395.** *Diplocentrus whitei*, male. **Figure 396.** *Opisthophthalmus glabrifrons*, female. **Figure 397.** *Pandinoides cavimanus*, female. **Figure 398.** *Urodacus novaehollandiae*, female. Ventral (388–391, 393–398) and ventrointernal (392) aspects. Scale bars: 1 mm (393–394, 396–398), 500 μm (388–392, 395). UV fluorescence.



Figures 399–404. Measurement and analysis of spatial patterns of macrosetae distributed on the distal ventral surface of the pedipalp movable finger. **Figures 399–401.** *Apistobuthus pterygocercus*, female (Buthidae). **Figure 399.** Ventral aspect of distal movable finger. Visible section of finger oriented with proximodistal axis approximately level horizontally. Black-filled circles: position markers of macrosetal sockets; L : length of visible distal section for normalizing proximodistal (x) and dorsoventral (y) positions of marked setae; DVMC: distal ventral macrosetal cluster; w : finger width at DVMC. Scale bar: 1 mm. UV fluorescence. **Figure 400.** Scatter plot of coordinates of macrosetae of DVMC (black-filled circles) and subdistal ventral macrosetae (gray-filled circles) in L -normalized morphospace (x/L , y/L). Gray curve: cumulative distribution function of macrosetal distribution along x -axis (CDF_x). **Figure 401.** Cumulative distribution function of nearest neighbor distances (NND) of macrosetae of DVMC (black curve) and subdistal ventral macrosetae (gray curve) in w -normalized morphospace (x/w , y/w). **Figures 402–404.** *Androctonus australis*, male (Buthidae). **Figure 402.** Ventral aspect of distal movable finger. Markers, variables, and parameters as in Fig. 399. **Figure 403.** Scatter plot of coordinates of macrosetae. Symbols and variables as in Fig. 400. **Figure 404.** Cumulative distribution function of w -normalized nearest neighbor distances (NND) of macrosetae. Variables and curves as in Fig. 401.



Figures 405–406. Variation in clustering metrics of distal ventral macrosetae on pedipalp movable fingers. Logarithmic horizontal bar charts of ratios of distal to subdistal ventral macrosetal counts (405) and mean w -normalized nearest neighbor distances (NND) of distal ventral macrosetae (406). Subdistal counts rescaled by ratio of distal section length to subdistal section length of analyzed finger images. Bars indicate observed ranges for each genus. Blue bars: ‘Buthus’ group (21 genera, 42 species); gray bars: other buthids (12 genera, 17 species); orange bars: non-buthids (23 genera, 26 species from 10 families).

We investigated the role of the DEMC in ocular grooming by video recording sponge-bathing in the ‘Buthus’ group species *Olivierus martensii*. To elicit grooming behavior, carapaces of adults were uniformly coated with a layer of moistened loess dust. Individuals responded to this treatment by initiating lengthy sponge-bathing episodes lasting up to an hour or longer. As reported in other species, oral exudate was spread over the appendages and body by the actions of chelicerae, pedipalps, legs and telson. Part of this process involved unilateral rhythmic flexing of the pedipalps in which the femur was rotated through an angle of $\sim 100^\circ$ about its trochanteral articulation (Figs. 424–431).

At one end of the oscillation cycle, the DEMC appeared to contact the ipsilateral median ocellus (Fig. 424); at the other end, the DVMC appeared to contact the contralateral median ocellus (Figs. 430–431). Over most of the cycle, the femur, patella and chela manus remained locked in a triangular configuration. During sponge-bathing, the anterior ventral surface of the telson was also observed to make contact with the median ocular tubercle (Fig. 435). These observations provide evidence supporting a role for both DEMC and DVMC in ocular grooming. Contact of DEMC and DVMC on median ocelli was recorded in multiple individuals (e.g., Figs. 432–434), showing that

this was not an acquired response of a single individual, but probably a stereotypic response governed by innate motor programs of this species.

Could the many other species in the ‘Buthus’ group equipped with a DEMC also utilize it as a lens cleaning brush? Comparative morphometrics offers a test of this hypothesis. As the femur swings around its basal point of articulation, the DEMC is predicted to sweep out an arc that intersects the ipsilateral median ocellus. This requires the distance of the DEMC centroid along the proximodistal axis of the femur to match the distance of the ipsilateral median ocellus from the anterolateral vertex of the carapace where the femur articulates (Fig. 436). A plot of these two variables in 95 individuals representing 55 species of the ‘Buthus’ group revealed a strong correlation and match of the physical distances, with most points aggregated close to the diagonal (Fig. 437). The morphometrics obey the geometric constraint dictated by the functional hypothesis. The physical distances were also matched across instars of different sizes (Fig. 229), allowing the DEMC to perform ocular grooming functions throughout the life of the animal.

Discussion

Taxonomic significance of external femoral macrosetae

We surveyed external femoral setation patterns of a broad sample of taxa from 17 currently recognized scorpion families. We found systematic differences between buthids and non-buthids, and between buthids belonging to the ‘Buthus’ group and other buthid groups. Density of setation was variable, ranging from moderately or heavily pilose, to sparse or glabrous. Setae were typically more numerous in the ‘Buthus’ group, and in some members of the ‘Charmus-Uroplectes’ group (*Parabuthus*, *Teruelius*, *Uroplectes*) and ‘Tityus’ group (*Centruroides*). In contrast, setation was typically sparse in non-buthids. The ECMS was a common motif whose development generally mirrored the aforementioned systematic trends in density. The number of ECMS setae was variable and not linked to development of the external median carina, i.e., strong carinae could lack setae, and weak carinae could bear multiple setae. The DEMC was mostly confined to the ‘Buthus’ group, in which it typically formed a dense, compact cluster (Fig. 188). In other buthid groups, it only occurred in setose genera, and it did not form a compact cluster. Differences between setation patterns of the major groups were quantified by their segregation in morphospace, with minor overlap between groups. We propose that the DEMC is a synapomorphy for the ‘Buthus’ group.

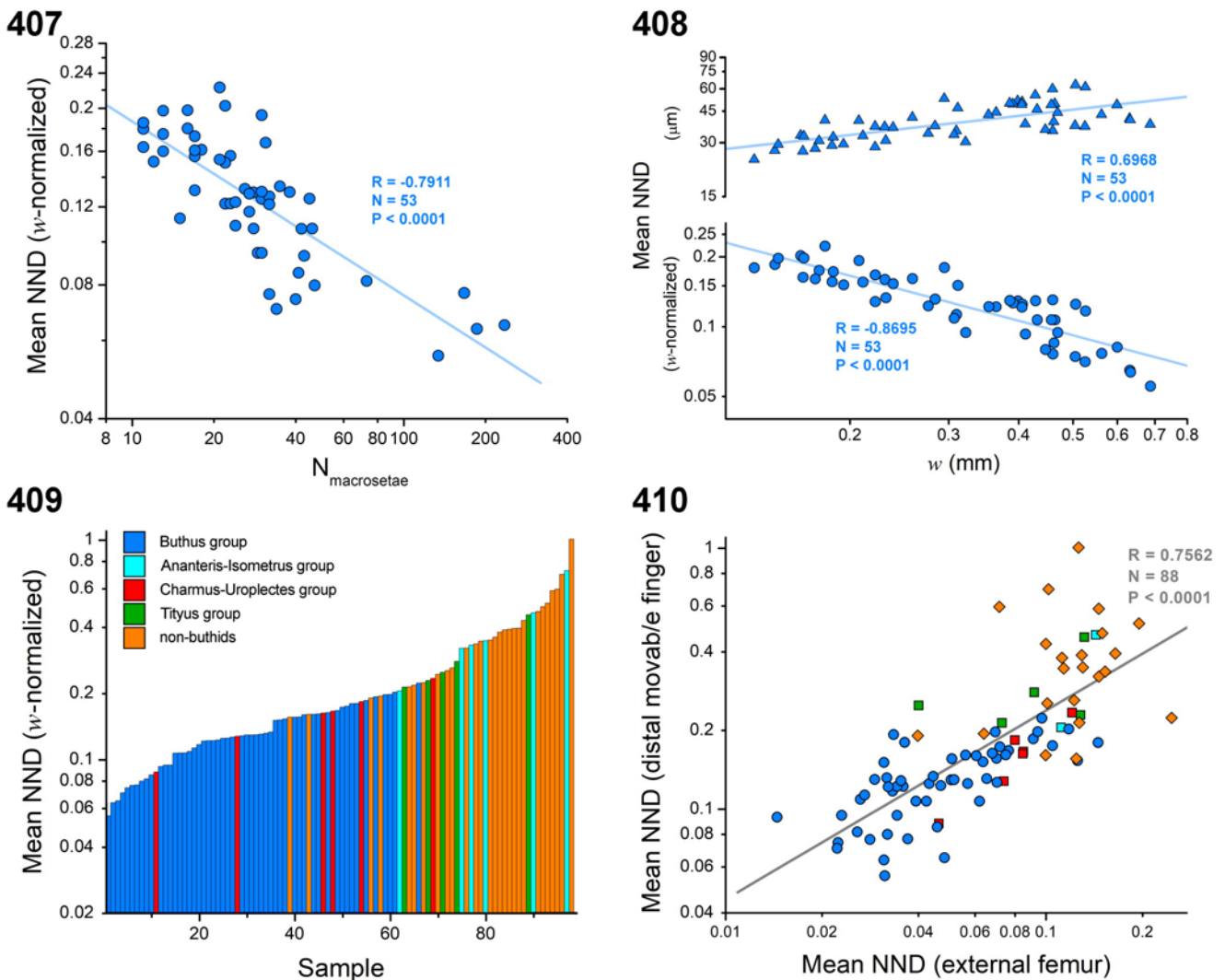
Within the ‘Buthus’ group, the DEMC varied considerably in size, shape and density. This variation exhibited taxonomic correlation at the genus level (Figs. 206–207). An analysis of setation in four sampled genera demonstrated their clear segregation in morphospace (Fig. 212). Suggested DEMC categories based on our samples are: short, dense, with short setae (*Androctonus*, *Buthus*, *Gint*, *Leiurus*, *Olivierus*); short,

dense, with long setae (*Buthacus*, *Liobuthus*, *Odontobuthus*, *Olivierus*, *Trypanothacus*); longer, less dense, with medium length setae (*Hottentotta*, *Mesobuthus*, *Olivierus*); long, dense, with short setae (*Apistobuthus*); sparser, with series of long setae (*Anomalobuthus*, *Kraepelinia*, *Orthochirus*, *Somalibuthus*, *Xenobuthus*, *Vachoniolus*); sparse, with short setae (*Compsobuthus*); and absent (*Microbuthus*, *Picobuthus*). More comprehensive species sampling is needed to characterize variation of DEMC configurations, and to test their diagnostic value at the genus level.

External femoral setation may also differentiate between species. For example, in *Centruroides*, there appears to be considerable interspecific variation in the density of setation. However, in *Olivierus martensii*, we found wide variation in the number of DEMC setae (Fig. 200), which would limit the diagnostic value of setal counts. On the other hand, pectinal tooth counts are a standard character in many species diagnoses, even though they can show similarly wide variation that may overlap between species. Although the diagnostic value of external femoral setation patterns awaits further investigation, our findings indicate that these patterns can be phylogenetically informative.

Taxonomic significance of external femoral trichobothria

Trichobothrial patterns can be a source of informative characters in the taxonomy and phylogeny of buthids. On the femur, α - vs. β -configuration of d_1 , d_3 , d_4 is a synapomorphy for the (‘Charmus-Uroplectes’ group, ‘Tityus’ group) clade (Fet et al., 2005; Lowe & Kovařík, 2022; Vachon, 1975). On the patella: (i) internal vs. external placement of d_3 relative to the dorsomedian carina is a synapomorphy for the ‘Buthus’ group (Fet et al., 2005); and (ii) more distal placement of esb_2 is a synapomorphy for the (‘Charmus-Uroplectes’ group, ‘Tityus’ group) clade (Fet et al., 2005; Lowe & Kovařík, 2022). On the chela manus, more distal placement of Eb_2 is a potential synapomorphy for the clade (‘Ananteris-Isometrus’ group, (Charmus-Uroplectes’ group, ‘Tityus’ group)) (Lowe & Kovařík, 2022). Trichobothrial patterns on the external surface of the femur have not been studied systematically. Two external trichobothria, e_1 and e_2 , are present in the vast majority buthids (by definition the orthobothriotaxic state). Exceptions are *Liobuthus*, with four (Vachon, 1958), and *Buthiscus*, with three (Vachon, 1952). Morphometric analysis of e_1 and e_2 positions measured from our UV images of the external femur, and extracted from published descriptions, revealed significant differences between the distributions of e_1 and e_2 of some buthid lineages. There was major segregation of ‘Buthus’ and ‘Tityus’ groups in the proximodistal position of e_1 , which tended to be more distal in the ‘Tityus’ group (Fig. 232). The ‘Ananteris-Isometrus’ and ‘Charmus-Uroplectes’ group were largely overlapped with minor segregation in the proximodistal position of e_2 , which tended to be more distal in the ‘Ananteris-Isometrus’ group (Fig. 233). These results indicate that external femoral trichobothrial positions are also relevant to the phylogenetic analysis of buthids.

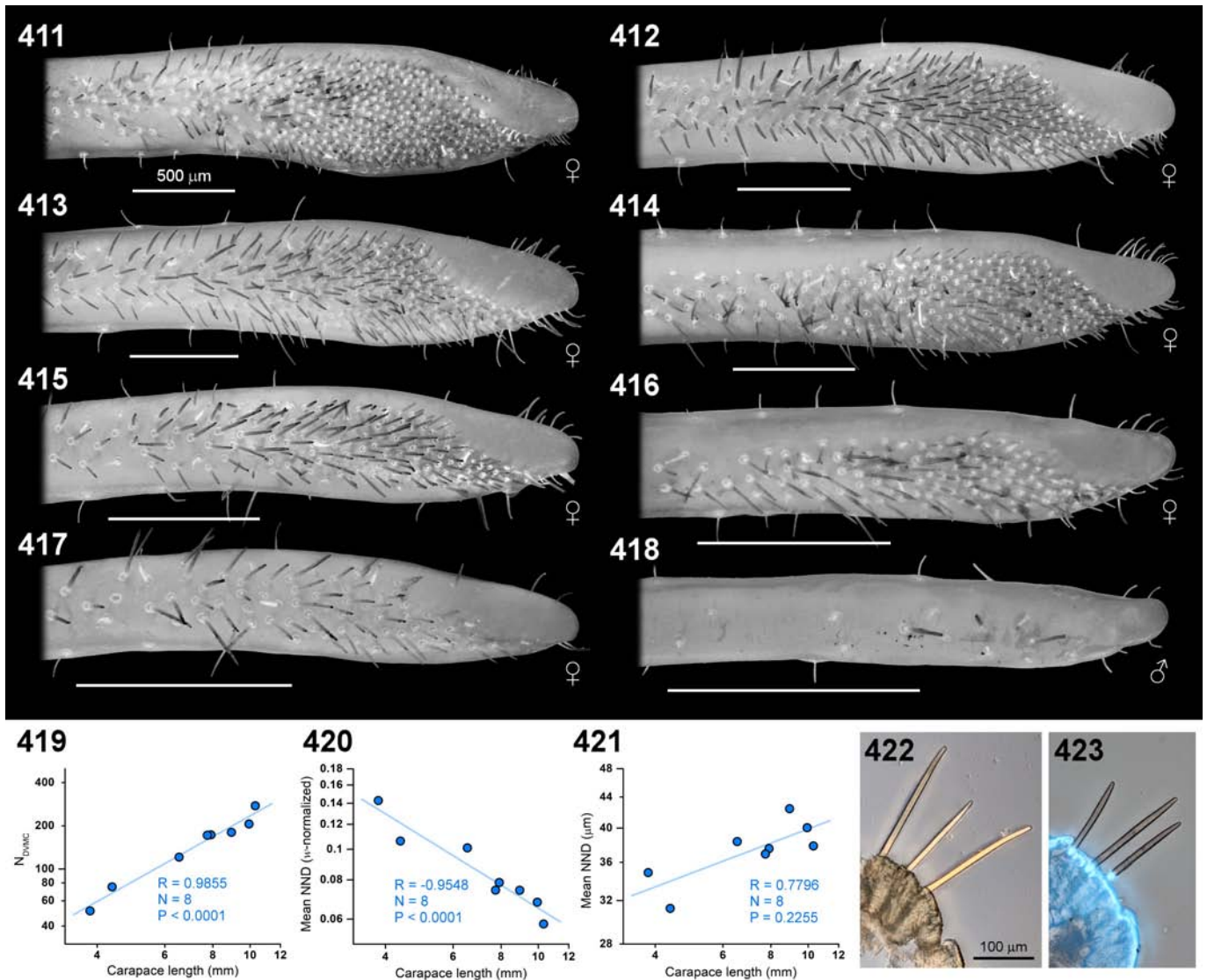


Figures 407–410. Variation in the density of setation on distal ventral movable finger. **Figure 407.** Logarithmic scatter plot of mean w -normalized NND vs. number of macrosetae in 'Buthus' group (blue circles). **Figure 408.** Lower plot: logarithmic scatter plot of mean w -normalized NND vs. w (= distal finger width), in 'Buthus' group (blue circles). Upper plot: mean absolute NND in μm of 'Buthus' group (blue triangles), plotted on the same abscissa. **Fig. 409.** Ranked vertical logarithmic bar plot of mean w -normalized NND of distal ventral macrosetae for 98 movable fingers. Blue bars: 'Buthus' group ($N = 53$); cyan bars: 'Ananteris-Isometrus' group ($N = 6$), red bars: 'Charmus-Uroplectes' group ($N = 6$); green bars: 'Tityus' group ($N = 5$); orange bars: non-buthids ($N = 28$). **Fig. 410.** Logarithmic scatter plot of mean w -normalized NND of distal ventral macrosetae of pedipalp movable finger vs. L -normalized mean NND of external femoral macrosetae. Blue circles: 'Buthus' group ($N = 53$); cyan squares: 'Ananteris-Isometrus' group ($N = 2$); red squares: 'Charmus-Uroplectes' group ($N = 6$); green squares: 'Tityus' group ($N = 5$); orange diamonds: non-buthids ($N = 22$). Gray line: linear least square regression fit to all points ($N = 88$); R : Pearson's correlation coefficient. Regression lines from linear least squares fits (407, 408, 410).

Taxonomic significance of macrosetae on ventral movable finger

Chaetotaxy on the ventral surface of the movable pedipalp finger has been not been studied systematically, and was not included in taxonomic descriptions. We surveyed a broad range of taxa and found large differences in patterns, numbers, clustering, and lengths of macrosetae on the distal and subdistal ventral movable finger. In most species of the 'Buthus' group, setation was relatively dense and typically arranged in two more or less regular longitudinal series running along the subdistal finger between ventrointernal and ventroexternal carinae. The density increased markedly in the distal region on

ventral and ventrointernal surfaces, forming the DVMC. The pattern was different in other buthids. In *Parabuthus*, dense, short setation on the subdistal finger was divided into two strips by a ventromedian carina. The density increased distally on the internal side, forming a DVMC. In other buthids, setation varied from dense to sparse or absent, was typically irregular with long setae, and a DVMC was formed only in some taxa (*Centruroides*, *Teruelius*, *Uroplectes*). In non-buthids there was wide variation in patterns, numbers, clustering, and lengths of macrosetae. A DVMC was only found in a vaejovid, *Vejovoidus longiunguis*. We propose that the serial arrangement of setae along the subdistal finger, and the consistent development of the DVMC, are synapomorphies for the 'Buthus' group.

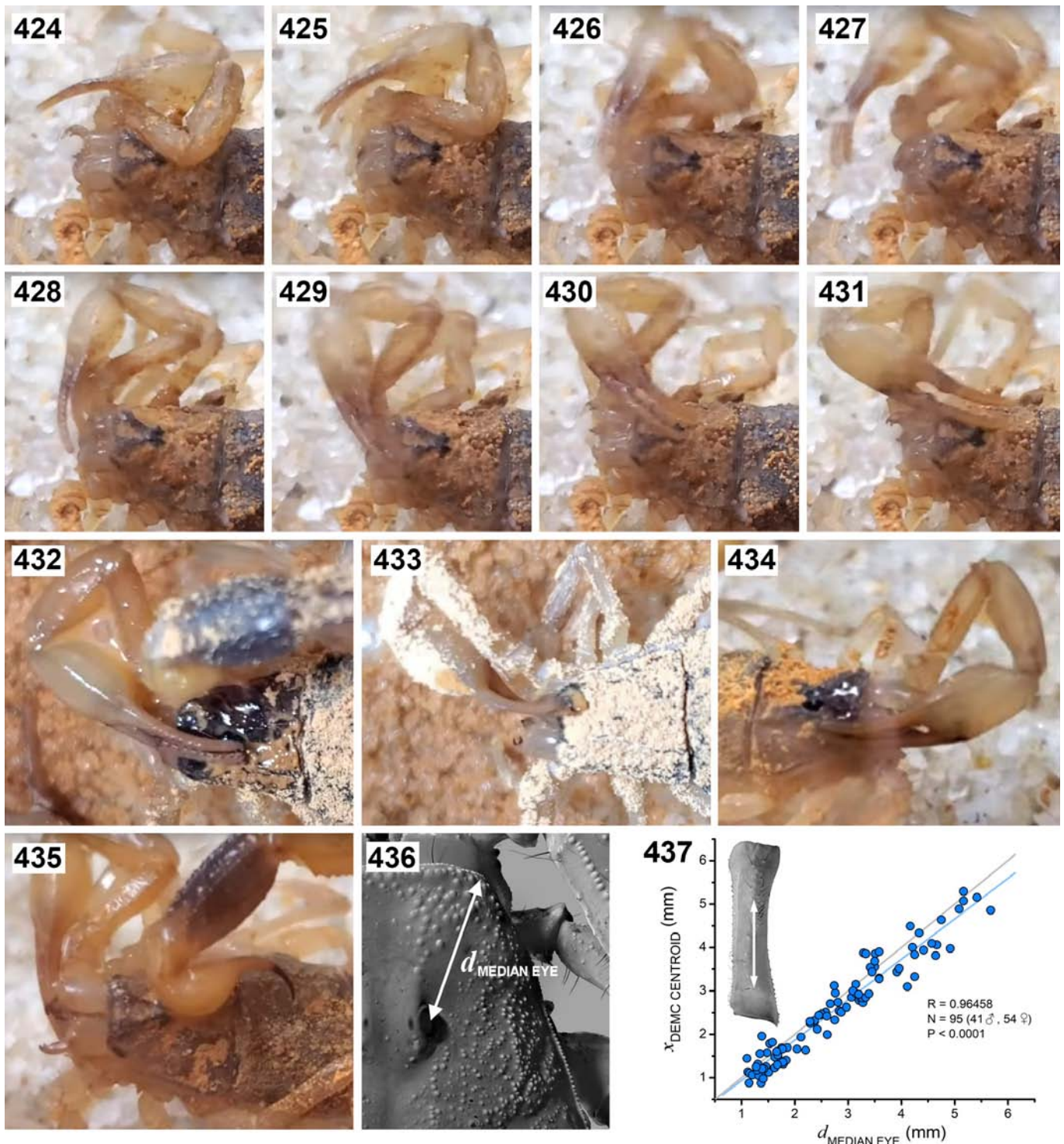


Figures 411–423: Ontogenetic variation and cuticular structure of DVMC (distal ventral macrosetal cluster) of movable finger of *Apistobuthus pterygocercus*. **Figures 411–418.** Ventral aspects of right (or left mirrored, 411, 414) distal movable finger of different instars, females (411–417) and male (418), with carapace lengths (mm): 10.32, 9.94, 8.94, 7.74, 6.54, 4.38, 3.83, and 2.84 respectively. Scale bars: 500 µm. UV fluorescence. **Figures 419–421.** Ontogenetic scaling of number and density of DVMC macrosetae. **Figure 419.** Number of DVMC macrosetae vs. carapace length. **Figure 420.** L-normalized mean nearest neighbor distance (NND) vs. carapace length. **Figure 421.** Mean absolute nearest neighbor distance (NND) vs. carapace length. **Figures 422–423.** Transverse ~40 µm sections of cuticle of left distal movable finger of adult female, intersecting DVMC, showing ventral macrosetae. Views under differential interference contrast (422), and Köhler illumination with UV epifluorescence (423). Scale bar: 100 µm (422–423).

Within the ‘Buthus’ group, DVMCs of different taxa varied in their densities of setation and in the lengths of their setae, but were generally similar in their sizes and shapes. A striking exception was the DVMC of *Apistobuthus*, which formed a large expanded patch of high density setation on a dilated subapical surface (Figs. 239–240, 252–253, 256–259). The number and relative density of setae in the DVMC of *A. pterygocercus* ranked the highest among all examined species. More generally, conspicuous differences in setal morphology and patterning of different buthid groups and non-buthid families are apparent even in our limited survey of distal fingers (Figs. 244–398). Finger setation deserves more attention as a potentially rich source of taxonomic characters.

Functional significance of the DEMC and DVMC

Locket (2001) cited an anecdotal report of Fleissner & Fleissner that the DEMC functions as a lens cleaning tool, wiping dust off the ipsilateral median ocellus. We found support for this in: (i) our observations of DEMC contact with the ipsilateral median ocellus during sponge-bathing in *Olivierius martensii* (Figs. 424–434), and (ii) the consistent positioning, in all examined buthid species, of the DEMC on the femur where it can make contact with the ipsilateral median ocellus during femoral rotation (Fig. 437). The Fleissner & Fleissner report did not mention wet cleaning by sponge-bathing, so it is possible that they were describing a more frequent wiping of dry debris by the DEMC. We have not observed such behavior in *O. martensii*.



Figures 424–437. Role of DEMC and DVMC in cleaning the median eyes. **Figures 424–435.** Frames captured from video recordings of sponge bathing activity in adult *Olivierus martensii* (Buthidae). **Figures 424–431.** Frames capturing various positions of right pedipalp during rhythmic oscillatory action of carapace cleaning. At opposite ends of oscillation, DEMC contacts ipsilateral median eye (416), and DVMC contacts contralateral median eye (422–423). **Figures 432–434.** Frames showing DVMC sweeping contralateral median eye in three other individuals. **Figure 435.** Frame showing wiping of median ocular tubercle by ventral surface of telson vesicle. **Figure 436.** Measurement of $d_{\text{MEDIAN EYE}}$ = distance between median eye and ipsilateral anterolateral vertex of carapace, example of *Trypanothacus barnesi*, ♂. **Figure 437.** Scatter plot showing matching of proximidistal coordinate of DEMC centroid ($x_{\text{DEMC CENTROID}}$) to distance of median eye from ipsilateral anterolateral vertex of carapace ($d_{\text{MEDIAN EYE}}$). R: Pearson’s correlation coefficient.

The sizes of particles that can be swept by a brush are determined by the physical spacing of brush bristles. In the DEMC, the mean absolute NND is measure of the average spacing between macrosetae. In the ‘Buthus’ group this varied over a range of ~150–300 μm (mean ~200 μm) (Fig. 203). These values match the diameters of the fine grains of sand that comprise much of the surface material in dune systems worldwide (Abolkhair, 1986; Ahlbrandt, 1979; Tsoar, 1990). DEMCs consisting of setae arranged regularly in single file would be capable of sweeping particles as small as fine dune sand. Those with setae arranged in broad patches may also be capable of sweeping smaller particles, such as very fine sand (50–100 μm) or silt (5–50 μm) (Blott & Pye, 2012). In addition, the longer, flexible setae in many DEMCs could bend and scrape the ocular surface with their shafts to remove particles smaller than the average spacing between setae. The dense, compact type of DEMC was found only in the ‘Buthus’ group, a major lineage distributed across the Palearctic deserts (Fet et al., 2005). It may have evolved as a specialized adaptation to prevent vision from being obscured by the loose sand and dust that is abundant in arid environments. In other buthids, DEMCs were present in *Parabuthus*, *Teruelius* and *Uroplectes*, genera inhabiting drier environments. DEMCs were absent from buthids found in humid, tropical habitats (e.g., *Grosphus*, *Tityus*, ‘Ananteris-Isometrus’ group) where dust is not likely to be a problem. The DEMC is not an ecomorphotypic feature of all arid-adapted scorpions, because we did not find DEMCs in picobuthoids of the ‘Buthus’ group (Figs. 79–80), the bothriurid genus *Brachistosternus* from arid and semi-arid habitats of South America (Figs. 127–129), and scorpion taxa of Nearctic deserts (e.g., vaejovids, *Hadrurus*). Dust on the ocelli either is not a problem for them, or is removed by some other grooming mechanism. In picobuthoids, the extremely short, clavate setae on the pedipalps may not be effective as brush bristles. It is conceivable that the transversely corrugated ventromedian carina on the anterior telson vesicle of picobuthoids (Lowe, 2010a) is used during grooming to dislodge encrusted soil from the carapace (i.e., wielded as in Fig. 435).

If the DEMC functions as an ocellar grooming tool, then it is predicted to be absent in troglobitic species lacking ocelli. This prediction was confirmed for *Belisarius xambeui* (Belisariidae) (Fig. 134). Its absence in eyeless endogean pseudochactid genera (*Aemngvantom*, *Troglokhamouanus*, and *Vietbocap*) was also confirmed by photographs of the external femur in Prendini et al. (2021). However, these cases may simply be instances of the general absence of DEMC in non-buthids, eyeless or not.

The apical finger location of the DVMC suggests that it functions to enhance tactile sensitivity of the fingertips as they probe the substrate. DVMC macrosetae arise from sockets connected to transcuticular canals that permit the passage of dendrites of mechanosensitive neurons, consistent with a sensory function. Thus, we were surprised to observe the apparent use of the DVMC for contralateral ocular grooming in the sponge-bathing routine of *O. martensii*. Dry-wiping by the DVMC is another possibility, although we have not observed it. The more

distal setae of the DVMC arise from the ventrointernal surface of the finger, where they are well oriented to brush the ocelli of an elevated median ocular tubercle. The DVMC could be dual use, functioning as both a sensory probe and an ocular grooming tool. In its grooming role, the setae can relay mechanoreceptive feedback signals to register contact with median ocelli. The same kind of feedback could be relayed by DEMC macrosetae during ocular grooming. Contralateral ocular grooming by the DVMC may seem redundant, given that each median ocellus can presumably be groomed by its ipsilateral DEMC. However, setae in the DVMC are more densely clustered, with mean absolute NNDs in the range of ~25–60 μm (mean ~40 μm) (Fig. 408), which includes the upper size range of silt. Perhaps the DVMC removes finer silt particles after coarser sand grains have been brushed off by the DEMC. Like the DEMC, the DVMC was mainly restricted to the ‘Buthus’ group, and a few other buthids from more arid habitats (*Parabuthus*, *Teruelius*, *Uroplectes*). The strong positive taxonomic correlation between DVMC and DEMC densities (Fig. 410) suggests coevolution driven by common environmental factors. An alternative non-sensory function of dense setation on the pedipalp fingers of arid-adapted scorpions was demonstrated for *Parabuthus transvaalicus* (Fig. 338–339). Chen et al. (2018) found that microscopic channels on the surfaces of the setae can accelerate dew collection. The microscopic surface structure of DVMC setae in other buthids is unknown. Experimental and behavioral studies on many more species of buthids are needed to test these functional hypotheses.

The unique DVMC of *Apistobuthus*, a highly expanded setation field on the tip of an extraordinarily elongated movable finger, is particularly intriguing. The genus displays a number of morphological specializations, some of which may be related to its psammophilic, or ultrapsammophilic, niche. Among the non-buthids that we studied, a DVMC was found only in *Vejovoidus*, another ultrapsammophile (Figs. 391–392). The DVMC of *Vejovoidus* is quite different from those of *Apistobuthus* and other ‘Buthus’ group genera. It is composed of a long series of more widely spaced macrosetae, with a mean absolute NND of ~250 μm , which is comparable to that of DEMCs in the ‘Buthus’ group (~200 μm). Since *Vejovoidus* lacks a DEMC, it may use its DVMC as a sand removal brush.

Acknowledgements

We gratefully acknowledge the many researchers and collectors who provided specimens examined in this study. In particular, study material was loaned or acquired thanks to the generosity, efforts and field assistance of: Rolf Aalbu, Andrew Gardner, Jim Dundon, Victor Fet, S. M. Farook, Blaine Hébert, Markus Heule, Michael Gallagher, Ian Harrison, David Hirst, Wendell Icenogle, František Kovařík, Chuck & Anita Kristensen, Steve Kutcher, Adam Locket, Samuel Miller, Shahrokh Navidpour, Michael Soleglad, Rolando Teruel, Alex Ullrich, Stanley Williams, Alex & Birgit Winkler, and Ersen Yağmur. We thank two anonymous reviewers for their comments.

References

- ABOLKHAIR, Y. M. S. 1986. The statistical analysis of the sand grain size distribution of Al-Ubay-lah barchan dunes, northwestern Ar-Rub-Alkhali desert, Saudi Arabia. *GeoJournal*, 13.2: 103–109.
- AHLBRANDT, T. S. 1979. Textural parameters of eolian deposits. Pp. 21–51 in: MCKEE, E. D. (ed.). *A Study of Global Sand Seas*. Geological Survey Professional Paper 1052. United States Government Printing Office, Washington.
- ARMAS, L. F. de. 1977. Nueva quetotaxia en Buthidae (Scorpionida). *Miscelanea. Zoologica*, La Habana, 6: 2–3.
- BASIBUYUK, H. H. & D. L. J. QUICKE. 1995. Morphology of the antenna cleaner in the Hymenoptera with particular reference to non-aculeate families (Insecta). *Zoologica Scripta*, 24 (2): 157–177.
- BAUER, R. T. 1981. Grooming behavior and morphology in the decapod Crustacea. *Journal of Crustacean Biology*, 1: 153–173.
- BAUER, R. T. 2013. Adaptive modification of appendages for grooming (cleaning, antifouling) and reproduction in the Crustacea. Pp. 337–375 in: WATLING, L. & M. THIEL (eds.). *The Natural History of the Crustacea. 1. Functional Morphology and Diversity*. Oxford University Press, Oxford, UK.
- BLOTT, S. J. & K. PYE. 2012. Particle size scales and classification of sediment types based on particle size distributions: Review and recommended procedures. *Sedimentology*, 59: 2071–2096.
- CAIN, S., E. GEFEN & L. PRENDINI. 2021. Systematic revision of the sand scorpions, genus *Buthacus* Birula, 1908 (Buthidae C.L. Koch, 1837) of the Levant, with redescription of *Buthacus arenicola* (Simon, 1885) from Algeria and Tunisia. *Bulletin of the American Museum of Natural History*, 450: 1–134.
- CHAMBERLIN, J. C. 1931. The arachnid order Chelonethida. *Stanford University Publications. University Series. Biological Sciences*. 7 (1): 1–284.
- CHEN, D., S. NIU, J. ZHANG, Z. MU, H. CHEN, D. ZHANG, Z. YAO, Z. HAN & L. REN. 2018. Superfast liquid transfer strategy through sliding on a liquid membrane inspired from scorpion setae. *Advanced Materials Interfaces*, 5, 1800802: 1–8.
- CHIRIVI-JOYA, D., L. BONILLA, A. GALINDO & G. FAGUA. 2021. Variation of cleaning organ structures and setae of pedipalp tarsus in the family Phrynidae (Arachnida: Amblypygi). *Arthropod Structure & Development*, 61, 101027: 1–13.
- CONSTANTINOU, C. 1985. Sponge bathing in the scorpion *Buthus occitanus*. *Entomologist's Monthly Magazine*, 121: 149–150.
- CONTRERAS FÉLIX, G. A. & J. L. NAVARRETE HEREDIA. 2024. Hidden in the cracks, a new species of scorpion from Michoacan, Mexico (Scorpiones: Vaejovidae). *Dugesiana*, 31 (2): 159–173.
- CRUZ, J. DE LA & L. F. DE ARMAS. 1980. Macroquetas digitales en Buthidae (Arachnida: Scorpionida). *Poeyana*, 199: 1–10.
- ENGEL, R. 2012. Novel discovery of lamellar papillae on the grooming organ in *Synsphyronus* (Garypidae: Pseudoscorpiones). *Arthropod Structure and Development*, 41: 265–269.
- FET, V., M. S. BREWER, M. E. SOLEGLAD & D. P. A. NEFF. 2006. Constellation array: a new sensory structure in scorpions (Arachnida: Scorpiones). *Boletín de la Sociedad Entomológica Aragonesa*, 38: 269–278.
- FET, V. & D. RECHKIN. 1989. Scorpion trichobothriotaxy: a principal component analysis. *Rivista del Museo Civico di Scienze Naturali "Enrico Caffi" (Bergamo)*, 14: 191–206.
- FET, V., M. E. SOLEGLAD & G. LOWE. 2005. A new trichobothrial character for the high-level systematics of Buthoidea (Scorpiones: Buthida). *Euscorpius*, 23: 1–40.
- FOELIX, R. & J. SCHABRONATH. 1983. The fine structure of scorpion sensory organs. I. Tarsal sensilla. *Bulletin of the British Arachnological Society*, 6 (2): 53–67.
- FRANCKE, O. F. 1977. Scorpions of the genus *Diplocentrus* from Oaxaca, Mexico (Scorpionida, Diplocentridae). *Journal of Arachnology*, 4: 145–200.
- FRANCKE, O. F. 1978. Systematic revision of diplocentrid scorpions from circum-Caribbean lands. *Special Publications of the Museum, Texas Tech University*, 14: 1–92.
- GONZÁLEZ-SANTILLÁN, E., M. A. GALÁN-SÁNCHEZ & L. L. VALDEZ-VELÁZQUEZ. 2019. A new species of *Centruroides* (Scorpiones, Buthidae) from Colima, Mexico. *Comptes Rendus Biologies*, 342 (9–10): 1–14. <https://doi.org/10.1016/j.crv.2019.10.002>

- GONZÁLEZ-SANTILLÁN, E. & L. PRENDINI. 2013. Redefinition and generic revision of the North American vaejovid scorpion subfamily Syntropinae Kraepelin, 1905, with descriptions of six new genera. *Bulletin of the American Museum of Natural History*, 382: 1–71.
- HARADON, R. M. 1983. *Smeringurus*, a new subgenus of *Paruroctonus* Werner (Scorpiones, Vaejovidae). *Journal of Arachnology*, 11: 251–270.
- HARADON, R. M. 1984a. New and redefined species belonging to the *Paruroctonus baergi* group (Scorpiones, Vaejovidae). *Journal of Arachnology*, 12: 205–221.
- HARADON, R. M. 1984b. New and redefined species belonging to the *Paruroctonus borregoensis* group (Scorpiones, Vaejovidae). *Journal of Arachnology*, 12: 317–339.
- HARADON, R. M. 1985. New groups and species of the nominate subgenus *Paruroctonus* (Scorpiones, Vaejovidae). *Journal of Arachnology*, 13: 19–42.
- HLAVAC, T. F. 1975. Grooming systems of insects: Structure, mechanics. *Annals of the Entomological Society of America*, 68 (5): 823–826.
- HUGHS, G. B. 2011. Morphological analysis of montane scorpions of the genus *Vaejovis* (Scorpiones: Vaejovidae) in Arizona with revised diagnoses and description of a new species. *Journal of Arachnology*, 39: 420–438.
- JAIN, P., H. FORBES & L. A. ESPOSITO. 2022. Two new alkali-sink specialist species of *Paruroctonus* Werner 1934 (Scorpiones, Vaejovidae) from central California. *ZooKeys*, 1117: 139–188. doi: [10.3897/zookeys.1117.76872](https://doi.org/10.3897/zookeys.1117.76872)
- JAIN, P., H. FORBES, J. A. GORNEAU & L. A. ESPOSITO. 2023. A new species of alkali-sink *Paruroctonus* Werner, 1934 (Scorpiones, Vaejovidae) from California's San Joaquin Valley. *ZooKeys*, 1185: 199–239. doi: [10.3897/zookeys.1185.103574](https://doi.org/10.3897/zookeys.1185.103574)
- KLADT, N., H. WOLF & H.-G. HEINZEL. 2007. Mechanoreception by cuticular sensilla on the pectines of the scorpion *Pandinus cavimanus*. *Journal of Comparative Physiology A*, 193: 1033–1043.
- KOVAŘÍK, F. 2000. Revision of family Scorpipidae (Scorpiones), with descriptions of six new species. *Acta Societas Zoologicae Bohemicae*, 64: 153–201.
- KOVAŘÍK, F. & G. LOWE. 2019. Scorpions of the Horn of Africa (Arachnida, Scorpiones). Part XVIII. *Gint banfasae* sp. n. from Somaliland (Buthidae). *Euscorpius*, 272: 1–14.
- KOVAŘÍK, F., G. LOWE, M. E. SOLEGLAD & J. PLÍŠKOVA. 2017. Scorpions of the Horn of Africa (Arachnida: Scorpiones). Part X. *Pandiborellius* stat. n. and *Pandinurus* (Scorpiones) with description of four new species from Eritrea and Ethiopia, and review of *Pandinus* sensu lato taxonomy. *Euscorpius*, 238: 1–103.
- KOVAŘÍK, F. & L. NJOROGE. 2021. *Somalibuthus sabae* sp. n., a new buthid scorpion from Kenya (Scorpiones: Buthidae). *Euscorpius*, 332: 1–19.
- KOVAŘÍK, F. & A.A. OJANGUREN AFFILASTRO. 2013. *Illustrated catalog of scorpions. Part II. Bothriuridae; Chaerilidae; Buthidae I. Genera Compsobuthus, Hottentotta, Isometrus, Lychas, and Sassanidotus*. Prague: Clairon Production, 400 pp.
- KRAEPELIN, K. 1894. Revision der Scorpione. II. Scorpionidae und Bothriuridae. *Beiheft zum Jahrbuch der Hamburgischen Wissenschaftlichen Anstalten*, 11: 1–248.
- LAWRENCE, R. F. 1968. The structure of the cleaning brush on the pedipalps of some African Amblypygi. *Journal of Zoology, London*, 154: 1–8.
- LEVY, G. & P. AMITAI. 1980. *Fauna Palaestina. Arachnida I. Scorpiones*. Jerusalem: The Israel Academy of Sciences and Humanities, 130 pp.
- LEVY, G., P. AMITAI & A. SHULOV. 1973. New scorpions from Israel, Jordan and Arabia. *Zoological Journal of the Linnaean Society*, 52 (2): 113–140.
- LOCKET, N. A. 2001. Eyes and vision. Pp. 79–106 in: BROWNELL, P. & G. POLIS (eds.). *Scorpion Biology and Research*. Oxford University Press, Oxford, UK.
- LOURENÇO, W. R. 1984. *Ananteris luciae*, nouvelle espece de Scorpion de l' Amazonie brésilienne (Scorpiones, Buthidae). *Journal of Arachnology*, 12 (3): 279–282.
- LOURENÇO, W. R. 1998. A new species of *Tityus* C. L. Koch, 1836 (Scorpiones, Buthidae) in Colombia, with a check list and key to the Colombian species of the genus. *Zoosystema*, 20 (3): 487–497.
- LOURENÇO, W. R. 2007. First record of the family Pseudochactidae Gromov (Chelicerata, Scorpiones) from Laos and new biogeographic evidence of a Pangaeon palaeodistribution. *Comptes Rendus Biologies*, 330 (10): 770–777.
- LOURENÇO, W. R. & D.-S. PHAM. 2010. A remarkable new cave scorpion of the family Pseudochactidae Gromov (Chelicerata, Scorpiones) from Vietnam. *ZooKeys*, 71: 1–13.

- LOWE, G. 2001. A new species of *Compsobuthus* Vachon, 1949 from central Oman (Scorpiones: Buthidae). Pp. 171–177 in: Fet, V. and P. A. Selden (eds). *Scorpions 2001. In Memoriam Gary A. Polis*. Burnham Beeches, Bucks: British Arachnological Society.
- LOWE, G. 2010a. New picobuthoid scorpions (Scorpiones: Buthidae) from Oman. *Euscorpius*, 93: 1–53.
- LOWE, G. 2010b. A New Species of *Odontobuthus* (Scorpiones: Buthidae) from Northern Oman. *Euscorpius*, 96: 1–22.
- LOWE, G. 2010c. The genus *Vachoniolus* (Scorpiones: Buthidae) in Oman. *Euscorpius*, 100: 1–37.
- LOWE, G. 2010d. Two new species of *Hottentotta* Birula, 1908 (Scorpiones: Buthidae) from northern Oman. *Euscorpius*, 103: 1–23.
- LOWE, G. 2018. The genera *Butheolus* Simon, 1882 and *Xenobuthus* gen. nov. (Scorpiones: Buthidae) in Oman. *Euscorpius*, 261: 1–73.
- LOWE, G. & V. FET. 2024. A survey of proximal sensilla associated with denticle subrows on scorpion pedipalp fingers (Arachnida: Scorpiones), with observations on scorpion fluorescence. *Euscorpius*, 382: 1–109.
- LOWE, G. & F. KOVAŘÍK. 2016. Scorpions of the Horn of Africa (Arachnida, Scorpiones). Part V. Two New Species of *Neobuthus* Hirst, 1911 (Buthidae), from Ethiopia and Eritrea. *Euscorpius*, 224: 1–46.
- LOWE, G. & F. KOVAŘÍK. 2019. Review of *Grosphus* Simon, 1880, with description of *Teruelius* gen. n., a new buthid genus from Madagascar (Scorpiones: Buthidae). *Euscorpius*, 281: 1–128.
- LOWE, G. & F. KOVAŘÍK. 2022. Reanalysis of *Teruelius* and *Grosphus* (Scorpiones: Buthidae) with descriptions of two new species. *Euscorpius*, 304: 1–40.
- LOWE, G., F. KOVAŘÍK, M. STOCKMANN & F. ŠTÁHLAVSKÝ. 2019. *Trypanothacus* gen. n., a new genus of burrowing scorpion from the Arabian Peninsula (Scorpiones: Buthidae). *Euscorpius*, 277: 1–30.
- LOWE, G., S. R. KUTCHER & D. EDWARDS. 2003. A powerful new light source for ultraviolet detection of scorpions in the field. *Euscorpius*, 8: 1–7.
- LOWE, G., E. A. YAĞMUR & F. KOVAŘÍK. 2014. A review of the genus *Leiurus* Ehrenberg, 1828 (Scorpiones: Buthidae) with description of four new species from the Arabian Peninsula. *Euscorpius*, 191: 1–129.
- MCWEST, K. J. 2009. Tarsal spinules and setae of vaejoviid scorpions (Scorpiones: Vaejovidae). *Zootaxa*, 2001: 1–126.
- MONOD, L., M. S. HARVEY & L. PRENDINI. 2013. Stenotopic *Hormurus* Thorell, 1876 scorpions from the monsoon ecosystems of northern Australia, with a discussion on the evolution of burrowing behaviour in Hormuridae Laurie, 1896. *Revue Suisse de Zoologie*, 120 (2): 281–346.
- MONOD, L., C. LEHMANN-GRABER, C. C. AUSTIN, B. IOVA & L. PRENDINI. 2023. Atlas of Australasian hormurid scorpions. I. The genus *Hormurus* Thorell, 1876 in Papua New Guinea. Exceptional morphological diversity in male and female copulatory structures suggests genital coevolution. *Revue suisse de Zoologie*, 130 (suppl.): 1–243.
- PRENDINI, L. 2000. Phylogeny and classification of the superfamily Scorpionoidea Latreille 1802 (Chelicerata, Scorpiones): an exemplar approach. *Cladistics*, 16: 1–78.
- PRENDINI, L. 2004. Revision of *Karasbergia* Hewitt (Scorpiones; Buthidae), a monotypic genus endemic to southern Africa. *Journal of Afrotropical Zoology*, 1: 77–93.
- PRENDINI, L., V. L. EHRENTAL & S. F. LORIA. 2021. Systematics of the relictual Asian scorpion family Pseudochactidae Gromov, 1998, with a review of cavernicolous, troglobitic, and troglomorphic scorpions. *Bulletin of the American Museum of Natural History*, 453: 1–149.
- PRENDINI, L. & S. F. LORIA. 2020. Systematic revision of the Asian forest scorpions (Heterometrinae Simon, 1879), revised suprageneric classification of Scorpionidae Latreille, 1802, and revalidation of Rugodentidae Bastawade et al., 2005. *Bulletin of the American Museum of Natural History*, 442: 1–480.
- PRENDINI, L., E. S. VOLSCHENK, S. MAALIKI & A. V. GROMOV. 2006. A ‘living fossil’ from Central Asia: The morphology of *Pseudochactas ovchinnikovi* Gromov, 1998 (Scorpiones: Pseudochactidae), with comments on its phylogenetic position. *Zoologischer Anzeiger*, 245 (3–4): 211–248.
- PURCELL, W. F. 1899. On the species of *Opisthophthalmus* in the collection of the South African Museum, with descriptions of some new forms. *Annals of South African Museum*, 1: 131–180.
- RAO, K. P. 1964. Neurophysiological studies on an arachnid, the scorpion *Heterometrus fulvipes*. *Journal of Animal Morphology and Physiology*, 11: 133–142.

- REBORA, M., G. SALERNO, S. PIERSANTI, J. MICHELS & S. GORB. 2019. Structure and biomechanics of the antennal grooming mechanism in the southern green stink bug *Nezara viridula*. *Journal of Insect Physiology*, 112: 57–67.
- ROSIN, R. & A. SHULOV. 1963. Studies on the scorpion *Nebo hierichonticus*. *Proceedings of the Zoological Society of London*, 140 (4): 547–575.
- SCHNEIDER, C. A., W. S. RASBAND & K. W. ELICEIRI. 2012. NIH Image to ImageJ: 25 years of image analysis. *Nature Methods*, 9 (7): 671–675. doi:10.1038/nmeth.2089
- SHULOV, A. & P. AMITAI. 1960. Observations sur les scorpions *Orthochirus innesi* E. Simon 1910, ssp. *negebensis* nov. *Archives de l'Institut Pasteur de l'Algérie*, 38 (1): 117–129.
- SISSOM, W. D., M. R. GRAHAM, T. G. DONALDSON & R. W. BRYSON. 2016. Two new *Vaejovis* C.L. Koch 1836 from highlands of the Sierra Madre Occidental, Durango, Mexico (Scorpiones, Vaejovidae). *Insecta Mundi*, 0477: 1–14.
- SOLEGLAD, M. E. & V. FET. 2001. Evolution of scorpion orthobothriotaxy: a cladistic approach. *Euscorpium*, 1: 1–38.
- SOLEGLAD, M. E., V. FET & F. KOVAŘÍK. 2005. The systematic position of the scorpion genera *Heteroscorpion* Birula, 1903 and *Urodacus* Peters, 1861 (Scorpiones: Scorpionoidea). *Euscorpium*, 20: 1–38.
- SOLEGLAD, M. E., V. FET & G. LOWE. 2011. Contributions to scorpion systematics. IV. Observations on the *Hadrurus* “*spadix*” subgroup with a description of a new species (Scorpiones: Caraboctonidae). *Euscorpium*, 112: 1–36.
- SANTIBÁÑEZ-LÓPEZ, C. E., O. F. FRANCKE B. & a. ORTEGA-GUTIERREZ. 2013. Variation in the spiniform macrosetae pattern on the basitarsi of *Diplocentrus tehuacanus* (Scorpiones: Diplocentridae): new characters to diagnose species within the genus. *Journal of Arachnology*, 41: 319–326.
- STAHNKE, H. L. 1967. *Diplocentrus bigbendensis*, a new species of scorpion. *Entomological News*, 28: 173–179.
- STAHNKE, H. L. 1968. Some diplocentrid scorpions from Baja California del Sur, Mexico. *Proceedings of the California Academy of Sciences*, 35 (14): 273–320.
- STAHNKE, H. L. 1971. Scorpion nomenclature and mensuration. *Entomological News*, 81: 297–316.
- ŠTUNDLOVÁ, J., F. ŠTÁHLAVSKÝ, V. OPATOVÁ, J. ŠTUNDL, F. KOVAŘÍK, P. DOLEJŠ & J. ŠMÍD. 2022. Molecular data do not support the traditional morphology-based groupings in the scorpion family Buthidae (Arachnida: Scorpiones). *Molecular Phylogenetics and Evolution*, 173(2020) 107511.
- TANG, V. 2022a. A new species of *Scorpiops* Peters, 1861 from Yunnan Province, China, with a preliminary review of its congeners in Yunnan (Scorpiones: Scorpiopidae). *Euscorpium*, 360: 1–45.
- TANG, V. 2022b. Reanalysis of the Yunnan population of *Scorpiops kubani* with a description of a new species, *Scorpiops lowei* sp. n. (Scorpiones: Scorpiopidae). *Euscorpium*, 361: 1–22.
- TANG, V. 2023. Description of the adult male *Scorpiops tongtongi* Tang, 2022, with further comments on the genus *Scorpiops* Peters, 1861 in China (Scorpiones: Scorpiopidae). *Euscorpium*, 377: 1–52.
- TANG, V., Q. JIA & L. LIU. 2023. A new monotypic genus and species from China, *Langxie feti* gen. et sp. n. (Scorpiones: Buthidae). *Euscorpium*, 370: 1–101.
- TANG, V., K. OUYANG, Z. LIU & F. ŠTÁHLAVSKÝ. 2024. Three new species of genus *Scorpiops* Peters, 1861 from Tibet, China (Scorpiones: Scorpiopidae), with implications for the diagnostic values of qualitative characters. *Euscorpium*, 394: 1–40.
- TERUEL, R. & C. TURIEL. 2020. The genus *Buthus* Leach, 1815 (Scorpiones: Buthidae) in the Iberian Peninsula. Part 1: four redescriptions and six new species. *Revista Ibérica de Aracnología*, 37: 3–60.
- TSOAR, H. 1990. Grain-size characteristics of wind ripples on a desert seif dune. *Geography Research Forum*, 10: 37–50.
- VACHON, M. 1952. *Étude sur les Scorpions*. Institut Pasteur d'Algerie, Alger, 482 pp.
- VACHON, M. 1958. A propos de *Liobuthus kessleri* Birula, Scorpion psammophile nouveau pour la faune iranienne. *Bulletin du Museum National d'Histoire Naturelle, Paris*, (2), 30: 422–426.
- VACHON, M. 1972. Sur l'établissement d'une nomenclature trichobothriale uniforme convenant à l'ensemble des Scorpions (Arachnides) et l'existence de trois types distincts de irichobothriotaxie. *Comptes Rendus de l'Académie des Sciences (Paris)*, Série D, 275: 2001–2004.

- VACHON, M. 1974. Étude des caractères utilisés pour classe les familles et les genre de Scorpiones (Arachnides). 1. La trichobothriotaxie en Arachnologie. Sigles trichobothriaux et types de trichobothriotaxie chez les scorpions. *Bulletin du Muséum National d'Histoire Naturelle Paris, Zoologie*, (3) 104 (140): 857–958.
- VACHON, M. 1975. Sur l'utilisation de la trichobothriotaxie du bras des pédipalpes des Scorpions (Arachnides) dans le classement des genres de famille des Buthidae Simon. *Comptes Rendus Hebdomadaires des Séances de l'Académie des Sciences*, (D), 281 (21): 1597–1599.
- VACHON, M. 1977. Contribution a l'étude des Scorpions Buthidae du nouveau monde. 1. Complément à la connaissance de *Microtityus rickyi* Kj.-W. 1956 de l'île de la Trinite. II. Description d'un nouvelle spece et d'un nouveau genre mexicains: *Darchenia bernadettae*. III. Cle de determination des genres de Buthidae du Nouveau Monde. *Acta Biologica Venezuelica*, 9 (3): 283–302.
- VACHON, M. 1979. Arachnids of Saudi Arabia, Scorpiones. *Fauna of Saudi Arabia*, 1: 30–66.
- VOLSCHENK, E. S. 2005. A new technique for examining surface morphosculpture of scorpions. *Journal of Arachnology*, 33: 820–825.
- WILLIAMS, S.C. 1966. Burrowing activities of the scorpion *Anuroctonus phaeodactylus* (Wood) (Scorpionida: Vejovidae). *Proceedings of the California Academy of Sciences*, ser.4, 34 (8): 419–428.
- WILLIAMS, S. C. 1970. A systematic revision of the giant hairy scorpion genus *Hadrurus*. *Occasional Papers of the California Academy of Sciences*, 87: 1–62.
- WORTHAM, J L. & L. G. KOSTECKA. 2019. Grooming behaviors and setal morphology in smasher and spearer mantis shrimps (Stomatopoda). *Journal of Crustacean Biology*, 39 (1): 11–21.
- YTHIER, E., J. CHEVALIER & W. R. LOURENÇO. 2020. A synopsis of the genus *Ananteris* Thorell, 1891 (Scorpiones: Buthidae) in French Guiana, with description of four new species. *Arachnida –Rivista Aracnologica Italiana*, 28: 2–33.